The Spinal Locomotor Circuit of the Larval Zebrafish: Anatomical Organization and Functional Components

A DISSERTATION
SUBMITTED TO THE FACULTY OF
UNIVERSITY OF MINNESOTA
BY

Timothy David Wiggin

IN PARTIAL FULFILLMENT OF THE REQUIREMENTS
FOR THE DEGREE OF
DOCTOR OF PHILOSOPHY

Mark A. Masino, Advisor

February 2015

Acknowledgements

I would like to acknowledge the wonderful support, mentorship and training provided by my advisor, Mark Masino. My coworkers in the Masino lab, Jack Peck, Jacob Montgomery, Aaron Lambert, Tatiana Anderson, Brittany Corwin and Balvindar Singh, have my gratitude for their help and friendship over the course of my time as a graduate student.

Table of Contents

List of Tables

List of Figures

CHAPTER 1: THE ROLE OF THE SPINAL CORD IN THE GENERATION OF LOCOMOTOR BEHAVIOR

Nervous Systems Permit Complex Animal Behavior

The nervous system is an adaptation that allows animals to engage in rapid, complex behaviors. Plants engage in chemical communication with conspecifics (Heil and Karban, 2010), and unicellular organisms are able to communicate (Waters and Bassler, 2005) and locomote (Yang et al., 1995), but the range of behaviors enabled by neural computations are unparalleled outside the animal kingdom. These advantages come at a cost: nervous systems are energetically demanding to maintain, consuming 2-8% of the typical vertebrate basal metabolism, and 20% of human basal metabolism (Mink et al., 1981). Both the behavioral importance and energetic cost of nervous systems are well illustrated by the life cycle of the ascidian *Ciona intestinalis* (sea squirt), a primitive chordate. Adult ascidians release larva that initially develop a nervous system that is comparable to other vertebrates (Meinertzhagen and Okamura, 2001). The larval ascidian swims and senses the environment until it finds a site to settle, at which point it attaches to a surface and initiates metamorphosis (Svane and Young, 1989). During metamorphosis, the ascidian becomes a sessile, filter feeding animal, and reabsorbs unnecessary larval tissues, including the central nervous system (Svane and Young, 1989). Without an appropriate nervous system, the ascidian larva would not be able to sense the environment and select a good location to settle. However, once that active behavioral task is complete,

the larval nervous system becomes an unnecessary energy expense. The study of the nervous system is therefore inextricably tied to the study of behavior, known as ethology. The work in this dissertation is primarily concerned with neuroethology, specifically with the neuronal circuits that drive locomotor behavior in fish. Additionally, because of the importance of the nervous system to human health and disease, neuroscience research is also an essential part of the biomedical research agenda. The research presented here may also be helpful for understanding how spinal locomotor systems are organized, which will be important for designing spinal cord therapeutics targeting injury or disease conditions (Ramer et al., 2014).

Organization of the Nervous System

Animal body plans are diverse with respect to symmetry, respiration, number of limbs, etc., and there is a corresponding diversity of nervous system organization. The vertebrate clade is named for a feature of their nervous system anatomy: the vertebra that surround the spinal cord. During development, vertebrates undergo neurulation, a process by which ectoderm is divided into the neural tube, neural crest cells and epidermis (Schoenwolf and Smith, 1990). Neural tube cells develop into the central nervous system (brain and spinal cord) and retina, neural crest cells develop into the peripheral nervous system, and epidermis develops into a variety of non-neuronal tissues (Schoenwolf and Smith, 1990; Wilson and Houart, 2004).

While the gross neuroanatomy of vertebrates is well conserved, the spinal cord varies somewhat in structure between vertebrate species. For example, tetrapods (reptiles, birds, amphibians and mammals) have specialized limb enlargements, while fish (jawless, cartilaginous and boney) lack these structures (Butler and Hodos, 2005). However, there are some features that are in common across the vertebrate clade. The spinal cord contains the cell bodies of motor neurons that innervate the muscles of the animals (Butler and Hodos, 2005), and the spinal cords of a wide diversity of vertebrates also contain a network (or multiple networks) of pre-motor interneurons called Central Pattern Generators (CPGs), a sample of which is presented in Fig. 1.1. The locomotor CPG is a neural circuit (or group of circuits) that is capable of producing motor neuron activity appropriate for locomotion even in the absence of descending input from the brain or sensory feedback (Marder and Calabrese, 1996). The locomotor CPG has been conserved across hundreds of millions of years of vertebrate evolution (Fig. 1.1), which suggests three things. First, the spinal locomotor CPG is indispensable for vertebrate survival. Second, the spinal circuits that drive locomotion may have common features across all vertebrates. Third, because the locomotor CPG has been modified to accommodate the unique behaviors of each animal, understanding which neuronal mechanisms are shared across CPGs and the role of these neuronal mechanisms in producing patterned motor output may provide insight into the fundamental computations that neural networks perform.

Conservation of CPG Neuronal Types Between Swimming Animals

While an extremely wide variety of vertebrates have a spinal locomotor CPG, the neural circuit that drives the rhythm and pattern of motor output is unknown or incompletely characterized in most animals (Guertin, 2009). Two vertebrates with well characterized locomotor CPGs are lampreys (several species including

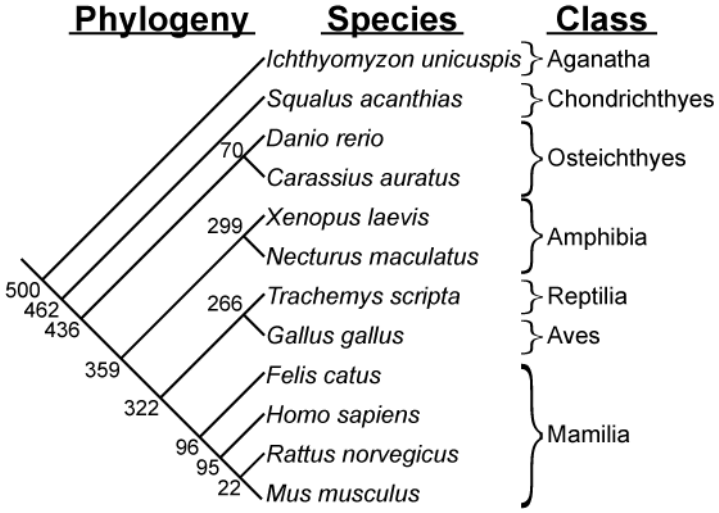

Figure 1.1 – Diversity of vertebrates with experimentally characterized spinal locomotor CPGs. *Left:* A cladeogram of selected vertebrates with published documentation of a spinal locomotor CPG. Numbers at each branch of the cladeogram indicate estimated time since the last common ancestor, in units of millions of years ago. Divergence time of Danio and Carassius is an upper bound based on Broughton et al. (2013), all other divergence times are the median estimate of TimeTree (Hedges et al., 2006). *Center:* Scientific name of species with documented CPG. Publications documenting each CPG are as follows: *Ichthyomyzon unicuspis* (lamprey): (Cohen and Wallen, 1980), *Squalus acanthias* (spiny dogfish): (Grillner et al., 1976), *Danio rerio* (zebrafish): (McDearmid and Drapeau, 2006), *Carassius auratus* (goldfish): (Fetcho and Svoboda, 1993), *Xenopus laevis* (frog): (Roberts et al., 1981), *Necturus maculatus* (mudpuppy): (Wheatley et al., 1992), *Trachemys scripta* (turtle): (Stein, 1978), *Gallus gallus* (chicken): (Jacobson and Hollyday, 1982), *Felis catus* (cat): (Miller and van der Meché, 1976), *Homo sapiens* (human): (Dimitrijevic et al., 1998), *Rattus norvegicus* (rat): (Cazalets et al., 1992), *Mus musculus* (mouse): (Jiang et al., 1999). *Right:* Class level divisions of the species in center column.

Ichthyomyzon unicuspis) and tadpoles (*Xenopus laevis*). These animals both swim using axial muscles to produce lateral undulation (Roberts et al., 1981; Williams et al., 1989). The similarity in the motor output is mirrored by similarities in the neuronal mechanisms of their CPGs (Table 1.1). In both animals, cholinergic motor neurons and glutamatergic sensory neurons are distributed across the rostrocaudal axis of the spinal cord (Roberts et al., 1998; Buchanan, 2001). The locomotor rhythm is generated by excitatory interneurons with

Table 1.1 – Homologous neurons in the tadpole and lamprey spinal cords

Neuron Name		*Transmitter*	*Morphology*	*Function*
Tadpole	*Lamprey*			
dIN	eIN	Glutamate	Ipsilateral, descending	Pre-motor excitation, network oscillator
cIN	iCC	Glycine	Commissural, descending	Contralateral inhibition of the excitatory network and motor neurons
aIN	LIN	Glycine	Ipsilateral, descending (aIN also have an ascending process)	Ipsilateral feed-forward inhibition of the CPG
Motor Neuron		ACh	Projection into ventral root	Excitation of muscle fibers
Rohon Beard	Dorsal Cells	Glutamate	Dorsal, ascending and descending	Sensory neuron
Kolmer Agduhr	Edge Cells	GABA	Contact the cerebrospinal fluid	Putative intra-spinal stretch receptors

Evidence supporting these descriptions is provided in the text. Descending neurons project caudally, ascending neurons project rostrally.

ipsilateral, caudally projecting axons that produce network oscillation through reciprocal connections (Cangiano and Grillner, 2005; Roberts et al., 2010). These ipsilateral excitatory neurons make direct synaptic connections with motor neurons and provide rhythmic synaptic drive (Buchanan and Grillner, 1987; Buchanan et al., 1989; Li et al., 2006; Sautois et al., 2007). Both CPGs also feature contralateral inhibitory connections that enforce side-to-side alternation (Buchanan, 1982; Dale, 1985). Both circuits also feature ipsilateral feed-forward inhibition, but this feature may be more important to rhythmicity in lamprey than in tadpole (Buchanan, 2001; Li et al., 2004). The lamprey spinal neurons without clear tadpole counterparts, such as giant interneurons, are only weakly active during swimming (Buchanan, 2001). Similarly, while the primary sensory neurons are similar in tadpole and lamprey, the sensory interneurons of the tadpole do not have clear lamprey homologs (Roberts et al., 1998; Buchanan, 2001). These differences show that spinal circuits were not completely unchanged following the divergence of tadpoles and lamprey but, remarkably, all of the interneurons that strongly participate in the generation of the locomotor pattern have morphological homologs in both species.

Weaknesses in the Homology Between Lamprey and Tadpole CPG Interneurons

A weakness of the comparison between lamprey and tadpole spinal neurons is that the developmental patterning of the neurons is not known in either animal, in part because most CPG neurons have not been labeled transgenically in either species (with some exceptions, e.g. Li W-C, et al. (2004)). Because of this, it is

possible that the similarity between lamprey and tadpole CPG interneurons is an example of convergence rather than conservation. Convergent evolution of locomotor circuits is hypothesized to explain similarities between leech and lamprey locomotion and locomotor circuits (Mullins et al., 2011), similar evolutionary pressures may have driven convergence between lamprey and tadpole locomotor systems. Convergent interneuron circuits that produce the same behavior (axial undulation) are interesting from the perspective of bio-mimetic design (Herrero-Carrón et al., 2011), but not informative for finding conserved elements of vertebrate CPGs.

Differences in Models of Higher Level Organization of Lamprey and Tadpole locomotor CPGs

There are strong homologies between the interneurons that drive the locomotor CPGs of lamprey and tadpole in both morphology and function, but the models of how these simple circuits are assembled into a spinal cord-wide network differ radically between the species. The lamprey literature is generally organized around a model in which each spinal segment (a section of spinal cord covered by a vertebra and innervating a single ventral root) contains an oscillator circuit (Buchanan, 2001; Grillner, 2006). Bilateral alternation is driven by intra-segmental commissural inhibition (presumably from iCC interneurons). The rostrocaudal delay in motor output necessary for undulation is modeled as the result of each spinal segment having slightly lower excitability than its rostral neighbor (Grillner and Wallen, 2002). In contrast, the tadpole literature has united

around a model in which the spinal interneurons are a continuous network with spatial gradients of connectivity that produce a rostrocaudal pattern of motor neuron activation (Wolf et al., 2009; Roberts et al., 2014). Both models produce motor output appropriate to the locomotor swim pattern in quantitative simulations (Matsushima and Grillner, 1990; Grillner and Wallen, 2002; Wolf et al., 2009). While there are substantial differences between the models, the models of the spinal circuits may differ more than the spinal circuits themselves. The lamprey spinal locomotor network can be modeled as a collection of interneurons without segmental boundaries, and it is unclear if the segmental hypothesis reflects the fundamental organization of the lamprey spinal cord or if it is an “accurate enough” simplification of the true neural circuit (Wallén et al., 1985; Wadden et al., 1997).

Lack of Homology Between Axial and Limbed Locomotor CPGs

Compared with the detailed networks of interneurons that have been characterized in lamprey and tadpole, the characterization of interneuron activity driving limbed locomotion is relatively immature (Stepien and Arber, 2008; Goulding, 2009). While significant work on the properties of the locomotor CPG has been performed in turtle (Stein, 2008) and cat (Jankowska, 2008), characterization of morphologically and/or genetically defined interneuron populations has been performed almost exclusively in rats and mice. The characterized interneuronal types are summarized in Table 1.2. Unlike the close

homology between the tadpole and lamprey interneurons, there is no obvious homology between the interneurons that compose limbed and non-limbed CPGs.

One potential explanation for this lack of homology is that limbed CPGs are fundamentally different from axial locomotor CPGs. This explanation removes the burden of bridging the gap between spinal locomotor CPGs across species, but does not account for ubiquity of spinal locomotor CPGs in vertebrates (Figure 1.1). If the tetrapod, and specifically mouse, locomotor CPG does not share homology with axial CPGs, one would expect that there was a transitional period during the development of limbed morphology when animals had limbs but not the mouse-like CPG, or a mouse-like CPG but no limbs. It is possible to apply this reading of the data to the salamander CPG, which has a mixture of axial-like and limbed-like properties (Charrier and Cabelguen, 2013), but the evidence to support this transition is not widespread.

An alternative explanation for the lack of apparent homology is that the conserved neuronal populations have adopted significantly different morphologies due to the rearrangement of the motor pools being driven by the CPG in swimming v. walking animals. Further complicating cross-species comparison, it is possible that functions performed by a single neuronal population in axial locomotion are driven by several specialized populations in tetrapods. In this view, Non-V2a Shox2^{+} neurons in mice (Table 1.2) are candidate homologs of dINs in tadpole and eINs in lamprey (Table 1.1) because

Table 1.2 – Characterized Mouse CPG Interneurons

Name	*Gene Expression*	*Transmitter*	*Projections*	*Function*
Dmrt3	Dmrt3	Inhibitory	Commissural	Hind limb left-right alternation, flexor/extensor coordination
V0v	Dbx1, Evx1	Glutamate	Commissural	Left-right alternation during high frequency locomotor rhythm
V0d	Dbx1	Inhibitory	Commissural	Left-right alternation during low frequency locomotor rhythm
V0c	Pitx2	Ach	Ipsilateral	Modulation of motor neuron excitability
Renshaw cells	En1	Inhibitory	Ipsilateral	Recurrent inhibition of motor neurons
Ia inter-neurons	En1	Inhibitory	Ipsilateral	Inhibition of antagonist muscle group
V1	En1	Inhibitory	Ipsilateral	Regulation of the frequency of the locomotor rhythm
V2b	Gata2/3	Inhibitory	Ipsilateral	Flexor/extensor alternation
$Shox2^{+}$ V2a	Chx10,Shox2	Glutamate	Ipsilateral	Burst robustness
Shox2	Shox2	Glutamate	Ipsilateral	Rhythm generation
V2a	Chx10	Glutamate	Ipsilateral	Left-right alternation during high frequency locomotor rhythm
V3	Sim1	Glutamate	Commissural	Burst robustness, left-right alternation

Support for interneuron descriptions: *Dmrt3:* (Andersson et al., 2012), *V0v:* (Lanuza et al., 2004; Grossmann et al., 2010; Talpalar et al., 2013), *V0d:* (Lanuza et al., 2004; Talpalar et al., 2013), *V0c:* (Zagoraiou et al., 2009), *Renshaw cells and Ia interneurons:* (Sapir et al., 2004; Talpalar et al., 2011), *V1*: (Sapir et al., 2004; Gosgnach et al., 2006), *V2b:* (Zhang et al., 2014), *$Shox2^{+}$ V2a and Shox2:* (Dougherty et al., 2013), *V2a:* (Crone et al., 2008, 2009; Dougherty and Kiehn, 2010; Dougherty et al., 2013), *V3:* (Zhang et al., 2008; Rabe et al., 2009; Rabe Bernhardt et al., 2012)

they are all excitatory interneurons that make reciprocal connections and support rhythm generation (Cangiano and Grillner, 2005; Roberts et al., 2010; Dougherty et al., 2013). The logic of this approach risks circularity: the CPG interneurons are assumed to have cross-species homologs, so neurons are sorted into *ad-hoc* homologous categories, which is then interpreted as evidence for homologous CPG interneurons. A less problematic strategy would be to use a feature with quantifiable homology to group neurons across species, and compare the function of these independently classified homolog neuronal populations. One promising feature that could be used to define neuronal populations is developmental gene expression (the basis of the V0,1,2,3 nomenclature used in Table 1.2 (Stepien and Arber, 2008)). Gene expression has several desirable qualities: Gene sequences provide a direct measure of conservation, gene expression profiles can be combined to increase the specificity of the neuronal sub-populations, and gene expression profiles can be used to design transgenic animals that label the same neuronal population *in vivo* across species (Suster et al., 2009). While the transgenic tools are available to perform these experiments in mice (Grossmann et al., 2010), comparable tools are not available in lamprey or tadpole. It would therefore be desirable to compare mouse interneurons with the interneurons of a transgenically tractable, axially locomoting animal.

The Larval Zebrafish as a Model of the Locomotor CPG

Compared with the tadpole and lamprey, the larval *Danio rerio* (zebrafish) is a newcomer to the study of spinal locomotor CPGs. The first whole cell recordings

from spinal neurons (Drapeau et al., 1999) and peripheral nerve recordings of fictive swimming (Masino and Fetcho, 2005) were both published in the last 15 years. Despite this relatively short history, recent work has demonstrated that the larval zebrafish is a powerful model organism for the study of locomotor circuits (Higashijima et al., 2004a; McLean et al., 2007; Liao and Fetcho, 2008; Pietri et al., 2009; Koyama et al., 2011; Eklöf-Ljunggren et al., 2012; Bagnall and McLean, 2014; Ljunggren et al., 2014). Both the interest in zebrafish spinal circuits and the speed of the progress are due to the advantages of larval zebrafish as a model organism: (1) Zebrafish breed regularly and produce over 100 embryos per mating (Westerfield, 2007), (2) Zebrafish embryos develop rapidly into free swimming larvae with coordinated swimming and hunting behavior as early as 4 days post fertilization (dpf) (Fuiman and Webb, 1988; Borla et al., 2002; Drapeau et al., 2002), (3) Zebrafish are ideal for high-throughput behavioral pharmacology because of the ease of collecting large numbers of animals, their small size, and their cutaneous permeability to small molecules (Rihel and Schier, 2012), (4) The genome of the zebrafish is well annotated, and sophisticated tools are available for generating transgenic animals (Kwan et al., 2007), (5) Zebrafish larvae are optically transparent, making it straightforward to perform whole mount, *in vivo* calcium imaging, optogenetics, and fluorescently targeted whole cell patch clamp (Higashijima et al., 2003; Liao and Fetcho, 2008; Arrenberg et al., 2009). These properties make larval zebrafish an ideal bridge to compare the interneurons of an axial locomotor CPG with the interneurons of the tetrapod mouse locomotor CPG.

Known Neuronal Types in the Larval Zebrafish Swimming CPG

Neural circuits for several motor behaviors are present in the larval zebrafish spinal cord, including swimming, struggle, and escape. Some interneurons are multi-functional and active during multiple behaviors (Liao and Fetcho, 2008), while others are only active during one behavior (Satou et al., 2009). Forward swimming is the predominant form of locomotion for larval zebrafish and the most comparable to other species (Fuiman and Webb, 1988), so I will focus on interneurons involved in this behavior. Characterization of the interneurons that make up the larval zebrafish swimming CPG can be divided into roughly two eras. Initially, neurons were characterized based on size and morphology via backfills of fluorescent dye (Hale et al., 2001). These backfills were the basis for a morphology-based naming scheme for neuron populations (e.g., MCoD neurons have a **M**ultipolar **Co**mmissural **D**escending morphology; (Hale et al., 2001)). This framework of named projection neurons has been complemented and refined by transgenes targeting developmental domains of the spinal cord (Higashijima et al., 2004a; Kimura et al., 2006; Suster et al., 2009), neurotransmitter phenotype (Liao and Fetcho, 2008), or enhancer trap gene expression (Wyart et al., 2009). Neuronal populations defined using these techniques have been targeted for whole cell patch, calcium imaging, ablation, and optogenetic manipulation. Based on these experiments, several cell populations putatively involved in the larval zebrafish locomotor CPG have been identified (Table 1.3):

- *V2a Interneurons (including CiD neurons)*

The best characterized of these neuronal populations are the V2a neurons. The V2a population is defined by the expression of the *alx* gene, the zebrafish homolog of *chx10* (Kimura et al., 2006). The majority of ipsilateral, caudally projecting (descending) interneurons express V2a markers (Kimura et al., 2006), so it is not surprising that the anatomically defined CiD neurons (Hale et al., 2001) are a subset of V2a neurons (Batista et al., 2008). V2a interneurons are glutamatergic projection neurons, all of which have a long caudal (descending) axon, and a subset of which also have a shorter rostral (ascending) axon (Batista

Table 1.3 – Characterized Zebrafish Swimming CPG Interneurons

Name	*Gene Expression*	*Transmitter*	*Morphology*	*Function*	*Tadpole Homolog*
V2a	Alx (aka Chx10)	Glutamate	Ipsilateral, descending	Pre-motor excitation of fast swimming	dIN
MCoD	Dbx1/Evx2	Glutamate	Commissural, descending	Pre-motor excitation of slow swimming	???
CoBL	Dbx1 Pax2/8	Glycine	Commissural, bifurcating	Left-right alternation	cIN
Inhibitory CoSA	Glyt2	Glycine	Commissural, ascending	Unknown, but active during locomotion	???
CiA	En1/Pax2	Glycine	Ipsilateral ascending	Inhibition of sensory and motor circuits	aIN

Evidence supporting these descriptions is provided in the text.

et al., 2008; Menelaou et al., 2014). Optogenetic activation of the V2a neurons is sufficient to drive fictive locomotion (Ljunggren et al., 2014), and ablation of a subset of V2a neurons perturbs the speed and reliability of fictive motor output (Eklöf-Ljunggren et al., 2012). V2a neurons make synaptic connections with motor neurons (Kimura et al., 2006; McLean et al., 2008; Bagnall and McLean, 2014), and provide the excitatory drive for intermediate and high speed swimming (McLean et al., 2007, 2008). These features of the V2a population suggest that they may be the zebrafish homologs of tadpole dINs and lamprey eINs (Table 1.1). One key attribute of the dINs and eINs that has not yet been reported in zebrafish V2a neurons is reciprocal excitatory connections that support rhythm generation (Li et al., 2006; Soffe et al., 2009). Given the amount of effort invested in characterizing the V2a neurons in zebrafish, including the distribution of their synaptic outputs, it is somewhat surprising that this synapse has not been reported (Menelaou et al., 2014). It may be that the reciprocal connectivity found in dINs and eINs has been divided among more than one specialized neuronal population in zebrafish, and the V2a neurons form an excitatory feedback circuit with another excitatory neuronal population that has yet to be characterized.

- *MCoD neurons (a subset of V0 neurons)*

The MCoD neurons are a second population of excitatory, pre-motor projection neurons (Hale et al., 2001; McLean et al., 2008; Satou et al., 2012). MCoDs derive from the V0 neuronal progenitor domain and are positive for *dbx1* and

evx2 (Satou et al., 2012), comparable to mouse V0v neurons (Table 1.2). Unlike V0v neurons, which are active during high-speed locomotion, MCoDs are active during slow swimming (McLean et al., 2008), and are necessary for its expression (McLean et al., 2007). The MCoDs do not have a clear homolog in the tadpole swim CPG, and may be evidence for increased complexity of the swim CPG in the larval zebrafish compared with other axially locomoting animals.

- *CoBL neurons (a subset of V0 neurons)*

The CoBL neurons are commissurally projecting, inhibitory interneuron population (Hale et al., 2001; Liao and Fetcho, 2008; Satou et al., 2012). CoBL neurons are a subset of V0 neurons that are positive for *dbx1*, *pax2* and *pax8* (Ikenaga et al., 2011; Satou et al., 2012). CoBL neurons are numerous, pre-motor neurons that fire in phase with ipsilateral motor neurons and suppress contralateral motor output (Liao and Fetcho, 2008). This function is similar to the function of inhibitory V0d neurons in mice (Table 1.2), commissural inhibitory cIN neurons in tadpole and iCC neurons in lamprey (Table 1.1). The swimming pattern when CoBL neurons are specifically ablated has not been characterized because genetic knock-outs of the cell population are lethal (Ikenaga et al., 2011). A specific transgenic line is needed to perform acute optogenetic silencing experiments to confirm the necessity of CoBL neurons for side-to-side alternation.

- *Inhibitory CoSA neurons*

Inhibitory CoSA neurons are the least well characterized of the putative zebrafish swimming CPG neurons. CoSA neurons were initially identified based on morphology and developmental order (Hale et al., 2001), but further investigation revealed that there are both excitatory and inhibitory neurons with this morphology (Higashijima et al., 2004b; Liao and Fetcho, 2008). Inhibitory CoSA neurons are rhythmically active during fictive swimming (Liao and Fetcho, 2008), but their specific role in locomotion is unknown.

- *CiA / V1 neurons*

The CiA / V1 neuron population is unusual in that all of the neurons derived from the V1 developmental domain have the CiA neuron morphology (Hale et al., 2001; Higashijima et al., 2004a). Therefore, in the context of larval zebrafish the names are synonymous, but for the purposes of cross-species comparison it is more informative to refer to the population as V1 neurons. Zebrafish V1 neurons are ipsilateral projection neurons that have an ascending axon and are active in phase with ipsilateral motor output (Higashijima et al., 2004a). They inhibit sensory reflex pathways during swimming, and provide phasic inhibition to motor neurons that may sharpen the timing of motor output (Higashijima et al., 2004a). Engrailed 1 (en1) expression can be measured in both larval zebrafish and tadpole (Higashijima et al., 2004a; Li et al., 2004), allowing confident identification of aIN neurons in tadpole as the homolog of zebrafish V1 neurons (Table 1.1). Mouse V1 neurons regulate locomotor speed (Table 1.2), but tadpole

V1 neurons have a minimal effect on rhythm generating neurons (Li and Moult, 2012), so cross-species homology does not allow a confident prediction of the functional role of zebrafish V1 neurons.

- *Summary*

While there is a significant amount known about the interneurons that compose the larval zebrafish swimming CPG, there is not a critical mass of cell types and synaptic connections to draw a reasonable CPG circuit diagram. Homology of structure and putative function of zebrafish and tadpole interneurons would suggest that the core elements of the zebrafish CPG have been identified (Table 1.1,1.3). However, zebrafish CPG neurons have been found that have no tadpole homolog (e.g., MCoDs), so it is possible that there are additional interneurons that are essential to locomotion in larval zebrafish but not found in tadpole.

Gaps in the Knowledge of the Larval Zebrafish Locomotor CPG

While significant progress has been made in the characterization of larval zebrafish interneurons, there are fundamental barriers to using these neurons to build a model of the swimming CPG.

One fundamental barrier is that there has not been a clearly articulated higher-level organization proposed for the larval zebrafish CPG. It is also not obvious what kind of higher level organization to propose based on the organization of other axially locomoting animals. The commonly held models of the lamprey and

tadpole CPGs are radically different; one is modeled as a series of segmental oscillators and the other as a continuous gradient (Grillner, 2006; Wolf et al., 2009). While some papers explicitly diagram (Severi et al., 2014), or describe (Charrier and Cabelguen, 2013) the larval zebrafish swimming CPG as a series of oscillators, the segmental model has not been carefully tested in larval zebrafish (but see McDearmid and Drapeau (2006)).

A second fundamental barrier is the lack of matching between interneurons and the features of zebrafish locomotion, or even a clear identification of the relevant features that need to be explained. There is evidence that different populations of excitatory pre-motor neurons are necessary to drive different frequencies of motor output (McLean et al., 2007, 2008; Eklöf-Ljunggren et al., 2012), but there is no clear hypothesis describing how these neurons are recruited. There is evidence that the spinal cord requires continuous drive to maintain motor output (Arrenberg et al., 2009; Kimura et al., 2013), and there is evidence that the spinal cord is capable of terminating motor output (McDearmid and Drapeau, 2006; Lambert et al., 2012), but there is no clear hypothesis for how swimming is terminated at the spinal level. There is evidence that rostrocaudal delay is actively regulated to keep the phase offset between segments constant across locomotor speeds (Masino and Fetcho, 2005), but there is no clear hypothesis for how rostrocaudal delay is set up and regulated.

The goal of this thesis is to attempt to address some of these fundamental barriers. In Chapter 2, I will present experimental work exploring the higher level organization of the larval zebrafish spinal cord as it relates to the production and termination of episodes of swimming. In Chapter 3, I will present similar work addressing the organization of the spinal cord as it relates to the production of rostrocaudal delay and side-to-side alternation. In Chapter 4, I will present preliminary work characterizing an excitatory interneuron population (V3 neurons) that may participate in locomotion, and may be necessary for speed dependent neuronal recruitment. Finally, in Chapter 5, I will describe how these results integrate with what is known about larval zebrafish locomotor circuits, and describe future directions for this research.

CHAPTER 2: ROSTRAL BIAS IN EPISODE GENERATION, AND FUNCTIONAL DISSOCIATION OF EPISODE GENERATION AND COORDINATION IN THE ZEBRAFISH SPINAL CPG

INTRODUCTION

Central pattern generators (CPGs) are neural circuits capable of producing a patterned motor output even in the absence of a patterned input (Marder and Calabrese, 1996). The spinal cord contains a CPG or CPGs that are important to the production of locomotion (Grillner, 2006). Despite the diverse methods vertebrates use for locomotion, there is evidence that components of the CPG are conserved across species (Grillner and Jessell, 2009; Kiehn, 2011). Larval zebrafish are an attractive species for studying motor systems (Fetcho and Liu, 1998; Fetcho, 2007; McLean and Fetcho, 2011). While the neuronal circuits for some motor behaviors such as escape (O'Malley et al., 1996; Satou et al., 2009; Koyama et al., 2011) and early touch response (Downes and Granato, 2006; Pietri et al., 2009) have been characterized, the CPG circuits that control swimming in larval zebrafish are less well characterized (Kimura et al., 2006; McLean et al., 2008; Eklöf-Ljunggren et al., 2012).

Zebrafish begin swimming at 3 days post fertilization (dpf) (Fuiman and Webb, 1988; Buss and Drapeau, 2001; Muller and Von Leeuwen, 2004) and perform infrequent episodes of locomotion that last several seconds (Buss and Drapeau, 2001). Later, at 4 dpf, larvae transition to perform more frequent but shorter

episodes of locomotor activity, sometimes described as a “beat and glide” pattern (Buss and Drapeau, 2001). The muscle contractions within these swimming episodes, in both swimming behaviors, are timed to alternate side-to-side and have rostrocaudal progression (Batty, 1984; Borla et al., 2002), which we collectively refer to as “coordination.” Similarly, paralyzed preparations of larval zebrafish produce episodes of peripheral nerve activity indicative of motor neuron firing (Masino and Fetcho, 2005). Within episodes, peripheral nerve activity is organized into discrete bursts that have the same coordinated pattern as trunk flexions in free swimming zebrafish larvae (Masino and Fetcho, 2005), similar to the correspondence between fictive and real behavior in several other swimming vertebrates (Grillner, 1974; Cohen and Wallen, 1980; Kahn and Roberts, 1982; Fetcho and Svoboda, 1993). Normal swimming in larval zebrafish at 4 dpf and later, both real and fictive, is defined by episodic organization and coordination.

When mapping a CPG, it is helpful to know the distribution of its neuronal components. One approach to characterizing the distribution of these CPG components is through the use of lesions (Ho and O’Donovan, 1993; Kjaerulff and Kiehn, 1996). There are two benefits to this approach. First, locomotor functions produced by spatially distinct neuronal circuits can be dissociated. Sagittal sections of the spinal cord have been used in several species to demonstrate that the locomotor rhythm does not depend upon connections that cross the midline (Kahn and Roberts, 1982; Kjaerulff and Kiehn, 1996; Cangiano and Grillner, 2003). Second, lesions can be used to simplify the system being

studied. Horizontal transections of the spinal cord have localized the CPG to the ventral spinal cord (Kjaerulff and Kiehn, 1996). Similarly, in a CPG composed of segmentally reiterated oscillators (Matsushima and Grillner, 1990), transections may allow investigation of simpler isolated oscillators.

Transections of the spinal cord produce “series” of contiguous spinal segments. Short series of spinal segments from dogfish and lamprey are sufficient to produce fictive locomotion regardless of rostrocaudal position in the spinal cord (Grillner, 1974; Cohen and Wallen, 1980). Among limbed vertebrates, the bulk of the locomotor circuits are located in the spinal limb enlargements. In some limbed vertebrate model systems, such as embryonic chick, there is not a strong effect of rostrocaudal position within the limb enlargement on the capacity of segments to produce the locomotor rhythm (Ho and O’Donovan, 1993). Other model systems show a strong effect of rostrocaudal position on rhythm generating capacity (Kjaerulff and Kiehn, 1996), including extreme examples where a CPG is located in one or two spinal segments (Deliagina et al., 1983; Wheatley et al., 1994). A previous report in larval zebrafish showed episodic motor neuron spiking in an isolated series of two body segments (McDearmid and Drapeau, 2006), however, the effect the of rostrocaudal position of the segments and the coordination of the pattern produced was not described. Given the differences in rostrocaudal distribution of CPG elements between species, it was our objective to characterize the rostrocaudal distribution of the swimming CPG in larval zebrafish.

We hypothesized several possible architectures for the larval zebrafish swimming CPG: 1) The CPG is composed of segmentally reiterated oscillators, 2) There is a single CPG distributed throughout the entire spinal cord, or 3) There is a single CPG located in a small region of the spinal cord. We evaluated the episodic structure and coordination of the fictive swim pattern produced by series of spinal segments of different lengths in response to N-Methyl D-Aspartate (NMDA), an activator of the larval zebrafish swimming CPG (McDearmid and Drapeau, 2006). We found that only longer series (≥12 of 33 total spinal segments) produced episodic fictive swimming, and that shorter series often produced continuous rhythmic bursting or sporadic, non-rhythmic bursting. Fewer rostral spinal segments (≥12) than caudal segments (≥23) were necessary to produce episodic swimming. We also found that the degree of coordination, that is, side-to-side alternation and rostrocaudal progression, was not different between preparations that produced episodic fictive swimming and those that produced tonic bursting. This result prompted us to propose a model of the larval zebrafish swimming CPG that separates the circuits for episode generation and coordination.

This content of this chapter has been previously published in the *Journal of Neurophysiology* (Wiggin et al., 2012).

MATERIALS AND METHODS

Animals and solutions

All procedures were approved by the Animal Care and Use Committee of the University of Minnesota Twin Cities. Wild type adult zebrafish (*Danio rerio,* Segrest Farms, Gibsonton, FL) were maintained in a zebrafish core facility. Adult zebrafish were set up to produce daily clutches of embryos with timed fertilization between 8:45 - 9:00am. Embryos and larval zebrafish were maintained in petri dishes filled with embryo water (60 µg/ml Instant Ocean® salt mix, Cincinnati, OH) in a 28.5°C incubator with a 14:10 light:dark cycle. Larval zebrafish 4 to 6 dpf were used in these studies. Chemicals and drugs were obtained from Sigma-Aldrich Chemical (St. Louis, MO), unless otherwise noted. Zebrafish Ringer's solution was composed of (in mM): 134 NaCl, 2.9 KCl, 1.2 $MgCl_2$, 2.1 $CaCl_2$, 10 HEPES buffer, 10 glucose, adjusted to pH 7.8 with NaOH (Legendre and Korn, 1994; Drapeau et al., 1999).

Procedure

The following procedure was adapted from Masino and Fetcho (2005). Zebrafish larvae were anesthetized for 5 minutes with 0.02% Tricaine-S (Western Chemical, Ferndale, WA) in Ringer's solution. For unilateral recordings, larvae were transferred to Sylgard®-lined dissecting dishes and pinned on their sides through the notochord using short pieces of fine tungsten wire (0.001" diameter). Typically, a rostral pin was placed between body segment (S) 5 and S8 and a caudal pin between S20 and S25 (Fig. 2.1A). In order to access the peripheral motor nerves and provide better perfusion access, the skin between the tungsten pins was removed using a sharp tungsten probe and fine forceps (Fine Science

Tools, Foster City, CA). For bilateral recordings, skin was removed from both sides of the larvae and the larvae were repositioned dorsal side up using additional pins to hold them in position. In order to prevent muscle contractions during recording, larvae were paralyzed using 5 µl of 0.1 mM α-bungarotoxin

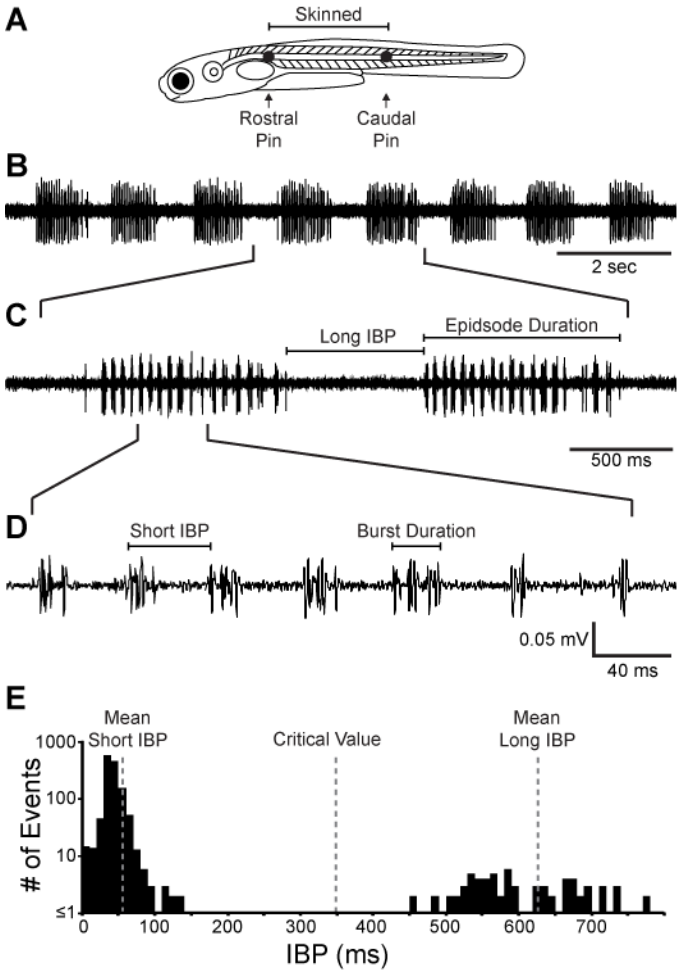

Figure 2.1 - Quantification of Episodic Organization. (A) A diagram of a typical unilateral fictive swimming preparation. Two tungsten pins (filled circles) were used to stabilize the larvae. The region between these pins was skinned. (B - D) Peripheral nerve recording from the midbody region of a spinalized zebrafish during bath application of 200 µM NMDA. (C) The episode duration and inter-episodic long IBP are indicated by horizontal lines. (D) The intra-episodic short IBP and burst duration are indicated by horizontal lines. The inverse of the IBP is the instantaneous burst frequency. (E) Histogram of IBP distribution from the representative recording in B - D. The values that were used to calculate Episodic Organization (critical value, mean short IBP and mean long IBP) are indicated by dashed vertical lines.

(Tocris, Ellisville, MO) added to the small amount (~15 µL) of Ringer's solution in the dissection dish. The larvae were kept in α-bungarotoxin for 10 minutes before superfusion with Ringer's solution began. Larvae were either left intact, spinalized (spinal cord transected at S3 in order to separate brain from spinal cord), or transected at multiple points along the body using a razor blade shard (FA-10 Feather S, Ted Pella, Redding, CA) clamped by a blade holder (Fine Science Tools, Foster City, CA). In the intact preparation, fictive swimming occurred spontaneously or was evoked by shining light on the fish. In the spinalized preparation, swimming was induced with 50 - 200 µM NMDA in Ringer's solution.

Electrophysiology

After transferring the larva to the stage of an Olympus BX51 WI microscope, (Center Valley, PA), superfusion with Ringer's solution at room temperature (21 - 25 °C) was started. Glass suction electrodes were fashioned from 1.5 mm o.d. x 1.12 mm i.d. glass tubes (A-M Systems, Sequim, WA) and pulled on a P-97 electrode puller (Sutter Instruments, Novato, CA). Electrodes were filled with Ringer's solution. Tip sizes ranged from 9 to 15 µm. The electrodes were placed in electrode holders that were inserted into headstages (50 MΩ) attached to an Axon Multiclamp 700B amplifier (Molecular Devices, Union City, CA). The electrodes were positioned over the peripheral nerves using micromanipulators (Siskiyou, Grants Pass, OR). Current clamp signals were digitized by an Axon Instruments Digidata 1440A (Molecular Devices, Union City, CA). Data were

recorded using pClamp 10 software (Molecular Devices, Union City, CA). Signals were sampled at 10 kHz and band pass filtered to 100 - 1000 Hz.

Data Analysis

Organized fictive swimming in larval zebrafish consists of motor neuron bursts clustered into episodes (Fig. 2.1B,C). A program written in Matlab (Mathworks, Natick, MA) was used to analyze episodically organized extracellular peripheral nerve voltage recordings. The program detected the presence or absence of activity at each voltage sample *(v(n))*. For each *v(n)*, the algorithm determined a voltage autocorrelation ($c_n(k)$) over a small window (3 ms) centered at *v(n)*. These "windowed" autocorrelations were computed as

$c_n(k)=\sum_{i=-N_0}^{i=N_0} v(n-i)v(n-i-k)$ (*Eq. 1*), where 3 ms windowing was implemented in *Eq. 1* by setting $N_0 = (3\text{ ms} * f_{sam})/2$, where f_{sam} is the sampling frequency, and by setting $v(j) = 0$ for j outside the interval $[n-N_0, n+N_0]$.

A subset of the autocorrelation values (lags) from *Eq. 1* were used to compute a test-statistic for each *v(n)* with the same lags ($\vec{k}_0 = [k_1, k_2, \ldots, k_m]$) used for all voltage samples. Building on *Eq. 1*, for each *v(n)*, a test-statistic c_n was computed as $c_n=\sum_{k=k_1}^{k=k_m}\sum_{i=-N_0}^{i=N_0} v(n-i)v(n-i-k)$, (*Eq. 2*), where *Eq. 2* is the sum of the $c_n(k)$ from *Eq.1* specified by $\vec{k}_0$. k was set at k = [1,2] because we found that these values effectively separate the distributions of the test statistics $\{c_n\}$ for

samples of noise and samples of activity across a broad range of recording quality.

Finally, activity was considered present at $v(n)$ only when c_n was greater than a detection threshold T. T was set as the maximum of a set of $\{c_n\}$ corresponding to the $\{v(n)\}$ in one contiguous second of the voltage recording where activity was confirmed to be absent (typically the first second of the recording), and was set this way for each individual voltage recording to account for differences in baseline noise levels. Fictive locomotor bursts were detected, grouped into episodes and the burst and episode properties were determined as follows: Episode duration is the time from the onset of the first burst of an episode to the offset of the final burst in the same episode (Fig. 2.1C). Burst duration is the time from the onset to the offset of each burst, as defined by c_n and described above (Fig. 2.1D). Burst frequency is the inverse of the inter-burst period (IBP), which is defined for each pair of bursts within episodes as the time from the onset of the first burst to the onset of the second burst (Fig. 2.1D). IBPs between episodes (Fig. 2.1C) are excluded from burst frequency analysis. Rostrocaudal delay per body segment is the time between the onset of each burst in the more rostral recording and the onset of the corresponding burst in the more caudal recording divided by the number of intervening body segments. Contralateral phase is measured on a cycle by cycle basis as the time between the onset of each burst

on the left and each corresponding burst on the right divided by the IBP of the left.

Because non-episodic swimming could not be processed using our Matlab program, the rostrocaudal delay and contralateral phase of non-episodically organized swimming was quantified using auto- and cross-correlation (Fig. 2.7). Signals were processed using python and the scipy signal library (http://www.scipy.org/) to rectify and low pass filter the signal to 90 Hz. Rostrocaudal delay was defined as the time of peak cross-correlation between the rostral and caudal signals (Fig. 2.7E). Rostrocaudal delay was normalized to the number of body segments separating the recording locations. Cross-correlation derived IBP was defined as the time of peak auto-correlation from 10 - 200 ms, and was converted to frequency by taking the reciprocal (Fig. 2.7C). Contralateral offset was defined as the average of the time of highest cross-correlation greater than zero and the absolute value of the time of the highest peak less than zero (Fig. 2.7G). Contralateral phase was defined as the contralateral offset divided by the IBP and expressed as a percentage.

Episodic Organization

In order to evaluate the degree to which the episodic structure of normal zebrafish locomotion was perturbed in these experiments, we developed a tool to quantify the degree of episodic organization (EO) of bursting. Because our Matlab program could not reliably identify bursts in non-episodically organized

recordings, Clampfit (Molecular Devices) was used to detect bursts using a voltage threshold. Because many bursts crossed the threshold multiple times, crossings with an inter-event period of less than 15 ms were grouped into a single burst. The 15 ms threshold was chosen based on our observation that in these recordings most crossings within a burst occur within 12ms and most inter-burst intervals are greater than 30ms. In normal swimming, the inter-episode interval is much longer than the intra-episode burst period. In order to separate "long" IBPs (inter-episode like) from "short" IBPs (intra-episode like), we defined a critical value for separating the IBPs into short and long as the mean of all IBPs plus two standard deviations (Fig. 2.1E). The means of the short and long IBPs were then calculated. EO is defined as the $\log_{10}$ ratio of the mean long IBP to the mean short IBP. To enhance readability, the EOs of spinalized and transected larvae are reported as a percentage of the EO of fictive swimming in spinalized larvae at the same NMDA concentration.

Statistical Analysis

For the comparisons between intact and NMDA induced fictive swimming along the rostrocaudal axis, data were analyzed using a 2 (intact, spinalized NMDA) x 3 (rostral, midbody, caudal) independent groups factorial design. All other tests were single factor, independent group designs. Tests for significance were carried out using one and two way ANOVAs and subsequent protected t-tests, or two tailed t-tests using SYSTAT software (Sigma Plot, San Jose, CA). The Pearson's correlation coefficient was calculated using R (http://www.r-

project.org/). Data with a $p < 0.05$ were accepted as statistically significant. Data are expressed as mean with SD.

RESULTS

The Larval Zebrafish Spinal Cord Produces Fictive Swimming Throughout its Rostrocaudal Extent

In order to determine the baseline bursting activity at points along the rostrocaudal axis of the spinal cord, we measured motor neuron bursts during fictive swimming in intact and spinalized larval zebrafish. Spontaneous fictive swimming episodes were recorded from intact larvae (*n* = 21 peripheral nerves, 3 larvae), and NMDA (50 μM) induced fictive swimming was recorded in spinalized larvae, that is, larvae with a spinal transection at body segment 3 (*n* = 37 peripheral nerves, 17 larvae; Fig. 2.2A). Series of contiguous spinal segments will be referred to by the body segment of the rostral and caudal boundaries; e.g., a spinalized zebrafish is referred to as S3-33.

Both spontaneous (intact) and chemically-evoked (spinalized) swimming consists of episodes (Fig. 2.1B) that are composed of high frequency bursts (Fig. 2.1C,D). In both intact and spinalized larvae, peripheral nerves along the rostrocaudal extent of the spinal cord produced episodes of fictive swimming. In order to compare the motor output produced by different regions of the spinal cord, we grouped the data into three anatomical divisions: rostral (S1 to S10), midbody (S11 to S20) and caudal (S21 to 33). There were statistically significant

differences in episode duration, burst duration and burst frequency between spontaneous (intact) and chemically-evoked (spinalized) fictive swimming (all $F > 6.8$, all $p < 0.01$; Fig. 2.2B-D). In intact larvae, there were no significant differences in the episode duration (Table 2.1, all $t < 0.01$, all $p > 0.99$), burst duration (Table 2.1, all $t < 0.88$, $p > 0.38$), or burst frequency (Table 2.1, all $t <$

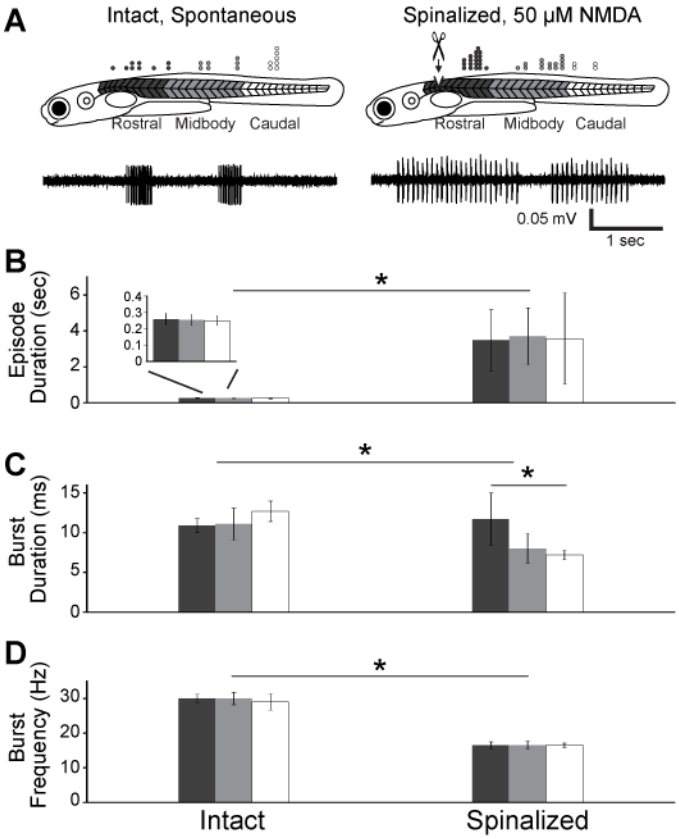

Figure 2.2 - Fictive swimming is produced throughout the rostrocaudal extent of the spinal cord. (A) Diagrams of larval zebrafish illustrating the design of the experiment. Recordings were performed in intact larvae (left) and spinalized larvae (right). The body of the larvae is divided into three regions: rostral (dark grey), midbody (light grey) and caudal (white). Circles above the illustration indicate location and number of recordings. Representative traces of spontaneous (intact) and chemically-evoked (spinalized) fictive swimming recorded in the midbody region are below the respective diagrams. (B-D) Plots of episode duration (B), burst duration (C) and burst frequency (D) against recording location and preparation type: rostral, midbody and caudal; intact (left) and spinalized (right). * Statistically significant difference.

0.71, all p > 0.57) along the rostrocaudal axis (Fig. 2.2B-D, left). In spinalized larvae, there were no significant differences in the episode duration (Table 1, all t < 0.39, all p > 0.7), or burst frequency (Table 2.1, all t < 0.07, all p > 0.95) along the rostrocaudal axis (Fig. 2.2 B,D, right), but the burst duration was significantly longer in the rostral region than in the midbody or caudal regions (Table 2.1, t > 3.2 , p < 0.002; Fig. 2.2C, right).

Table 2.1 – Properties of Fictive Swimming along the Rostrocaudal axis

Preparation	*Recording Location*	*Episode Duration (ms)*	*Burst Duration (ms)*	*Burst Frequency (Hz)*
Intact, Spontaneous	Rostral	257 (34)	10.9 (0.89)	30 (1.2)
	Midbody	254 (30)	11.1 (2.0)	30 (1.8)
	Caudal	250 (28)	12.7 (1.3)	29 (2.3)
Spinalized, 50 μM NMDA	Rostral	3,484 (1,694)	11.7 (0.58)	16.5 (1.0)
	Midbody	3,707 (1,575)	8.0 (0.67)	16.5 (1.1)
	Caudal	3,575 (2,554)	7.2 (1.3)	16.5 (0.6)

Values are means (SD)

Fictive Swimming Characteristics Vary with NMDA Concentration

To determine the effect of NMDA concentration on the properties of fictive swimming, we recorded activity from peripheral nerves in spinalized larvae (*n* = 6) at three concentrations of NMDA: 50, 100 & 200 μM (Fig. 2.3). Because the burst duration of NMDA-induced fictive swimming differs along the rostrocaudal axis (Fig. 2.2) and to simplify our analysis, all recordings were performed in the midbody region due to its relative accessibility. Episodic fictive swimming was

observed at all three NMDA concentrations (Fig. 3A). Increasing NMDA concentration significantly decreased episode duration (Table 2.2, $F = 20.3$, $p < 0.001$; Fig. 2.3B). Increasing NMDA concentration also significantly increased the number of episodes produced per minute (Table 2.2, $F = 28.8$, $p < 0.001$; Fig. 2.3C). NMDA concentration did not have a significant effect on burst duration (Table 2.2, $F = 2.3$, $p = 0.13$; Fig. 2.3D), but increased burst frequency at 200 μM NMDA (Table 2.2, all $t > 4.0$, all $p < 0.006$; Fig. 2.3E). To determine the independence of burst frequency and episode duration, we tested their correlation. There was a significant negative correlation between episode

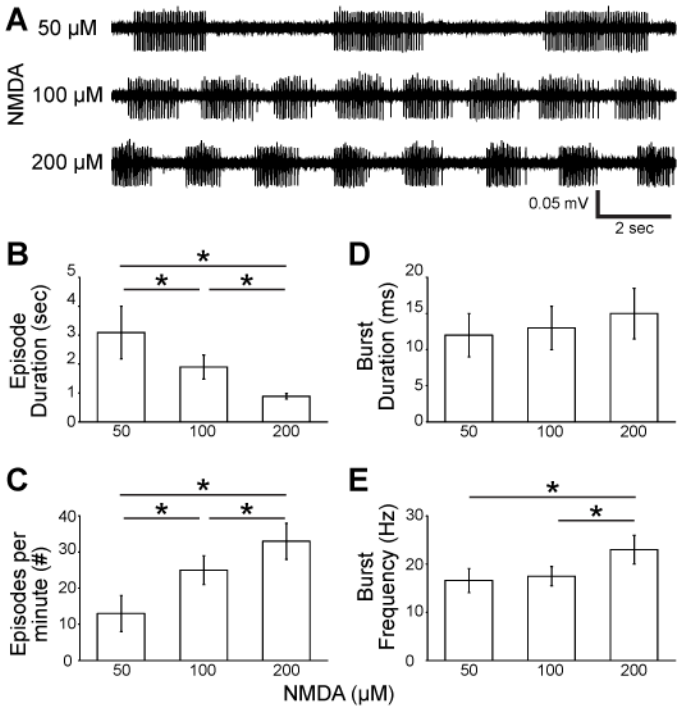

Figure 2.3 - The characteristics of fictive swimming depend on NMDA concentration. (A) Representative traces of NMDA induced fictive swimming in a spinalized larval zebrafish at 50, 100 and 200 μM NMDA. (B-E) Plots of episode duration (B), episodes per minute (C), burst duration (D) and burst frequency (E) against NMDA concentration: 50, 100 and 200 μM. * Statistically significant difference.

duration and burst frequency across NMDA concentrations (r = -0.63, t = -3.2, p = 0.006), but there was no correlation between episode duration and burst frequency across preparations within NMDA concentrations (r = 0.05, t = 0.2, p = 0.84).

Table 2.2 – Properties of Chemically Evoked Fictive Swimming in Reduced Preparations of Larval Zebrafish

Preparation	*NMDA Concentration (μM)*	*Episode Duration (ms)*	*Episodes per Minute*	*Burst Duration (ms)*	*Burst Frequency (Hz)*
S3-33	50	3,150 (952)	12 (4.6)	11.2 (1.2)	15 (1.4)
	100	1,950 (459)	24 (4.2)	12.0 (1.9)	16 (1.2)
	200	898 (87)	33 (5.1)	13.8 (3.0)	21 (2.7)
S10-33	200	1,130 (372)	n.d.	10.6 (1.1)	19.5 (5.8)
S3-15	200	1,425 (386)	n.d.	8.9 (1.4)	18.3 (4.0)
S8-20	200	1,087 (412)	n.d.	9.8 (4.8)	16.3 (4.0)

Values are means (SD), n.d. = not determined

Series of Contiguous Spinal Segments Retain the Ability to Produce Fictive Swimming Following Spinal Transection

To characterize the rostrocaudal distribution of the spinal locomotor circuit in spinalized (S3 transection) larval zebrafish, we performed a series of spinal transections at S8, S10, S15 or S20, dividing the spinal cord into series of spinal segments of different lengths. In all spinalized larvae with an additional spinal transection, episodically organized bursting was no longer observed at 50 μM NMDA (*n* = 24; Fig 2.4B-D). When the NMDA concentration was increased to

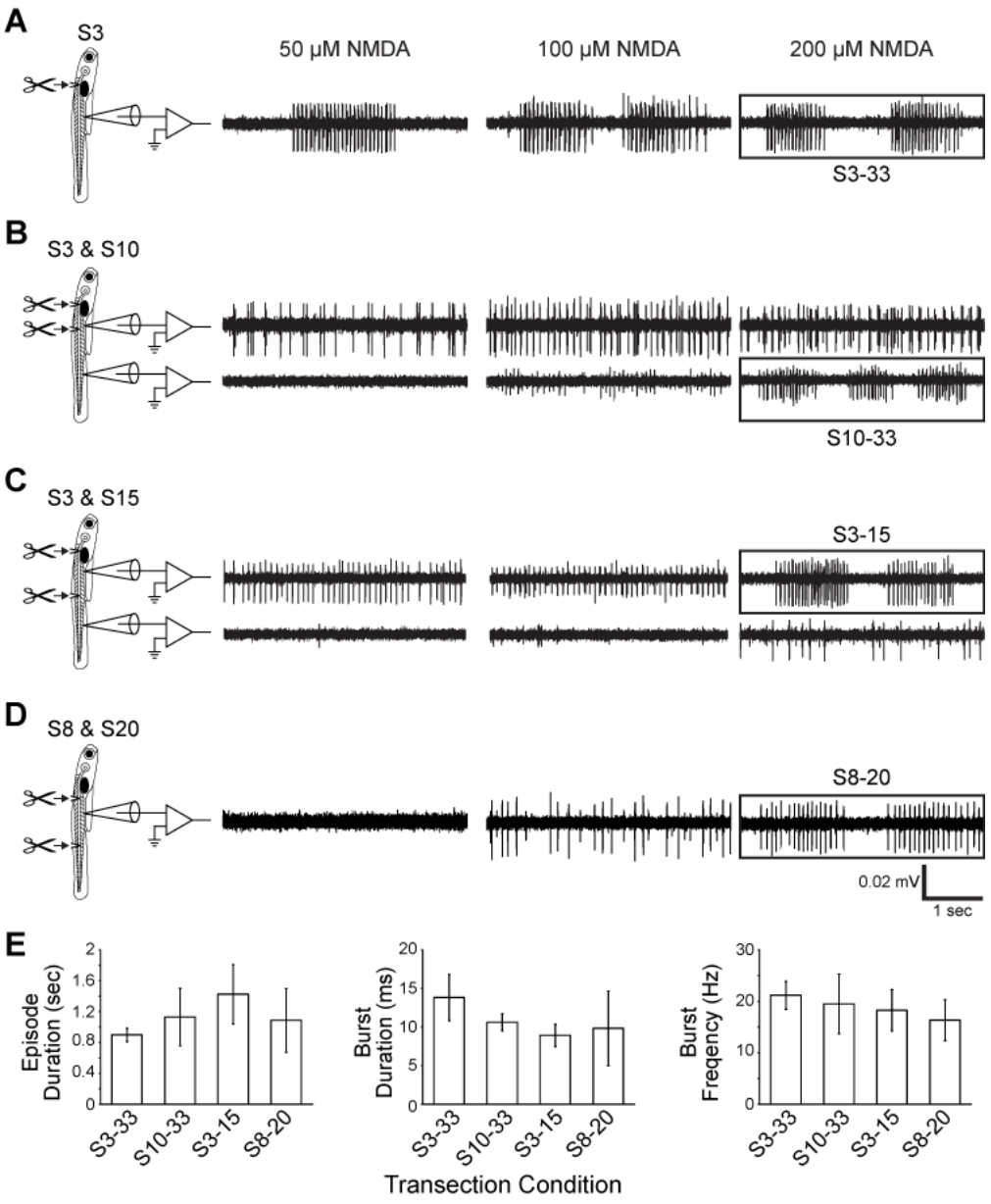

Figure 2.4 - The length and location of contiguous segments determines the episodic nature of NMDA induced fictive swimming. (A-D) Representative traces illustrating the typical fictive motor output from each contiguous spinal region. Chemically-induced fictive locomotor activity in is shown at 50, 100 and 200 µM NMDA. A black box indicates experimental conditions that produce episodically organized fictive swimming that is quantified in panel E. (A) Fictive swimming activity produced by a spinalized larva. (B) Activity from S3-10 (top trace) and S10-30 (bottom trace). C) Activity from S3-15 (top trace) and S15-33 (bottom trace). (D) Activity from S8-20. (E) Plots of episode duration (left), burst duration (middle) and burst frequency (right) against the series of contiguous spinal segments producing fictive swimming.

200 μM, some of the series of contiguous spinal segments produced episodically organized bursting (Fig. 2.4B-D). In spinalized larvae transected at S10 (*n* = 5; Fig. 2.4B), the caudal portion of the spinal cord (S10-33) produced normal, episodically organized bursting, while the rostral portion of the spinal cord (S3-10) produced regular, non-episodic bursting. In spinalized larvae transected at S15 (*n* = 5; Fig. 2.4C), the rostral portion of the spinal cord (S3-15) produced episodically organized bursting, while the caudal portion (S15-33) produced low frequency, sporadic bursting. In larvae transected at S8 and S20 (*n* = 6; Fig. 2.4D), the midbody series (S8-20) in most (4 of 6) larvae produced episodic bursting. The fictive swimming produced showed no significant differences in episode duration (Table 2.2, F = 2.3, p = 0.12; Fig. 4E). There was a non-significant trend toward shorter burst duration in shorter series of spinal segments compared to spinalized larvae (Table 2.2, F = 3.0, p = 0.07; Fig. 2.4E). There were no significant differences in burst frequency (Table 2.2, F = 1.0, p = 0.41) among the spinalized larvae and shorter series of spinal segments at 200μM NMDA (Fig. 4E).

Rostral Spinal Segments Have Greater Capacity for Producing Episodic Fictive Swimming

To map the distribution of episode organizing capacity along the rostrocaudal extent of the spinal cord, we compared the degree of episodic organization (EO) produced by series of contiguous spinal segments by their length and location along the spinal cord. EO is a tool for quantifying the degree to which bursts are

organized into episodes (see *Methods*; Fig. 2.5A). To provide more closely matched lengths of spinal segments between rostral and caudal series, we

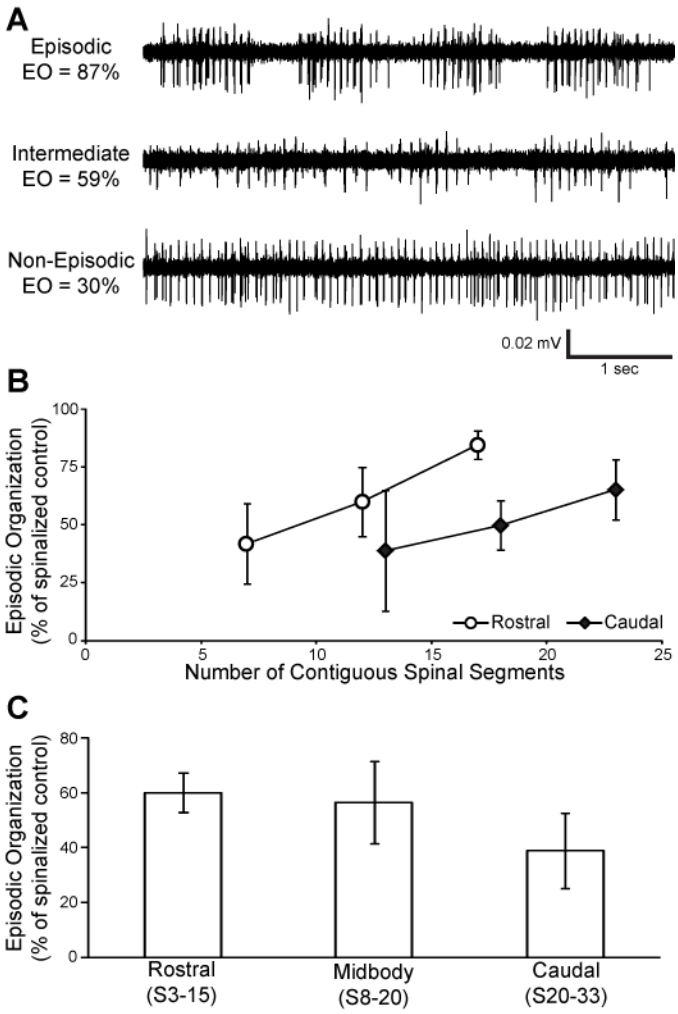

Figure 2.5 - Production of episodic fictive swimming is rostrally biased. (A) Representative traces illustrating the patterns of bursting that correspond to episodic, intermediate and non-episodic EO scores. Fictive swimming was evoked by 200 μM NMDA. (B) Plot of % EO against the length of the series of contiguous spinal segments. The length of rostral spinal regions (open circular markers) was measured from the transection at S3 to the location of a more caudal transection. The length of caudal spinal regions (filled diamond markers) was measured from the site of the midbody transection to S33. The rostral series were: S3-10, S3-15 and S3-20. The caudal series were: S10-33, S15-33 and S20-33. (C) Plot of % EO against transection type: rostral (S3-15), midbody (S8-20) or caudal (S15-30). Data were normalized to the average EO of spinalized larvae in 200 μM NMDA.

measured bursting produced by spinalized larvae additionally transected at S20 (n = 4) as well as S10 and S15 (Rostral: 7, 12 & 17 segment series; Caudal: 13, 18 & 23 segment series). Because high NMDA concentrations were more likely to produce episodic fictive swimming in all series of spinal segments, 200 μM NMDA was used for this analysis. There was a positive correlation between the number of contiguous spinal segments and EO both for the rostral series (S3-10, S3-15 and S3-20) and for the caudal series (S10-33, S15-33 and S20-33) ($r > 0.99$ for both; Fig. 2.5B). Rostral series of spinal segments produced greater EO per contiguous spinal segment than caudal series (rostral = 5.3% (SD 0.6), caudal = 2.9% (SD 0.1), $t = 7.3$, $p = 0.018$). When comparing series of contiguous spinal segments that are roughly the same length (12-13 spinal segments) but from different regions of the spinal cord, there was a trend toward the rostral spinal segments producing fictive swimming with a higher EO than the caudal spinal segments, but this trend was not statistically significant (S3-15 = 71% (SD 18), S8-20 = 66% (SD 16), S20-33 = 46% (SD 31), $F = 1.7$, $p = 0.22$; Fig. 2.5C).

Coordination of Episodically Organized Bursting in Transected Spinal Cord

To determine if bursting produced by series of contiguous spinal segments are coordinated (that is, produce side-to-side alternation and rostrocaudal progression), we performed two point recordings on spinalized and transected larvae. Quantification of delay and phase was performed using the first burst of each episode as a phase marker. Spinalized larvae produced fictive swimming

with side-to-side alternation (n = 3) and rostrocaudal progression (n = 3) in the presence of 200 μM NMDA (Fig. 2.6A). The S10-33 series, the shortest caudal series of contiguous spinal segments that produced episodically organized fictive swimming (EO = 67% (SD 13)), produced bursting with side-to-side alternation (n

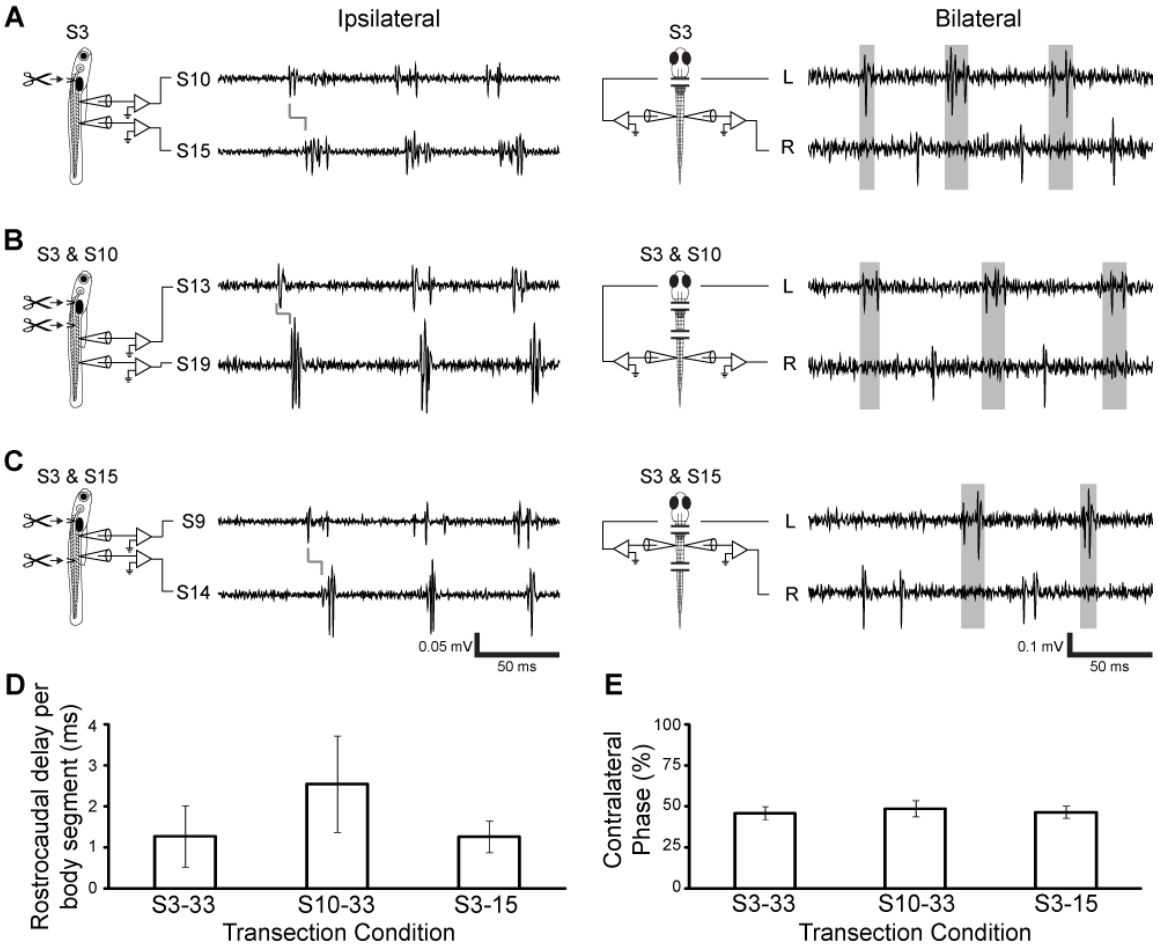

Figure 2.6 - Episodic fictive swimming is coordinated following spinal transection. (A-C) Representative traces from ipsilateral (left) and bilateral (right) two point recordings in spinalized larvae. Fictive swimming was induced by bath application of 200 μM NMDA. Rostrocaudal delay in each ipsilateral record is indicated by a gray line. The timing of bursts from the left channel of each contralateral record is indicated by a filled gray box. (A) Spinalized larvae. (B) Transected larvae recorded in the S10-33 series. (C) Transected larvae recorded in the S3-15 series. (D, E) Plot of ipsilateral delay (D) and contralateral phase (E) against transection conditions: spinalized (S3-33), S10-33 and S3-15.

= 3) and rostrocaudal delay (n = 3; Fig. 2.6B). The S3-15 series, the shortest rostral series of contiguous spinal segments that produces episodic fictive swimming (EO = 61% (SD 15)), also produced bursting with side-to-side alternation (n = 3) and rostrocaudal delay (n = 3) (Fig. 2.6C). Neither the rostrocaudal delay per body segment (S3-33 = 1.3ms (SD 0.75), S10-33 = 2.5ms (SD 1.2), S3-15 = 1.3ms (SD 0.38), F = 2.5, p = 0.15) nor the contralateral phase (S3-33 = 45% (SD 3.9), S10-33 = 49% (SD 5.0), S3-15 = 47% (SD 3.6), F = 0.36, p = 0.71) were significantly different between spinalized larvae and shorter series of spinal segments (Fig 2.6D,E).

Coordination of Non-Episodic Bursting in Transected Spinal Cord

Among the transection conditions that do not produce episodically organized bursting, some (e.g. S3-15, 100 μM NMDA; Fig. 2.4C) produced highly regular bursting (burst frequency = 14Hz (SD 0.82), coefficient of variation = 0.48Hz (SD 0.21)). Given the regularity of these bursts, we hypothesized that the putative episodic organization circuit was either inactive or functioned in an abnormal fashion that did not lead to episode termination, but that other swimming-related circuits were active. The S3-15 series transitioned from producing tonic bursting (EO = 26% (SD 2.1)) to episodic bursting (EO = 61% (SD 1.5)) when the NMDA concentration was increased from 100 μM to 200 μM. Therefore, to determine the necessity of episodic organization for coordination, we compared the coordination of bursts produced by this series of segments in 100 μM NMDA to the coordination of bursts produced in 200 μM (n = 3 per group). Because the

bursting in 100 μM NMDA was non-episodic, we could not use the first burst of each episode as a phase marker (as in Fig. 2.6). Instead, we used cross- and auto-correlation to measure the inter-burst period (IBP) and burst frequency of individual recordings and the relative timing of bursts between recording sites. In

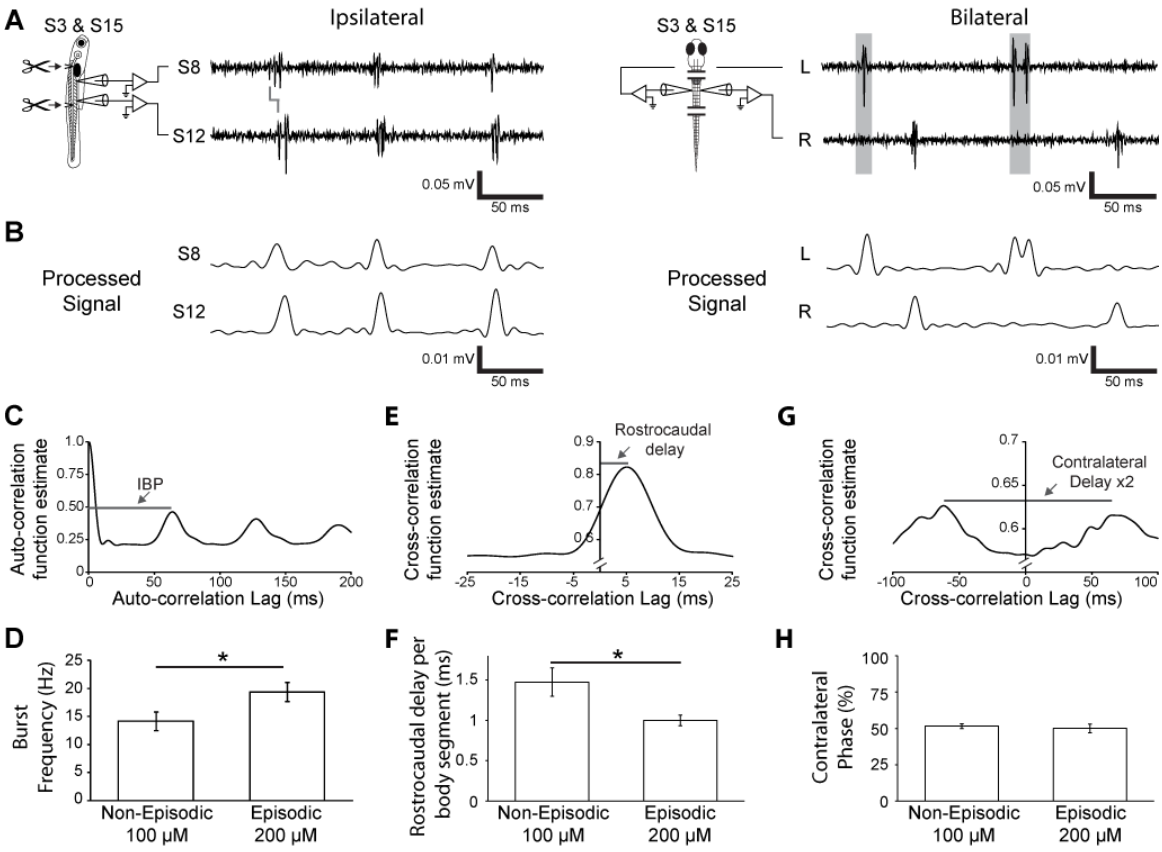

Figure 2.7 - Non-episodic bursting is coordinated following spinal transection. (A) Representative traces from ipsilateral (left) and contralateral (right) two point recordings of fictive swimming in the S3-15 series. Bursting was induced by bath application of 100 μM NMDA. Rostrocaudal delay in the ipsilateral record is indicated by a gray line. The timing of bursts from the left channel of each contralateral record is indicated by a filled gray box. (B) The traces from A following processing. (C) Auto-correlation of the left processed signal in B. The gray line shows the IBP. (D) Plot of the burst frequency determined by autocorrelation against NMDA concentration: 100 μM NMDA and 200 μM NMDA. (E) Cross-correlation of the left processed signal in B. The grey line shows the rostrocaudal delay. (F) Plot of the rostrocaudal delay against NMDA concentration. (G) Cross-correlation of the right processed signal in B. The grey line shows the contralateral delay reflected across 0 ms lag. (H) Plot of the contralateral phase against NMDA concentration. * Statistically significant difference.

order to facilitate correlation of biphasic bursts (Fig. 2.7A), recordings were rectified and low-pass filtered at 90Hz (Fig. 2.7B), and auto- and cross-correlations of the processed signal were performed (Fig. 2.7C,E). The burst frequency of the S3-15 series was significantly slower in 100μM than in 200μM NMDA (100μM = 14Hz (SD 1.6), 200μM = 19Hz (SD 1.7), $t = 3.4$, $p = 0.043$, Fig. 7D). The non-episodic bursting produced by the S3-15 series in 100 μM NMDA had a rostrocaudal delay per body segment significantly greater than zero (1.48ms (SD 0.18), $t = 14.6$, $p = 0.005$). Rostrocaudal delay per body segment was significantly longer in 100 μM than 200 μM NMDA (200μM = 1.00ms (SD 0.07), $t = 4.4$, $p = 0.02$, Fig. 2.7F). Contralateral phase was found by dividing the contralateral delay by the IBP (Fig. 2.7G). There were no significant differences between the contralateral phase of the S3-15 series in 100 μM and 200 μM NMDA (100μM = 52% (SD 0.02), 200μM = 50% (SD 0.03), $t = 0.8$, $p = 0.49$; Fig. 2.7H).

DISCUSSION

We have shown that fictive locomotion is produced along the rostrocaudal extent of the spinal cord in larval zebrafish (Fig. 2.2) and that this locomotor pattern can be generated from reduced series of spinal segments (Fig. 2.4). In the transected spinal cord, rostral spinal segments have greater potential for generating episodically organized fictive swimming (Fig. 2.5). The episodic fictive swimming produced by these series is coordinated normally (Fig. 2.6). Based on these findings, we return to our initial three hypotheses regarding the spatial distribution

of the swimming CPG: 1) The CPG is composed of segmentally reiterated oscillators, 2) There is a single CPG distributed throughout the entire spinal cord, or 3) There is a single CPG located in a small region of the spinal cord. Our results are inconsistent with the third hypothesis. Neither the rostral (S3 - S10) nor caudal (S15 - S33) regions are necessary for organized locomotion (Fig. 2.5). While those transections leave open the possibility that the midbody segments S10 - S15 contain a critical population of neurons, the S8-20 series contains the largest contiguous midbody region but does not produce the most organized swimming (Fig. 2.5). Based on these results, we conclude that there are no critical segments or series of segments in the larval zebrafish swimming CPG. Our finding that there is a linear trend of EO against number of contiguous segments (Fig. 2.5) is suggestive of either a robust, distributed CPG or of segmentally reiterated oscillators that are too weak to drive fictive swimming independently, but we cannot distinguish between these possibilities on the basis of these data. We also found that normal functioning of the circuit responsible for generation of episodic organization is not necessary for coordination of motor bursts (Fig. 2.7). Our results support the hypothesis that the zebrafish swimming CPG is composed of functionally separable circuits, one of which organizes episodes and another that coordinates bursting side-to side and rostrocaudally.

The Entire Spinal Cord Produces the Same Pattern of Fictive Swimming

Based on our observations of free-swimming larvae, we predicted that there might be different patterns of motor neuron bursting in the midbody and tail of the

larvae. For example, one type of free-swimming behavior, slow start swimming, has a relatively tight lateral undulation in the midbody region that rapidly increases in amplitude in the far caudal region (Muller and Von Leeuwen, 2004). We proposed that this motion could be due to the whip-like snapping of a passive tail. To determine the spatial distribution of motor activity, we measured peripheral nerve activity at points along the rostrocaudal axis of the larvae. Our prediction of a passive tail was not observed in the range of swim frequencies or spinal segments recorded in our experiments (Fig. 2.2). Instead, the entire spinal cord produced the same pattern of motor neuron bursting. We concluded that the motor neuron output is distributed throughout the cord, though the interneurons that generate the motor pattern may not be.

Fictive Swimming Characteristics are Dependent on NMDA Concentration

Concentrations of NMDA between 50 and 200μM reliably evoked fictive swimming in spinalized larval zebrafish (Fig. 2.3). High concentrations of NMDA produce short duration episodes of high frequency bursting, while low concentrations produce long duration episodes of lower frequency bursting. The correlation we observed between burst frequency and episode duration across NMDA concentrations is not observed across preparations following application of the same concentration of NMDA. This suggests that the effect of NMDA concentration accounts for the covariance of these variables and that episode duration and burst frequency are independent of one another.

Series of Spinal Segments Produce Fictive Swimming Following Transection

We performed a series of spinal transections that divided the spinal cord into isolated series of contiguous segments (Fig. 2.4). Under some conditions, these isolated series of spinal segments produced episodically organized fictive locomotion that was not statistically different from the output produced by spinalized larvae. The effect of these transections was to raise the threshold for production of organized episodes from 50 uM to 200 uM NMDA, and for some transection conditions, to abolish the capacity for generating episodically organized fictive swimming. The necessity of higher NMDA concentration may be due to removing ascending and descending intra-spinal excitatory projections (e.g. Satou et al. (2012)) or due to an injury-induced decrease in neuronal excitability. We found that rostral series of segments shorter than 12 segments were not able to produce episodic swimming (Fig. 2.4, 2.5), and that more than 20 body segments were necessary to produce episodic swimming in the caudal region. This finding differs from a previous report that two isolated body segments were sufficient to produce locomotor-like bursting (McDearmid and Drapeau, 2006). There are several potential explanations for this discrepancy, including effects of strain, larval stage, NMDA concentration, and transection technique. We believe the most parsimonious explanation arises from the intrinsic properties of motor neurons. McDearmid and Drapeau (2006) performed whole cell recordings from individual motor neurons while we use peripheral nerve recordings. Zebrafish motor neurons have intrinsic bursting properties (Buss et al., 2003) that may be activated by high doses of NMDA, possibly giving

the appearance of episodic fictive swimming when recording from an individual neuron. However, these oscillations would not likely be correlated between motor neurons, and therefore would not be observed with peripheral nerve recording, unless a CPG was driving their activity.

The Rostral Spinal Cord has Greater Episode Organizing Potential

In these experiments, we found that rostral body segments are more capable of producing episodically organized swimming than caudal body segments following transection (Fig. 2.5). This difference is most dramatically demonstrated by the difference in motor output between the rostral series S3-15 and the caudal series S15-33 (Fig. 2.4C). Despite the rostral bias for episode generation, rostral spinal segments are not necessary for the production of episodes (Fig. 2.4). This finding is inconsistent with the hypothesis that the swimming CPG is localized to a small region of the cord, and suggests a more distributed model. The strong linear trend we find between the number of body segments and the EO score of the swim pattern (Fig. 2.5) could be interpreted in two ways. On the one hand, it could be that the episode circuit is segmentally reiterated. Based on this structure, we would predict repeating interneuron populations with progressively weaker net synaptic drive onto their targets. On the other hand, it could be that the episode organizing circuit is composed of a non-segmentally organized network of neurons spread throughout the spinal cord. Based on this structure, we would predict a gradient of synaptic output from the episode circuit and an interneuron distribution that does not align to segmental boundaries. Modeling

studies in tadpole (Wolf et al., 2009) provide a quantitative framework for the distributed hypothesis, but determining which hypothesis is more likely will require additional characterization of neuronal distribution throughout the larval zebrafish spinal cord.

Coordination of Bursts is Independent of Episodic Organization

We found that by manipulating the concentration of NMDA, we activated the putative coordination circuit without observing discretely organized episodes (S3-15, 100 μM NMDA; Figs. 2.4C, 2.7). The functional dissociation between the episode organization circuit and the coordination circuit we have observed is similar to models of the leech swimming circuit (Kristan et al., 2005) and multi-level models of the mammalian CPG (McCrea and Rybak, 2008). Therefore, we propose the following preliminary model of the functional organization of the zebrafish spinal locomotor CPG:

The hindbrain acts as an activator (Mori et al., 1978; Noga et al., 1988; Li et al., 2006; Arrenberg et al., 2009; Soffe et al., 2009) and makes excitatory connections with the spinal episode circuit (Hägglund et al., 2010; Li et al., 2010). The episode circuit acts as a gating center and makes excitatory connections (Buss and Drapeau, 2001; Kyriakatos et al., 2011) with the spinal coordination circuit. The coordination circuit sculpts excitatory input from the episode circuit into a coordinated output and makes excitatory and inhibitory connections with motor neurons (McLean et al., 2008; Kyriakatos et al., 2011). When the hindbrain

initiates a locomotor episode, it sends an excitatory signal to the episode circuit, initiating an up-state of high activity. The episode circuit excites the coordination circuit, which then begins driving the motor neurons in a coordinated fashion. The episode generator up-state self-terminates, ending the excitation to the coordination circuit. In the absence of excitation, the coordination circuit is silenced and the motor neurons stop firing.

Conclusions

In summary, using transections of the larval zebrafish spinal cord, we demonstrate the spatial and functional organization of the episode and coordination circuits in the spinal CPG. We show that there is a strong effect of rostrocaudal position on the ability of series of spinal segments to produce episodic swimming. Further, we show that normal coordination of bursting is not dependent upon episodic organization. Future work is necessary to determine whether or not the episode organization and coordination circuits are segmentally organized and how the putative episode and coordination circuits interact with one another.

CHAPTER 3: COORDINATION OF FICTIVE MOTOR ACTIVITY IN THE LARVAL ZEBRAFISH IS GENERATED BY NON-SEGMENTAL MECHANISMS.

INTRODUCTION

Locomotion in vertebrates is organized by spinal neural circuits called central pattern generators (CPGs) that are capable of driving patterned motor neuron output even in the absence of patterned synaptic input (Marder and Calabrese, 1996). Despite their importance, the cellular basis for most vertebrate CPGs is still incompletely characterized (Stepien and Arber, 2008; Goulding, 2009). Because there is evidence for evolutionary conservation of CPG elements such as cell types (Grillner and Jessell, 2009), two vertebrate species with characterized locomotor CPGs, lamprey (Grillner and Wallen, 2002) and tadpole (Roberts et al., 1998), are frequently used as the basis of models of locomotor CPGs in other animals (Grillner, 2006) (but see also (Dougherty and Kiehn, 2010)).

One model of the vertebrate spinal locomotor CPG proposes that it is composed of a series of reiterated circuits with connecting projections (Hill et al., 2003; Grillner, 2006). This segmental CPG model is comparable to the known organization of several invertebrate locomotor CPGs. For example, in crayfish and leech the locomotor CPGs are composed of segmentally reiterated groups of neurons with local connections that coordinate alternation in antagonist motor

neurons and with longer range projections that drive rostral to caudal propagation (Kristan et al., 2005; Mulloney and Smarandache-Wellmann, 2012; Smarandache-Wellmann et al., 2014). The segmental CPG model is supported also supported by experimental evidence in vertebrates. Lesion studies have demonstrated that rhythmic, coordinated motor output can be evoked using tonic excitatory drive from as few as 2 spinal intact segments in chicks (Ho and O'Donovan, 1993), rats (Kjaerulff and Kiehn, 1996), lamprey (Cangiano and Grillner, 2003), and salamanders (Charrier and Cabelguen, 2013). Complementing this experimental evidence, computational models of the lamprey locomotor CPG that use spinal segments as the units of circuit reiteration accurately reproduce swimming output (Matsushima and Grillner, 1990; Grillner and Wallen, 2002).

One deficiency in the segmental CPG model is that there is little anatomical evidence for segmental distribution of interneurons that would make up the segmental CPGs (Wallén et al., 1985). An alternative is a continuous model of the vertebrate spinal locomotor CPG, which is proposed as an unsegmented, continuous collection of neurons with gradients of soma and synaptic density that drive appropriately timed motor output. Based on anatomical distributions of neurons, quantitative continuous models of the lamprey (Wadden et al., 1997) and tadpole (Wolf et al., 2009; Roberts et al., 2014) locomotor systems have been developed that produce swimming-like motor output. Continuous CPG models of rhythm generation have also been proposed for the mammalian

locomotor circuit based on the properties of motor deletions in fictive locomotion (McCrea and Rybak, 2008).

The larval zebrafish is a useful model of locomotion because it has well developed genetic tools and shares many genetic markers of cell type with mammals, but has a simpler motor output than quadruped locomotion (Fetcho and McLean, 2010). Larval zebrafish swim in a “beat-and-glide” pattern composed of brief episodes of active swimming separated by periods of inactivity (Buss and Drapeau, 2001). During each episode, the larvae undulate using side-to-side lateral alternation and rostrocaudal progression of the body wave (Batty, 1984; Borla et al., 2002). Fictive swimming in both intact and spinalized larval zebrafish retains the episodic nature of free-swimming larvae (Masino and Fetcho, 2005; McDearmid and Drapeau, 2006). Within each episode, bursts are produced along the body with a rostrocaudal delay and bursts alternate on each side of the body (Masino and Fetcho, 2005). These burst-timing relationships drive the undulatory movement of the free-swimming larvae, and throughout this paper we refer to them collectively as “coordination.” In a previous study we demonstrated that the production of episodes of activity in larval zebrafish depends upon a distributed spinal circuit, and that rostrocaudal delay and side-to-side alternation are independent of episode production (Described in Chapter 2 of this document, and published as Wiggin et al., (2012)). In this study, we tested the hypothesis that larval zebrafish have segmentally reiterated locomotor circuits for production of rostrocaudal delay and side-to-side alternation. We

found that the motor output of the spinal cord following transection or reduction of inhibitory synaptic strength is not consistent with a segmental CPG model, and is more consistent with a continuous CPG model.

This content of this chapter has been previously published in *Public Library of Science (PLoS) ONE* (Wiggin et al., 2014).

METHODS

Ethics Statement

All procedures were approved by the Animal Care and Use Committee of the University of Minnesota Twin Cities, Approval #1305-30622A.

Animals and solutions

Wild type adult zebrafish (*Danio rerio*, Segrest Farms, Gibsonton, FL) were maintained in the University of Minnesota Zebrafish Core Facility. Group breeding tanks of adult zebrafish were set up daily to produce clutches of embryos with timed fertilization between 8:45 and 9:00am. Embryos and larval zebrafish were maintained in 100 mm petri dishes filled with embryo water (60 µg/ml Instant Ocean® salt mix, Cincinnati, OH) and 0.0002% methylene blue in a 28.5°C incubator with a 14:10 light:dark cycle. All experiments were carried out using larval zebrafish 4 to 6 days post fertilization (dpf). At this age, the sex of the larvae is not determined (Liew et al., 2012). Chemicals and drugs were obtained

from Sigma-Aldrich Chemical (St. Louis, MO), unless otherwise noted. Zebrafish extracellular saline was composed of (in mM): 134 NaCl, 2.9 KCl, 1.2 $MgCl_2$, 2.1 $CaCl_2$, 10 HEPES buffer, 10 glucose, adjusted to pH 7.8 with NaOH and 300 mOsm with sucrose (Legendre and Korn, 1994; Drapeau et al., 1999).

Peripheral Nerve Recordings

Larval zebrafish were prepared for peripheral nerve (PN) recordings as previously described (Masino and Fetcho, 2005). Briefly, larval zebrafish were anesthetized with 0.02% Tricaine-S (Western Chemical, Ferndale, WA) in extracellular saline, pinned in a Sylgard®-lined dissecting dish, and skin was removed from the regions of the body to be recorded. Larvae were paralyzed using 5 µl of 0.1 mM α-bungarotoxin (Tocris, Ellisville, MO) added to the small volume (~15 µL) of extracellular saline in the dissection dish. Paralyzed larvae were transected while bathed in extracellular saline using a razor blade shard to completely sever the spinal cord and overlying muscle (razor blade: FA-10 Feather S, Ted Pella, Redding, CA). Transections nicked, and occasionally severed, the notochord and completely separated the musculature, including the dorsal muscle. Larvae were allowed to recover for 20 - 30 minutes following transection and prior to peripheral nerve recordings. Larvae used for unilateral PN recordings (to measure rostrocaudal delay) were pinned with one side of the larva facing up. Larvae used for bilateral PN recordings (to measure side-to-side alternation) were rotated into a dorsal-up position so that both sides of the larva

were accessible. Larvae were continuously superfused with extracellular saline during all recordings.

Experimental Groups

In this study we used a range of reduced spinal cord preparations of larval zebrafish. Spinalized larvae and reduced preparations only produced fictive motor output when it was evoked by NMDA. NMDA was superfused for approximately 20 minutes prior to the beginning of PN recordings, and continued throughout the recording. The NMDA concentration used was 100 μM unless otherwise noted.

The experimental conditions were as follows: 1) Spinalized preparations were transected at body segment 3 (S3) to separate the spinal cord from the hindbrain. 2) Rostral-10 preparations were transected at S3 and S14, leaving 10 intact segments between the transection sites centered on S8. 3) Rostral-5 preparations were transected at S5 and S11, leaving 5 intact segments centered on S8. 4) Middle-10 preparations were transected at S6 and S17, leaving 10 intact segments centered on S11. 5) Middle-5 preparations were transected at S10 and S16, leaving 5 intact segments centered on S13. 6) Caudal-5 preparations were transected at S16 and S22, leaving 5 intact segments centered on S19.

Segments were counted using the anal pore as the marker for the ventral side of S15 and the first visible segment caudal to the head as S1. Because of ambiguity in determining the location of body segment landmarks between larvae, it is likely that the borders of these transected regions were offset rostrally or caudally by up to 1 body segment, but the number of body segments was consistent between dissections. All experimental groups contained larvae from at least 2 clutches.

Electrophysiology

PN recordings were performed as previously described (Masino and Fetcho, 2005). Briefly, larvae were placed on the stage of an upright microscope (Olympus BX51 WI, Center Valley, PA), and continuously superfused with extracellular saline at room temperature (20 – 22 °C). PN recordings were obtained using glass suction electrodes with tip sizes ranging from 9 to 15 μm. Recordings of laterally mounted larvae were obtained from the intermyotomal cleft adjacent the horizontal septum; paired recordings of dorsoventrally mounted larvae were obtained from the intermyotomal clefts on opposite sides of the larvae. Signals were obtained using an Axon Instruments Multiclamp 700B amplifier and acquired with an Axon Instruments Digidata 1440A controlled by pClamp 10 software (Molecular Devices, Union City, CA).

Analysis of Peripheral Nerve Recordings

We used a custom Matlab (Mathworks, Natick, MA) program developed in our laboratory to detect fictive swimming in PN recordings automatically, as

previously described (Wiggin et al., 2012). Briefly, for each voltage sample ($v(n)$), the voltage autocorrelation ($c_n(k)$) was computed over a small window (3 ms) centered at $v(n)$. A subset of the autocorrelation values were used to compute a test-statistic (c_n) for each $v(n)$, where c_n is the sum of the $c_n(k)$ in the range k = [1,2]. This range of k was chosen empirically to optimize burst detection and noise rejection in low amplitude recordings. Activity was considered present at $v(n)$ when the test statistic was greater than a detection threshold T. T was set for each recording as the maximum value of the test statistic in a region of the recording that was visually inspected and confirmed to not contain any bursting activity (typically the first second of the recording). If the test statistic remained above threshold for at least 3ms, the supra-threshold voltage samples were identified as a burst.

We defined the properties of fictive motor output as follows: Burst Duration was the time between the test statistic rising above threshold and falling below threshold. Burst Frequency was the inverse of the mean inter-burst period (IBP), which was defined for each pair of bursts as the time from the midpoint of the first burst to the midpoint of the second burst. IBPs longer than 200ms were excluded from quantification because, in unperturbed swimming, these IBPs are times between episodes rather than part of the intra-episode locomotor rhythm. This IBP threshold is longer than would be strictly necessary based on typical zebrafish behavior in order to accommodate the phenomenon of “missed” bursts.

A “missed” burst is a time when a burst is expected based on the locomotor rhythm, but not detected by the PN recording. We do not have evidence that missed bursts reflect changes in the underlying behavior, instead we believe that they are due to under-sampling the motor pool. In order to avoid inappropriately partitioning activity into separate episodes because of missed bursts, we use an IBP threshold twice as long as would be sufficient if we assumed perfect burst detection.

Phase Vector Sum Analysis

We used a phase-based analysis to quantify the changes in rostrocaudal delay and side-to-side alternation (Fig. 3.1). One PN recording was *a priori* designated as the phase leader and the other as the phase follower. For bilateral recordings, the left side of the animal was the leader, and in unilateral recordings of rostrocaudal delay, the more rostral recording site was the leader. In the phase leader recording, the IBP of each pair of chronologically adjacent bursts was calculated. Burst pairs with an IBP greater than 2x the mean of that record were excluded from further analysis because of the possibility of missed bursts distorting the phase calculation. The time period between each pair of bursts in the leader recording was checked for the presence of a burst in the phase follower recording (Fig. 3.1A,B). If one or more follower bursts were present, the phases (in radians) were calculated as

$2\pi \times \frac{Follower.Burst.Time - Leader.Burst.Time_1}{Leader.Burst.Time_2 - Leader.Burst.Time_1}$, where subscripts 1 and 2 indicate

the initial and final bursts of the pair of bursts in the leader recording, respectively. After the follower phases were calculated, they were converted into unit vectors in a polar plane (Fig. 3.1C). Standard vector addition was used to calculate the vector sum of all burst phase vectors, and the magnitude of the

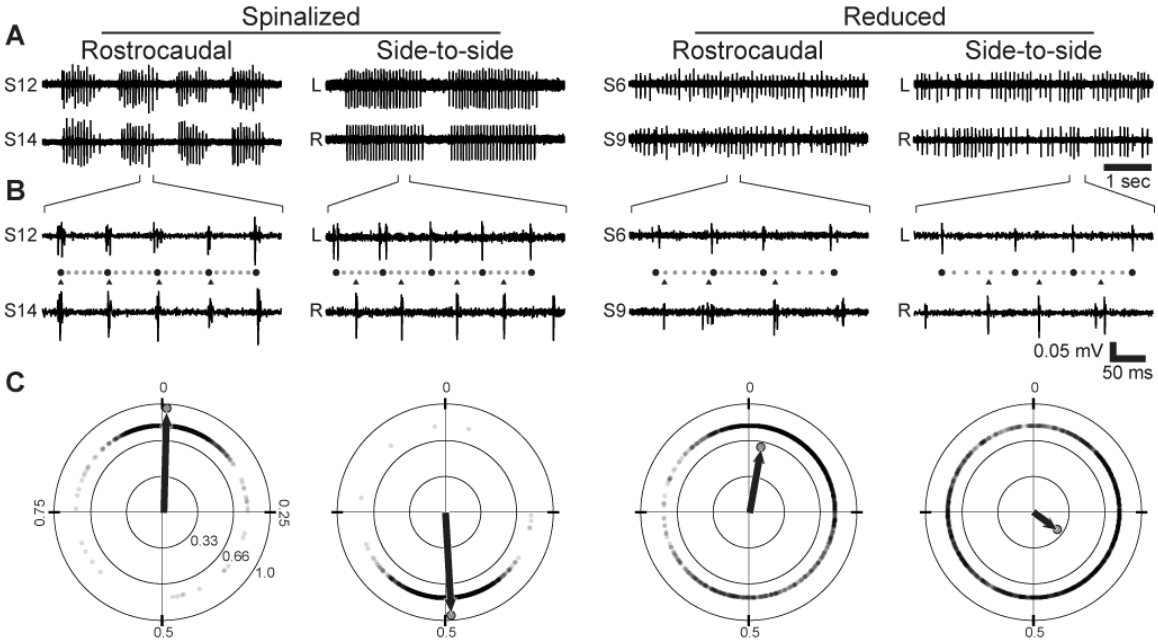

Figure 3.1 – Phase Vector Sum Analysis of Fictive Motor Output. (A) PN recordings of fictive motor output produced by representative spinalized larvae (left traces) and reduced spinal cord preparations (right traces). Left (L) and right (R) sides of the body are indicated in traces showing side-to-side alternation. The rostrocaudal location of each recording is indicated by segment number (e.g. S12) in traces showing rostrocaudal progression. (B) The indicated regions of the top traces at a finer time scale. The relative phases of the bursts in the paired recordings are illustrated using circles (phase markers) and triangles (follower burst times). Black circles indicate burst times, smaller gray circles divide each burst period into 6 equally long intervals. (C) Polar plots showing the phase of each burst (small gray circles) from the follower recording site relative to bursts from the leader recording site, for each group indicated above the plot. Individual burst phases are plotted at an arbitrary radius for illustrative purposes, they are treated as unit vectors when calculating vector sums. Concentric circles are plotted at distances of 0.33, 0.66 and 1.0 from the fixed point; cross-hairs separate the quadrants. The normalized vector sums of the bursts from each representative preparation are illustrated by an arrow and a large gray circle at the terminal point.

resulting vector sum was divided by the total number of phase vectors, normalizing it to the range 0 – 1. Finally, the phase of the vector sum was divided by 2π, converting from radians into the range 0 – 1. This process produced a single mean phase vector for each preparation that has two parameters: 1) *Θ*, the phase angle of the vector, a measure of mean phase offset between the leader and follower. 2) *r*, the vector magnitude, a quantification of the degree of consistency of the phases of each follower burst relative to the leader (Fig. 3.1C). For rostrocaudal recordings, the phase was divided by the number of segments separating the recording sites, yielding phase lag per body segment.

Statistical Analysis

Measurement of the variability of burst period and rostrocaudal delay is necessary to quantify the stability of the motor rhythm and the reliability of rostrocaudal delay, respectively. Variance and standard deviation are both sensitive to the effects of outliers, so we chose a more robust statistic for comparing the variability of groups to one another: the Median Absolute Deviation (MAD) (Hampel, 1974). Tests for significant differences in episode and burst properties, the magnitude of the phase vector and MAD values were carried out using one-, two- and three-way ANOVAs and subsequent protected *t*-tests. The value and deviation of the phase angle for each group was calculated using circular statistics, and the Watson-Williams test was used to test for significant differences between groups. Statistical tests were carried out using SigmaPlot 12 software (SyStat Software, San Jose, CA), Microsoft Excel

(Microsoft, Seattle, WA), or the Matlab CircStat toolbox (Berens, 2009). An α level of 0.05 was used to determine statistical significance. Linear data are expressed as the mean and standard deviation, phase data are expressed as the circular mean with angular variation.

RESULTS

NMDA Induces Non-Episodically Organized Fictive Motor Activity in the Reduced Larval Zebrafish Spinal Cord

The only published method for inducing fictive locomotion in spinalized zebrafish larvae and reduced larval zebrafish spinal cords is bath application of NMDA (McDearmid and Drapeau, 2006; Lambert et al., 2012; Wiggin et al., 2012). The episodic character of intact and spinalized fictive locomotion is disrupted by spinal transections in a graded fashion depending upon the quantity and region of spared spinal cord (Wiggin et al., 2012). In this study, we used small isolated regions of the spinal cord (5 or 10 segments, approximately 15% or 30%, respectively, of the full cord; Fig. 3.2A). NMDA (100 μM) induced fictive locomotion in these reduced preparations was qualitatively different from spinalized swimming because it lacked episodic structure (Fig. 3.2B). We quantified the parameters of fictive motor output from the following experimental groups (described in *Methods*): Spinalized (n = 11) Rostral-10 (n = 9), Middle-10 (n = 8), Rostral-5 (n = 6), Middle-5 (n = 6), Caudal-5 (n = 6). Burst frequency and burst duration did not vary between the groups (One-way ANOVAs; all $F_{(5,40)} < 2.17$; all $p > 0.07$; Fig. 3.2C,D).

Rostrocaudal Phase Consistency and Motor Rhythm Stability are Impaired in Reduced Spinal Cord Preparations

A segmental model of the spinal locomotor network (Fig. 3.3A) would predict that the phase relationship between the fictive motor outputs of two segmental CPGs should depend on the connections (direct or indirect) between the segments and the state of each segmental CPG. In contrast, a non-segmental model of the locomotor network (Fig. 3.3B) would predict that the coordination of fictive motor output at two points along the rostrocaudal axis of the larva would depend upon

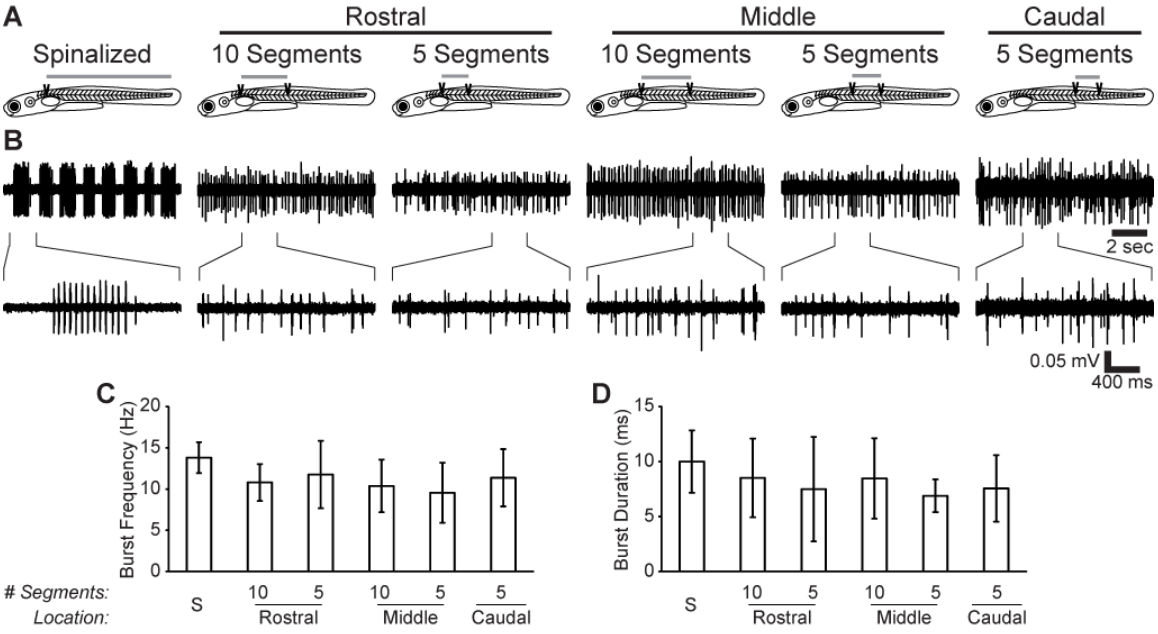

Figure 3.2- NMDA Induces Fictive Motor Activity in Spinalized and Reduced Larval Zebrafish. (A) Schematic diagrams of Spinalized, Rostral-10, Rostral-5, Middle-10, Middle-5, and Caudal-5 preparations. Dark wedges indicate the sites of spinal transections, and gray bars above each larva indicate the spared spinal cord region used for recordings subsequent to transection. (B) Representative traces showing fictive motor activity in each of the experimental conditions below its respective schematic diagram. Bottom traces show the indicated region at a finer time scale. (C-D) Plots of burst frequency (C) and burst duration (D) in each experimental group. The bar labeled “S” is the spinalized group.

the integrity of the entire circuit. To determine if rostrocaudal delay is affected by reducing the number of contiguous spinal segments surrounding the PN recordings, we performed two-point unilateral PN recordings of fictive motor output produced by isolated regions of the larval zebrafish spinal cord (Spinalized, n = 9; Rostral-10, n = 9; Middle-10, n = 8; Rostral-5, n = 6; Middle-5, n = 6; Caudal-5, n = 6; Fig. 3.3C). We measured coordination of the motor output using phase vector sum analysis, and we measured the stability of the motor rhythm using the median absolute deviation (MAD) of the burst period (see *Methods*). PN recordings were performed 1 to 4 segments apart (mean: 2.16(SD 0.75)); phase delay was normalized to phase per segment. Mean rostrocaudal phase delay per segment did not differ among the experimental groups (Watson-Williams test; $F_{(5,37)}$ = 0.77; p = 0.58; Fig 3.3D). However, there was a significant effect of experimental group on phase consistency (One-way ANOVA; $F_{(5,37)}$ = 23.2; p < 0.001; Fig 3.3E). Post-hoc tests revealed that spinalized larvae had higher phase consistency than all groups but Rostral-10 (Corrected t-tests; all t > 2.8; all p < 0.04), that 10 segment experimental groups had higher phase consistency than 5 segment experimental groups (Corrected t-tests; all t > 3.1; all p < 0.025), and that there were no significant differences among the 5 segment experimental groups. The trends revealed by the post-hoc tests were confirmed by a two-way ANOVA of only the Rostral-10, Rostral-5, Middle-10, and Middle-5 experimental groups that showed a significant main effect of number of segments ($F_{(1,25)}$ = 26.2; p < 0.001), but no main effect of location of segments or interaction of number of segments and location (all $F_{(1,25)}$ <1.8; all p > 0.19). There was also

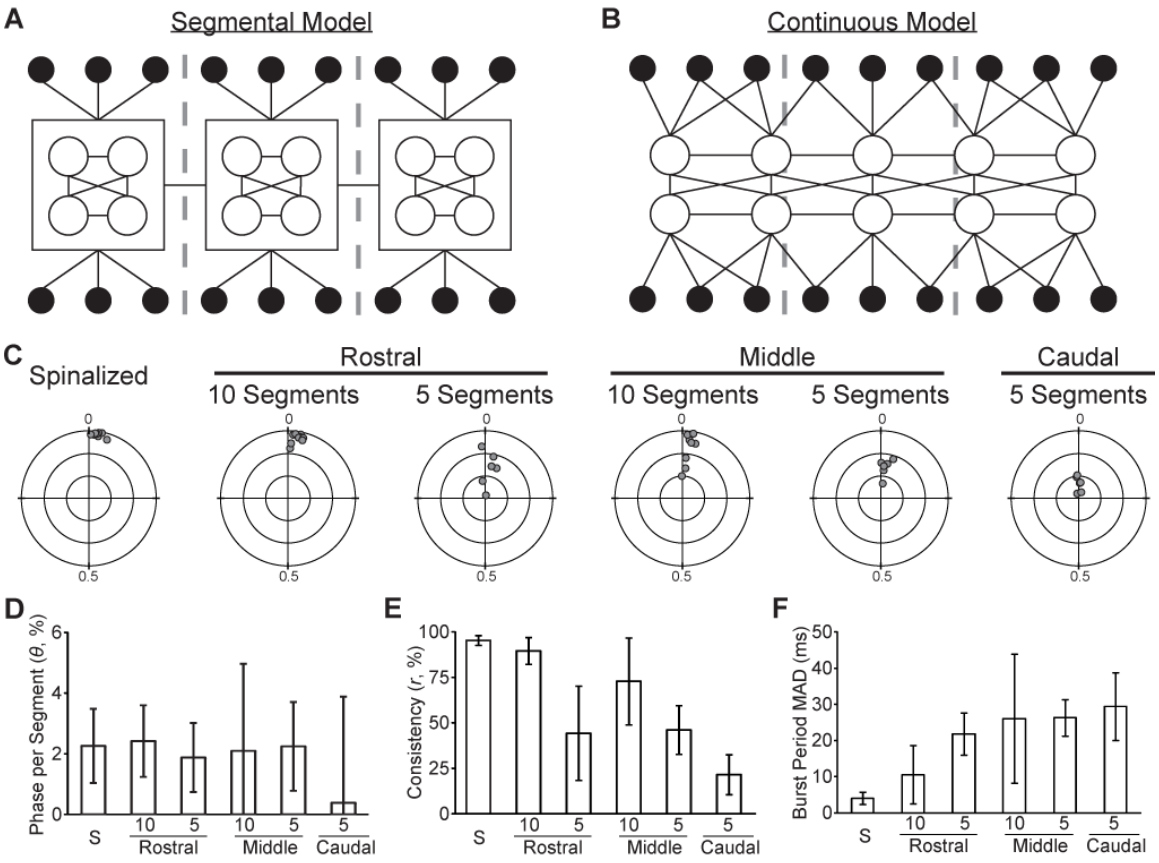

Figure 3.3 – Rostrocaudal Phase Consistency and Motor Rhythm Stability are Decreased by Spinal Transection. (A-B) Diagrams of segmental (A) and continuous (B) models of the spinal locomotor CPG. The models show the spinal circuit with the rostrocaudal axis horizontal and the mediolateral axis vertical. Body segment boundaries are shown with gray dashed lines. In both models, each segment contains two groups of motor neurons (black-filled circles), each group innervating one lateral hemi-segment. In both models, interneurons (open circles) form synaptic connections (black lines) with each other and with motor neurons. In the segmental model (A), each segment contains a reiterated interneuron circuit that controls local motor neurons and communicates with other segmental circuits. In the continuous model (B), interneurons are distributed and form synaptic connections based on inter-somatic distance and are independent of segmental boundaries. In both models, patterns of interneuron connectivity are strictly illustrative and should not be interpreted as definite synaptic connections between defined interneurons. (C) Polar plots showing the normalized rostrocaudal phase vector sum (gray circle) of each preparation in the experimental group indicated above the plot. Concentric circles are plotted at distances of 0.33, 0.66 and 1.0 from the fixed point; cross-hairs separate the quadrants. (D-F) Plots of mean phase delay per segment (D), mean phase consistency (E), and mean burst period MAD (F) of each experimental group. The bar labeled “S” is the spinalized group. Significant differences are not indicated due to the number of pair-wise comparisons (see text in *Results*).

a significant effect of experimental condition on the burst period MAD (One-way ANOVA; $F_{(5,37)} = 8.1$; $p < 0.001$; Fig. 3.3F). Post-hoc tests revealed that spinalized larvae had lower burst period variability than all other groups but Rostral-10 (Corrected *t*-tests; all $t > 3.4$; all $p < 0.018$). Rostrocaudal coordination of fictive motor output is impaired in reduced larval zebrafish spinal cord. The number of spared segments, but not the rostrocaudal location of the segments, determines the degree of impairment. This effect may be either due to injuring a distributed coordination circuit or due to unstable oscillation of segmental CPGs.

Side-to-Side Phase Consistency and Motor Rhythm Stability are Impaired in Reduced Spinal Cord Preparations

A segmental CPG model of the spinal locomotor network (Fig. 3.3A) would predict that phase relationships between the contralateral sides of the same segment should depend only on the operation of each segmental circuit and not on inter-segmental connections. Alternatively, a continuous CPG model of the spinal locomotor network (Fig. 3.3B) would predict that the coordination between contralateral sides of a single segment of the larva would depend upon the integrity of the entire circuit. To determine if side-to-side alternation is affected by reducing the number of contiguous spinal segments, we performed two-point bilateral PN recordings of fictive motor output produced by isolated regions of the larval zebrafish spinal cord (Spinalized, $n = 7$; Rostral-10, $n = 7$; Middle-10, $n = 6$; Rostral-5, $n = 6$; Middle-5, $n = 6$; Fig. 3.4A). We measured coordination of the motor output using the phase vector sum analysis, and we measured the stability

of the motor rhythm using the MAD of the burst period. There was a significant effect of experimental group on side-to-side phase (Watson-Williams test; $F_{(4,27)}$ = 7.1; p < 0.001; Fig 3.4B). This difference was driven by the Middle-5 group, which differed significantly from the spinalized and Rostral-10 larvae (Corrected Watson-Williams test; all p < 0.025). The Middle-5 larvae had extremely low phase consistency (Fig. 3.4C), and the mean phase of this group is likely not functionally meaningful. There was also a significant effect of experimental group on phase consistency (One-way ANOVA; $F_{(4,27)}$ = 23.2; p < 0.001; Fig 3.4C). Post-hoc tests revealed that spinalized larvae were more consistent than all of the experimental groups of reduced spinal cord preparations (Corrected *t*-tests;

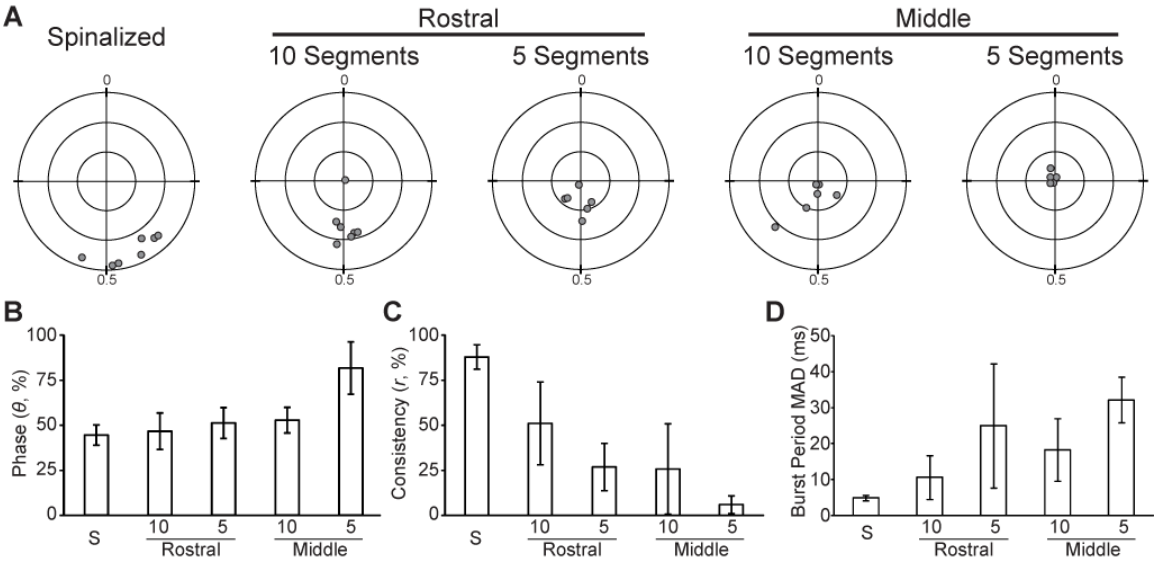

Figure 3.4 – Side-to-Side Phase Consistency and Motor Rhythm Stability are Decreased by Spinal Transection. (A) Polar plots showing the normalized contralateral phase vector sum (gray circle) of each preparation in the experimental group indicated above the plot. Concentric circles are plotted at distances of 0.33, 0.66 and 1.0 from the fixed point; cross-hairs separate the quadrants. (B-D) Plots of mean phase offset (B), mean phase consistency (C), and mean burst period MAD (D) of each experimental group. The bar labeled "S" is the spinalized group. Significant differences are not indicated due to the number of pair-wise comparisons (see text in *Results*).

all $t > 4.1$; all $p < 0.002$). A two-way ANOVA of Rostral-10, Rostral-5, Middle-10, and Middle-5 groups showed significant main effects of both the position of segments ($F_{(1,21)} = 9.5$; p = 0.006), and the number of segments ($F_{(1,21)} = 8.7$; p = 0.008) with no significant interaction. There was also a significant effect of experimental condition on the burst period MAD (One-way ANOVA; $F_{(4,27)} = 9.0$; $p < 0.001$; Fig. 3.4D). Post-hoc tests revealed that spinalized larvae had lower burst period variability than 5 segment transected preparations (Corrected *t*-tests; all $t > 3.9$; all $p < 0.004$). Side-to-side alternation of fictive motor output is impaired in reduced zebrafish spinal cord and both the number of spared segments and the rostrocaudal location of the segments determines the degree of impairment. There is also a significant decrease in the stability of the motor rhythm in the reduced spinal cord conditions. The decrease in coordination may be due to either injuring a distributed coordination circuit or to unstable oscillation of hemisegmental CPGs.

Side-to-Side Alternation is Impaired More than Rostrocaudal Delay in Reduced Spinal Cord Preparations

To compare the effect of spinal cord reduction on rostrocaudal and side-to-side coordination, we performed a three-way ANOVA (recording type X number of segments X rostrocaudal location) on the phase consistency of the reduced spinal cord experimental groups shared between the unilateral and bilateral PN recording experiments (Rostral-10, Rostral-5, Middle-10, and Middle-5; Figs. 3,4). Spinal transections impaired the phase consistency of side-to-side

alternation significantly more than the rostrocaudal delay ($F_{(1,46)}$ = 48.5; p < 0.001). Consistent with the two-way ANOVA results, rostral segments produced more consistent phase delays than middle segments and 10 segment regions of contiguous spinal segments produced more consistent phase delays than 5 segment regions (all $F_{(1,46)}$ > 8.8; all p < 0.005), but there were no significant interactions. There were no significant differences between the burst period MAD recorded in unilateral and bilateral experiments (Two-way ANOVA; $F_{(1,59)}$ = 0.03; p = 0.86).

Both Intra-segmental and Inter-segmental Coordination are Disrupted by Spinal Transections

The preceding experiments were not sufficient to exclude either the segmental or continuous model of the spinal CPG. The graded disruption of coordination observed in progressively reduced larval zebrafish spinal cord would be predicted by a continuous CPG model, but could also be explained by the disruption of rhythm generation in putative segmental CPGs. However, the models make different predictions about the effect of transection on the fictive motor output of an individual segment. The segmental model (Fig. 3.3A) predicts that the coordination of output from a single motor pool would be unaffected by spinal transections or decreased motor rhythm stability. On the other hand, the distributed CPG model (Fig. 3.3B) does not require that motor neurons within a segment have any more shared drive or synchronous output than motor neurons in different segments.

To test the hypothesis that coordination within a segment is unaffected by spinal transection, we compared the timing of fictive motor output from two points on a single hemi-segment and from two ipsilateral hemi-segments in reduced spinal

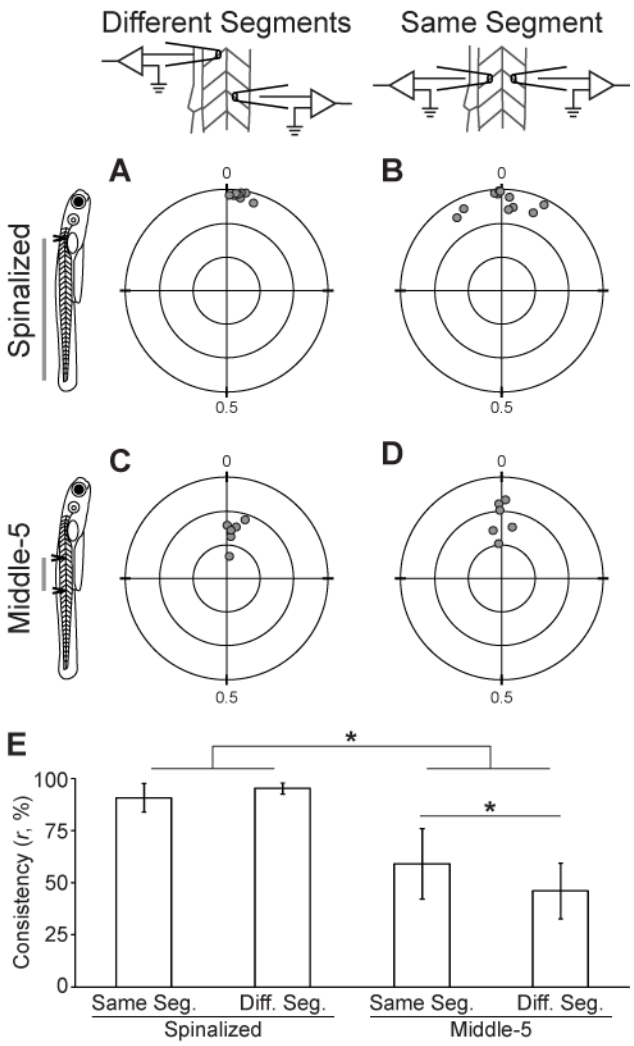

Figure 3.5 – Both Intra-segmental and Inter-segmental Coordination are Disrupted by Spinal Transections (A-D) Polar plots of the normalized phase vector sum (gray circles) of Spinalized (A,B) and Middle-5 (C,D) preparations recorded at two locations at a rostrocaudal offset (A,C) or on the same body segment (B,D). Concentric circles are plotted at distances of 0.33, 0.66 and 1.0 from the fixed point; cross-hairs separate the quadrants. (E) Plot of mean vector sum consistency (*r*) of the four experimental groups above. * Statistically significant difference.

cord preparations (Fig. 3.5). We performed same segment ipsilateral PN recordings on spinalized (n = 11; Fig. 3.5B*)* and Middle-5 larvae (n = 6; Fig. 3.5D). Data from different-segment recordings of spinalized and Middle-5 larvae presented in Fig. 3.3 are reproduced here for purposes of comparison (Fig. 3.5A,C). There is a greater spread of mean phase in the spinalized same-segment recordings than in the spinalized different-segment recordings (Fig. 3.5A,B). The greater spread is due to the different-segment mean phase being divided by the number of segments between the recordings (see *Methods*), an operation that does not apply to same-segment recordings. There was a significant main effect of spinal cord reduction on phase consistency (Two-way ANOVA; $F_{(1, 27)}$ = 113.9; p < 0.001; Fig. 3.5E), consistent with our previous results (Fig. 3.3). There was no main effect of recording in the same-segment versus different segments on phase consistency (Two-way ANOVA; $F_{(1, 27)}$ = 1.3; p = 0.27; Fig. 3.5E), but a post-hoc test did show that Middle-5 same segment recordings are significantly more coordinated than Middle-5 different segment recordings (Corrected t-test; t = 2.2; p = 0.04). These results indicate that motor neuron coordination within a body segment is significantly reduced by spinal transection, which is inconsistent with the segmental CPG model. The small difference in coordination between Middle-5 same segment and Middle-5 different segment recordings could be due to weak intra-segmental coupling of the motor neurons or a bias toward shared synaptic input within a segment (Bagnall and McLean, 2014).

Reduced Synaptic Inhibition Reversibly Reduces Coordination and Burst Period Stability

Transection experiments allowed us to measure the effect of reducing ascending and descending synaptic input on the coordination of fictive motor output. These lesions disrupt episodic organization and are irreversible. Strychnine, a glycine receptor antagonist, has been demonstrated to reduce swimming speed without reducing tail beat frequency or disrupting episodic organization, presumably through weakening each cycle of swimming (Mirat et al., 2013). In order to determine if fictive motor coordination can be disrupted independently of disrupting episodic organization, we pharmacologically suppressed inhibitory neurotransmission with strychnine. We used a strychnine concentration (1 μM) that has been shown to significantly decrease glycinergic neurotransmission (Higashijima et al., 2004a). The combination of 100 μM NMDA and 1 μM strychnine evoked fictive motor output in which adjacent bursts fused into continuous activity, which made side-to-side alternation impossible to measure. Based on a concentration response experiment, we found that reducing the concentration of NMDA to 50 μM produced fictive locomotion where coordination could be assessed effectively, and therefore we used this lower NMDA concentration for all strychnine experiments. Strychnine (1 μM) significantly changed the properties of 50 μM NMDA-evoked fictive swimming in spinalized larvae without disrupting the episodic nature of the motor output (n = 6; Fig. 3.6). Episode frequency was significantly increased by strychnine while episode duration was significantly reduced (One-way repeated measures ANOVA; all

$F_{(2,10)} > 8.7$; all $p < 0.006$; Fig 3.6C,D). Changes in episode frequency and duration were not reversed following washout (>30 minutes). Burst frequency and burst duration were reversibly increased by strychnine (One-way repeated measures ANOVAs; all $F_{(2,10)} > 6$; all $p < 0.02$; Fig 3.6E,F).

We also found that strychnine had significant effects on both phase consistency

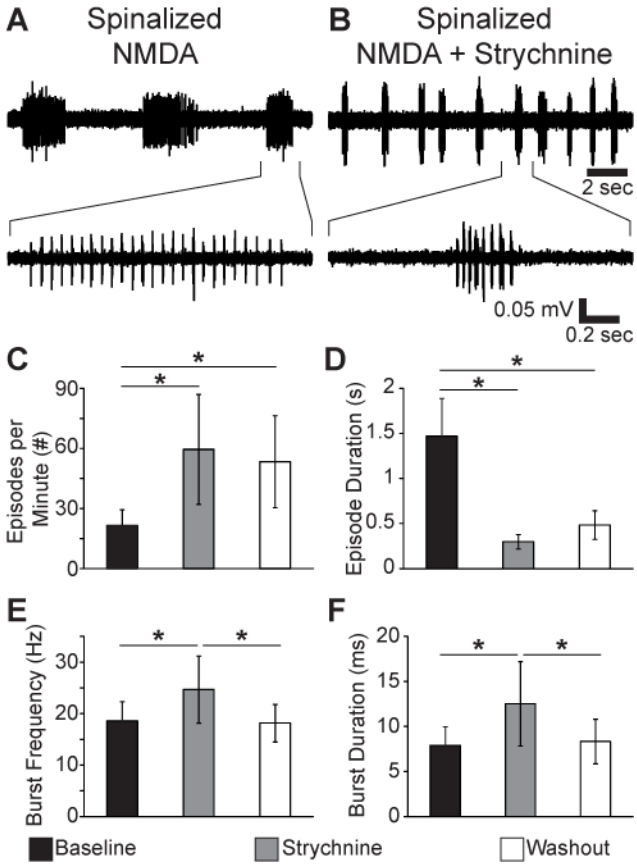

Figure 3.6 – Reduced Synaptic Inhibition Perturbs Spinalized Fictive Motor Output Without Disrupting Episodic Structure. (A-B) Representative traces of the fictive motor output from a representative spinalized larva in 50 μM NMDA (A) and following application of 1 μM Strychnine (B). Top traces are episodes of fictive motor activity; bottom traces show bursts in the indicated regions at a finer time scale. (C-F) Plots of episode frequency (C), episode duration (D), burst frequency (E) and burst duration (F) in Baseline (50 μM NMDA), Strychnine (50 μM NMDA, 1 μM Strychnine), and Washout (50 μM NMDA) conditions. * Statistically significant difference.

and motor rhythm stability (Fig. 3.7). Examining the traces of rostrocaudal delay in these spinalized preparations before and after application of strychnine did not reveal an obvious coordination defect (*n* = 6; Fig. 3.7A), however the vector sum analysis revealed a significant decrease in rostrocaudal phase consistency (One-

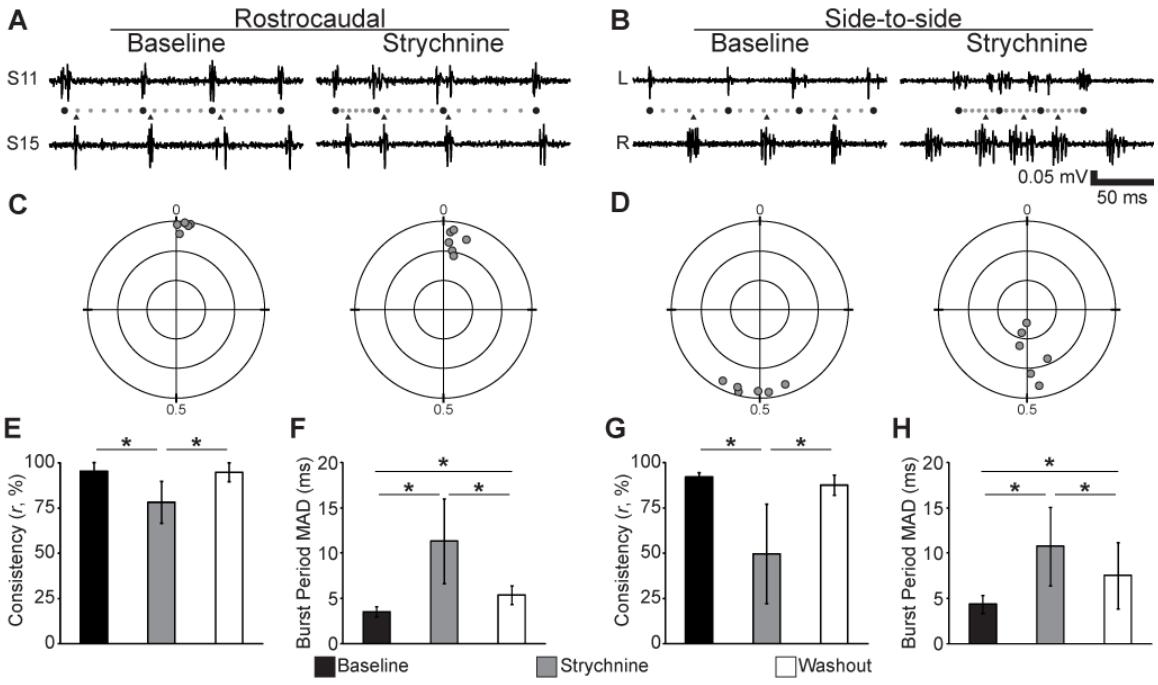

Figure 3.7 – Reduced Synaptic Inhibition Reversibly Reduces Both Rostrocaudal and Side-to-Side Phase Consistency. (A-B) Representative traces of fictive motor activity recorded on the same side of the spinalized larvae in different segments (A) or on opposite sides of the larva in the same segment (B). Within each panel, left traces are activity at baseline (50 μM NMDA) and right traces are the activity in the same larva following addition of 1 μM strychnine. (A) The relative phases of the bursts in the paired recordings are illustrated using circles (phase markers) and triangles (follower burst times). Black circles indicate burst times, smaller gray circles divide each burst period into 6 equally long intervals. (C-D) Polar plots of the normalized phase vector sum (gray circles) of each preparation in the experimental group indicated above the plot. Concentric circles are plotted at distances of 0.33, 0.66 and 1.0 from the fixed point; cross-hairs separate the quadrants. (E-F) Plots of mean phase consistency (*r*) and mean burst period MAD against condition for ipsilateral recordings. (G-H) Plots of mean phase consistency (*r*) and mean burst period MAD against condition for contralateral recordings. * Statistically significant difference.

way repeated measures ANOVA; $F_{(2,10)}$ = 16.7; p < 0.001; Fig 3.7C,E). There were more obvious changes in the burst structure of side-to-side alternation in strychnine, such as the overlap of bursts on contralateral sides of the body (n = 6; Fig. 3.7B). Strychnine caused a significant decrease in side-to-side phase consistency (One-way repeated measures ANOVA; $F_{(2,10)}$ = 15.0; p < 0.001; Fig. 3.7D,G). There were no significant differences in phase consistency between the baseline and washout (Corrected t-tests; all t < 0.52; all p > 0.62). The significant decreases in phase consistency of rostrocaudal delay and side-to-side alternation were accompanied by significant increases in burst period MAD (One-way repeated measures ANOVAs; all $F_{(2,10)}$ > 10.9; all p < 0.003; Fig. 3.7F,H). Strychnine had no significant effect on the mean rostrocaudal phase delay per segment or the mean phase of side-to-side alternation (One-way repeated measures ANOVAs; all $F_{(2,10)}$ < 2.7; all p > 0.11). Reducing inhibitory neurotransmission in spinalized larval zebrafish decreased both the phase consistency and stability of the motor rhythm, an effect like that of spinal transections, but without disrupting episodic organization.

Rostrocaudal Coordination is Impaired by Reduced Inhibitory Neurotransmission Independent of Motor Rhythm Stability

Reduced inhibitory neurotransmission resulted in the concurrent disruption of coordination and the stability of the fictive motor rhythm. In order to exclude the effect of an unstable motor rhythm as the cause of the decreased coordination, we considered a situation where locomotor bursts are produced in the absence

of an ongoing locomotor rhythm: the first burst of each episode of fictive swimming (Fig. 3.8A). The distribution of first burst rostrocaudal delays appeared to be broader in strychnine than at baseline or washout (Fig. 3.8B). We quantified variability of the first burst delay in the time domain by measuring the mean rostrocaudal delay and the MAD of the delay (Fig. 3.8C,D). There was no

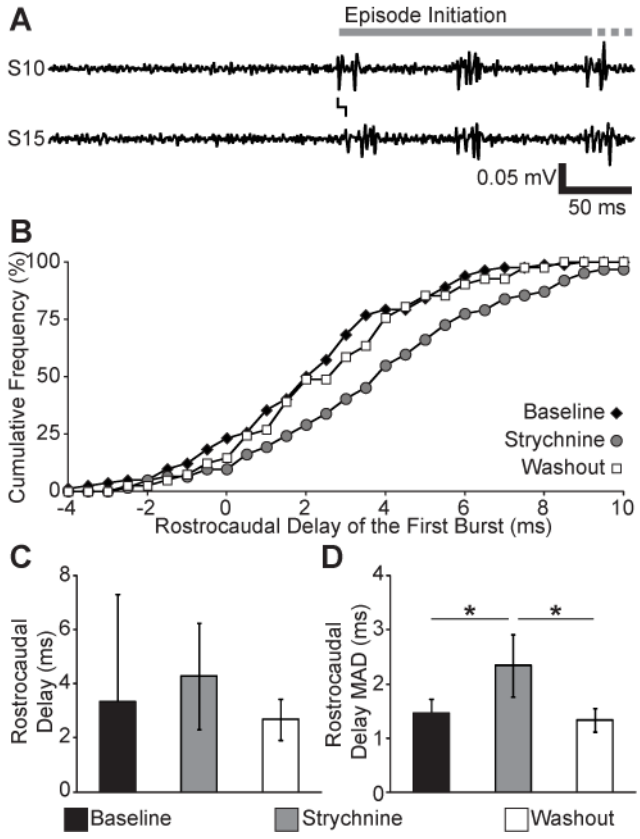

Figure 3.8 – Reduced Synaptic Inhibition Significantly Reduces the Consistency of the Rostrocaudal Delay of Episode Initiation. (A) Representative traces showing the initiation of an episode of fictive swimming in Baseline conditions (spinalized, 50 μM NMDA). The gray bar shows the time in the trace occupied by the episode, the line between the traces shows the rostrocaudal delay between the first burst in the PN recordings. This episode continued past the time window shown in the trace, reflected by gray dots. (B) Cumulative histogram of rostrocaudal delay for a representative preparation in Baseline (black diamonds), Strychnine (gray circles; 50 μM NMDA, 1 μM strychnine) and Washout (white squares; 50 μM NMDA) conditions. (C-D) Plots of the mean rostrocaudal delay (C) and the MAD of rostrocaudal delay (D) against condition. * Statistically significant difference.

significant effect of strychnine on the mean rostrocaudal delay of the first burst of each episode (One-way repeated measures ANOVA; $F_{(2,10)} = 0.94$; $p = 0.42$; Fig. 3.8C). There was a significant effect of strychnine on the MAD of the delay of the first burst of each episode (One-way repeated measures ANOVA; $F_{(2,10)} = 17.9$; $p < 0.001$; Fig 3.8D), due to increased variability in the strychnine condition (Corrected *t*-tests; all $t > 4.8$; all $p < 0.001$). There was no significant difference in rostrocaudal delay MAD between the baseline and washout (Corrected *t*-test; $t = 0.68$; all $p = 0.51$). Both the first-bust analysis and the phase vector sum of all bursts show the same effect of strychnine: decreasing the consistency of locomotor coordination. Because the disruption of rostrocaudal delay by strychnine is found in the absence of an on-going locomotor rhythm we conclude that the perturbation is not caused by an unstable locomotor rhythm, and therefore that strychnine disrupts coordination independent of disrupting episodic organization.

DISCUSSION

In this study we characterized the coordination of fictive motor activity produced by intact and perturbed larval zebrafish spinal cords. In spinalized preparations, this fictive motor output could be accurately described as “fictive swimming” because it retained the characteristics of larval zebrafish locomotion: episodic organization and coordination (Fuiman and Webb, 1988; Muller and Von Leeuwen, 2004; Figs. 3.1-3.4). Fictive motor output in reduced spinal cord preparations lacked episodic organization, and both the stability of the motor

rhythm and the consistency of rostrocaudal and side-to-side phase relationships were reduced (Figs. 3.1-3.4). Reduced phase consistency would make muscle forces add less efficiently on a cycle-by-cycle basis, weakening each tail stroke and likely impeding important survival behaviors. Therefore, we argue that phase consistency captures a behaviorally relevant aspect of swimming that is impacted by our experimental manipulations. Neither the lack of episodes nor the disruption of the motor rhythm was responsible for the decreased phase consistency (Figs. 3.7,3.8). This result is also not solely a function of the level of overall excitation, since 100 μM NMDA drove bursting at equal frequencies in all preparations (Fig. 3.2); a good proxy measurement for global excitation (Wiggin et al., 2012; Fig. 2.3). Instead, the transections appear to have directly disrupted the circuits controlling rostrocaudal delay and side-to-side alternation.

Coordination Relies on a Non-Segmental Circuit

The primary goal of these experiments was to determine which of two competing models (segmental CPGs or continuous gradient) of the spinal locomotor circuit better describe the larval zebrafish spinal cord. In the previous chapter, we demonstrated that rostrocaudal and side-to-side coordination were not impaired in reduced preparations of 12 or more spinal segments (Wiggin et al., 2012). Therefore we have not repeated these experiments, and in this chapter we have focused on transections that spare fewer (10 or 5) spinal segments in order to determine their effect on coordination. These transection experiments

demonstrated that fictive motor coordination diminishes as the number of intact spinal segments decreases (Figs. 3.3,3.4).

Rostrocaudal coordination between two adjacent segments does not depend solely on direct connections between the segments, and side-to-side coordination does not solely depend upon commissural connections between opposing hemi-segments. Instead, both rostrocaudal and side-to-side coordination depend on how much of the surrounding spinal cord is intact. This finding is especially surprising for side-to-side alternation, a process that could plausibly take place completely within a segment. The segmental CPG model could explain these data if each segmental CPG were perturbed so that they produced an unstable motor rhythm and intra-segmental coupling were too weak to entrain the outputs. Exploring this alternative hypothesis, we found that spinal transection compromised the stability of the motor rhythm (Figs. 3.3,3.4). However, we also found that spinal transections reduce phase consistency within hemi-segments (Fig. 3.5), which would not be predicted by a segmental model even when rhythm stability is compromised.

Based on these results, we conclude that the spinal locomotor network of the larval zebrafish is unlikely to consist of segmental CPGs. The reduction of coordination we observed is better explained by an unsegmented locomotor system, similar to models of the tadpole locomotor CPG (Wolf et al., 2009). In the computational model of the tadpole locomotor system, rostrocaudal delay of

motor neuron firing results from a non-segmental gradient of descending excitatory neurons and their synapses (Wolf et al., 2009). Removing the excitatory gradient and making the neuronal/synaptic density equal along the spinal cord results in a loss of rostrocaudal delay (Wolf et al., 2009). Using this paradigm, one would predict that a transection that removed many of these projection neurons from the circuit would reduce the strength of the synaptic gradient necessary to maintain a rostrocaudal delay.

The loss of side-to-side coordination that we observed following spinal transections (Fig 3.4) was not predicted by either the segmental or a gradient-driven model of the locomotor system (Grillner, 2006; Wolf et al., 2009). We hypothesize that the loss of side-to-side alternation following transection is due to the loss of commissural inhibition from neurons distributed throughout the spinal cord (Cowley and Schmidt, 1995; Hirata et al., 2005). There are four identified classes of commissural inhibitory interneurons in the larval zebrafish, of which only the CoSA and CoBL neurons are active during swimming (Liao and Fetcho, 2008). Both of these neuronal classes have long-range projections (~10 body segments) that would be disrupted by spinal transections. We hypothesize that even through CoBL neurons are relatively abundant, the overlapping projection fields of CoSAs and CoBLs distributed throughout the spinal cord are necessary to produce consistent side-to-side alternation.

Episode Generation and Coordination are Independent

One limitation of spinal transection experiments is that the degree of transection necessary to disrupt coordination also disrupts episode generation (Fig. 3.2; see also Chapter 2). Consistent with previous findings (Buss and Drapeau, 2001; Ljunggren et al., 2014), disrupting glycinergic neurotransmission does not disrupt episodic organization (Fig. 3.6). We found that strychnine has the effect of reducing the stability of the locomotor rhythm and reducing phase consistency of spinalized fictive motor output (Fig. 3.7). The coordination deficit revealed by phase vector addition of all bursts was recapitulated in an analysis of only the first burst of each episode, which eliminates the disruption of the locomotor rhythm as the cause of reduced coordination (Fig. 3.8). These results confirm and extend the results of our previous report (Wiggin et al., 2012), demonstrating that there is a dissociation between episodic organization and coordination. One caveat to these findings is the possibility that homeostatic processes following the elimination of inhibition may unmask mechanisms different from those that ordinarily drive locomotion (Moult et al., 2013), but we have no direct evidence that this is the case. A possible future direction of this research would be to use optogenetic tools (e.g., ArchT (Han et al., 2011)) to synaptically isolate regions of the spinal cord reversibly and with greater spatial resolution. An optogenetic approach, in addition to greater precision, would allow cell type selectivity based on neurotransmitter profile or projection pattern (Rabe et al., 2009; Ljunggren et al., 2014), and may reveal the topography of functional networks.

Conclusions

Our findings are inconsistent with larval zebrafish having a segmented locomotor CPG. These findings make it difficult to sustain the body segment as an important feature of the larval zebrafish locomotor system in the organization of the pre-motor network. Instead, both the present study and recent work on larval zebrafish pre-motor interneurons (Eklöf-Ljunggren et al., 2012; Bagnall and McLean, 2014; Ljunggren et al., 2014) suggest that the larval zebrafish CPG is an unsegmented network of microcircuits. Short-range connections between interneurons and from interneurons to motor neurons are almost certainly important features of this network, but the utility of describing these connections as “intra-segmental” is unclear.

We hypothesize that the larval zebrafish locomotor CPG is functionally segregated as follows: Episodes of locomotion are initiated and maintained by synaptic drive originating in the V2a neurons of the hindbrain (Arrenberg et al., 2009; Kimura et al., 2013). The spinal cord, despite its inability to initiate or maintain a locomotor episode, has an episode termination mechanism, demonstrated by the termination of episodes in spinalized larvae (McDearmid and Drapeau, 2006) and the modulation of episode duration at the spinal level (Lambert et al., 2012). The episode termination mechanism: 1) requires >12 intact segments of the spinal cord to effectively suppress motor output (Wiggin et al., 2012; Fig. 2.4), 2) has better performance when the circuit is strongly excited (Wiggin et al., 2012; Fig. 2.4), and 3) does not require glycinergic

neurotransmission (Fig. 3.6). Independent of episode generation, there are a collection of microcircuits that drive rhythmic motor output with appropriate phase relationships along the larvae. The coordination circuit is distributed throughout the spinal cord and requires ~10 intact segments to perform well (Fig. 3.3,3.4). The coordination circuit requires excitatory and inhibitory neurotransmission (Fig. 3.7). Spinal V2a neurons are likely one source of excitation in the coordination circuit (Bagnall and McLean, 2014; Ljunggren et al., 2014), and inhibition is likely supplied by both ipsilateral and contralateral projection neurons (Higashijima et al., 2004a; Liao and Fetcho, 2008).

The functional dissociation we find between burst period variability and coordination mirror functional dissociations of these properties between genetically defined ventral excitatory interneurons in the mouse spinal CPG (Dougherty et al., 2013). It is unclear to what degree the larval zebrafish and mouse CPGs share spatial organization. In the hindlimb region of the spinal cord, the properties of locomotor deletions are well explained by ipsilateral pattern-forming networks that coordinate the activity of flexor and extensor motor pools (McCrea and Rybak, 2008; Zhong et al., 2012). In contrast to an interdependent flexor-extensor network, some recent data support the existence of independent unit burst generators (UBGs) located adjacent to their motor neuron outputs (Hägglund et al., 2013). Even if the UBG hypothesis is correct in the lumbar region, conceiving of the mammalian spinal cord as a collection of equipotent UBGs distributed along the spinal cord would be an oversimplification (Cazalets,

2005). In contrast to a UBG architecture, we did not find evidence for coordination circuits adjacent to their axial motor output in the larval zebrafish. However, the finding that motor neuron activity is produced in all of our reduced preparations (Fig. 3.2) suggests that it is possible that localized motor circuits exist for functions other than episode generation and coordination. Regardless of the degree of conservation of specific neuronal structures between zebrafish and other animals, cross species comparisons are often instrumental in developing deeper understanding of each system (Marder and Goaillard, 2006).

CHAPTER 4: A POPULATION OF VENTRAL GLUTAMATERGIC INTERNEURONS (V3) IS NECESSARY FOR APPROPRIATE RECRUITMENT OF MOTOR NEURONS DURING FICTIVE LOCOMOTION

INTRODUCTION

Spinal locomotor circuits are present in all studied vertebrates (Chapter1, Fig. 1.1), but the neuronal mechanisms that drive locomotor output have been characterized only in a few axially locomoting species (Grillner and Wallen, 2002; Roberts et al., 2010). These neuronal circuits, often called Central Pattern Generators (CPGs), have resisted complete characterization in mammals for over a century (eg. Brown (1914)), while the CPGs of many invertebrate species have been thoroughly explored during the same time period (Marder and Calabrese, 1996). One reason for the greater degree of success in investigating invertebrate CPGs is the ability to identify interneurons with the same function and synaptic connectivity within and across animals (Bullock, 2000), which is a substantially more difficult task in vertebrates. Not coincidentally, the vertebrate species in which it has been most consistently possible to identify similar spinal cord neurons across animals (tadpole and lamprey) are also those with the best characterized locomotor CPGs (Grillner and Wallen, 2002; Roberts et al., 2010).

One relatively recent strategy for identifying comparable neurons and neuronal populations across animals in the vertebrate spinal cord is based on developmental gene expression (Stepien and Arber, 2008). The vertebrate spinal

cord develops from dorsoventrally-stratified neuronal progenitor cell domains, which subsequently develop into stratified neuronal populations with mutually exclusive gene expression markers (Briscoe et al., 2000). In dorsal to ventral order, the ventral neuronal populations that arise are: V0, V1, V2, Hb9/MN and V3 (Stepien and Arber, 2008; Kwan et al., 2009). Within the spinal cord, expression of *evx1*, *en1*, *chx10*, or *sim1*, is sufficient to identify a neuron as a member of the V0, V1, V2 or V3 interneuronal class, respectively (Briscoe et al., 2000; Lee et al., 2004). This tightly controlled gene expression profile makes it possible to transgenically target each neuronal population for perturbation and physiological characterization (e.g., Lanuza et al., 2004; Liao and Fetcho, 2008).

The neurons labeled by each developmental marker are frequently not homogeneous populations, but these markers have nevertheless led to a greatly refined understanding of the neuronal bases of locomotion, especially in the mouse (Table 1.2). In larval zebrafish, the functional properties of inhibitory V0 (Liao and Fetcho, 2008), V1 (Higashijima et al., 2004a) and excitatory V2a neurons (Eklöf-Ljunggren et al., 2012; Ljunggren et al., 2014; Menelaou et al., 2014) have been characterized (see also Table 1.3). One population that has not been thoroughly characterized in mouse or zebrafish are the V3 interneurons.

The V3 neurons are developmentally defined ventral-medial glutamatergic neurons with commissural projections (Zhang et al., 2008). The function of V3 neurons in mice has been explored using two genetic ablation strategies. In one

strategy, the genes encoding the axon guidance proteins DCC and Netrin are knocked out (KO) or mutated, greatly reducing the numbers of neurons that send an axon to the contralateral side of the spinal cord (Rabe et al., 2009). DCC KO mice have reduced contralateral projections from all neuronal populations while Netrin KO mice have a comparable reduction in all populations except for the V3 neurons (Rabe et al., 2009; Rabe Bernhardt et al., 2012). By comparing DCC and Netrin KO mice, it is possible to determine if there is a specific locomotor effect of *adding* commissural V3 signaling. NMDA-induced fictive locomotion in DCC KO mice (no V3 projections) lacks left-right coordination, while fictive locomotion in Netrin KO mice (intact V3 projections) has simultaneous left and right bursting (Rabe Bernhardt et al., 2012). This difference implies that V3 neurons provide timed excitatory drive to the contralateral spinal cord, but this timed activity is not sufficient to produce normal left-right alternation of motor output. An alternative genetic strategy is to selectively express a toxin in the V3 population, *subtracting* them from the network. Inhibition of synaptic release from the V3 neurons using tetanus toxin light chain disrupts left-right alternation during real and fictive locomotion and reduces locomotor robustness (Zhang et al., 2008). Finally, mouse V3 neurons express activity related genes following treadmill running and forced swim, indicating that the V3 neurons are more active than baseline when the animals are moving (Borowska et al., 2013). These results are consistent with the hypothesis that the V3 neurons provide timed excitation to the spinal network during locomotion. However, because neither the *in vivo* activity of V3 neurons during locomotion nor the effect of acute silencing

of V3 neurons has been observed in mouse or zebrafish, the role of V3 neurons in locomotion remains unclear. We hypothesize that the V3 neurons provide excitatory drive in the CPG, and the objective of this study was to characterize their functional role in the zebrafish spinal locomotor CPG.

The data presented in this Chapter are preliminary in nature, and therefore it is not possible to draw strong conclusions about the function of the V3 neurons. Our preliminary results show that it is possible to identify V3 neurons in larval zebrafish using the Tg(VGlut2:DsRed) and Tg(VGlut2:Gal4) transgenic lines. Consistent with a pre-motor excitatory population, the V3 neurons are numerous and present along the rostrocaudal extent of the spinal cord. The V3 neurons have dense, bilaterally projecting, local innervation of the ventral spinal cord and motor neuron region, and a proportion of the population has a descending projection. V3 neurons are active during stimulus-evoked fictive locomotion, but laser ablation of V3 neurons does not affect the properties of fictive locomotor output. The effect of the V3 neurons appears to be more subtle in zebrafish than in mice, and preliminary data suggest that V3 neurons promote appropriate recruitment of motor neurons at different locomotor frequencies.

MATERIALS AND METHODS

Generation of Larval Zebrafish

All procedures were approved by the Animal Care and Use Committee of the University of Minnesota Twin Cities. Wild type and transgenic adult zebrafish

(*Danio rerio,* Segrest Farms, Gibsonton, FL) were maintained as previously described (Wiggin et al., 2012, 2014). The transgenic lines used in these experiments were: Tg(VGlut2:dsRed) (Miyasaka et al., 2009), Tg(Nkx2.2a:GFP-CAAX) (Kucenas et al., 2008), Tg(VGlut2:Gal4) (Satou et al., 2013), and Tg(UAS:Kaede) (Scott et al., 2007). In-crossed and out-crossed transgenic larvae at 4 – 6 days post fertilization (dpf) were used in these experiments. Larval zebrafish were maintained in petri dishes filled with embryo water (60 µg/ml Instant Ocean® salt mix, Cincinnati, OH) and 0.005% Methylene Blue in a 28.5°C incubator with a 14:10 light:dark cycle.

Confocal Microscopy

In vivo fuorescent confocal microscopy of larval zebrafish was performed using a fixed-objective, upright microscope (Olympus FV-1000, Center Valley, PA). Larvae were anesthetized in zebrafish ringers solution (Wiggin et al., 2012, 2014) with 0.02% Tricaine (MS-222; Western Chemical, Ferndale, WA). Anesthetized larvae were embedded laterally in a fluorodish (World Precision Instruments, Sarasota, FL) filled with 1.5% low-melting point agarose in zebrafish ringers solution and covered with additional saline containing anesthetic. Photoconversion of Keade was performed using the bleach function of the FV-1000 to direct a 405 µm laser spot onto a Kaede-expressing cell targeted for conversion (5% laser intensity, 7 seconds, single pulse). The embedding procedure resulted in small variations in the orientation of the spinal cord such that the larvae were not precisely level and square with respect to the imaging

plane. Following confocal stack acquisition, Fiji (Schindelin et al., 2012) was used to rotate the image in order to correct these errors.

Soma Distribution Analysis

Quantification of the distribution of V3 cell bodies was performed using Fiji (Schindelin et al., 2012) and custom Matlab code (Mathworks, Natick, MA). Confocal microscopy was used to collect overlapping stacks of images documenting the expression of Tg(VGlut2:DsRed) and transmitted light morphology. Images were acquired at high magnification (40X / NA 0.8 objective) and a z-axis resolution of 1.3 μm. The fields of view in each stack overlapped with their neighbors by at least 10% of the width to permit accurate stitching, and included the full width of the spinal cord and dorsal root ganglia (DRG) in the field of view. The collection of stacks were stitched into a single 3-D image of the caudal hindbrain and spinal cord (Preibisch et al., 2009). The Fiji cell counter tool was used to identify the coordinates of all V3 neurons in the rostral 2 mm of the larval spinal cord (out of a total length of ~3 mm), the coordinates of the DRG neuron clusters, and the position of the dorsal and ventral edges of the spinal cord. The markers tracing the dorsal and ventral edges of the spinal cord were used to calculate local tangent lines to the dorsal and ventral edges of the spinal cord at the rostrocaudal position of each V3 neuron. The equation of a line perpendicular to the ventral tangent and intersecting the V3 neuron was calculated, which I will refer to as the “V3 plumb line.” The rostrocaudal distance of each V3 neurons was calculated as the distance along the ventral surface of

the spinal cord between the spinal cord/hindbrain junction (Segment 2/3 boundary (S2/3)) and the V3 plumb line intersection with the ventral surface. The dorsoventral height of the spinal cord at the location of each V3 neuron was calculated as the distance between the intersections of the V3 plumb line with the dorsal surface and the ventral surface, respectively. The distance of the V3 neuron from the ventral surface of the spinal cord was also measured along the plumb line. The z-axis position DRG neurons on each side of the spinal cord were used as boundary points of the lateral edges of the spinal cord, and a linear fit to the DRG neurons on each side of the animal was used to calculate the edges of the spinal cord at each rostrocaudal position in the imaging area. The midline slice and spinal cord width were calculated at the rostrocaudal position of each V3 neuron, along with the distance from midline of the V3 neuron.

Peripheral Nerve Recordings

Peripheral nerve (PN) recordings were performed and analyzed as previously described (Wiggin et al., 2012, 2014). In brief, the larvae were anesthetized, the skin was carefully removed from the recording region, and larvae were paralyzed with of 0.1 mM α-bungarotoxin (Tocris, Ellisville, MO) to prevent muscle contractions. The anesthetic was removed to allow the larvae to perform fictive behavior, and a suction electrode (tip diameter: 9-15 μm) was placed over the intermytomal cleft to record motor neuron axons. Fictive motor bursts were identified using custom Matlab code (Wiggin et al., 2012, 2014).

Calcium Imaging and Analysis

Calcium imaging was performed using Calcium Green 1 AM (Life Technologies, Grand Island, NY) loaded either into all spinal neurons (for V3 imaging experiments), or exclusively into motor neurons (for motor neuron recruitment experiments). A Calcium Green stock was made by dissolving 50 µg of dye in 20% Pluronic F-127, 80% DMSO (Life Technologies, Grand Island, NY) at a concentration of 0.25% weight/volume.

For imaging of V3 neurons, the Calcium Green stock was diluted 1:5 in zebrafish ringers solution, a small quantity of the working solution was pressure injected into the spinal cord of Tg(VGlut2:DsRed) zebrafish larvae, and the preparations were allowed to incubate for 1 – 2 hours. Following incubation, the larvae were prepared for PN recording and transferred to the stage of a confocal microscope. A field of view in which several V3 neurons were well labeled by the dye was selected for imaging, and a PN recording was acquired. Data were acquired in 10 second trials during which one electrical stimulation was delivered to the head of the larvae to evoke an episode of fictive swimming. Multiple trials (typically 4) were acquired for each field of view, with at least one minute between trials. Optical and electrophysiological data acquisition was synchronized by using the sync output of the microscope to trigger acquisition of the PN recording.

For imaging of motor neurons, the skin was removed from a region of a zebrafish larva, and Calcium Green stock was diluted 1:50 in zebrafish ringer solution and

bath applied to the exposed muscles of the larva. The Calcium Green was sequestered into motor neurons via the peripheral motor axons. Sensory neurons were not strongly loaded by this procedure, possibly because of damage to sensory processes during the removal of skin. Following a 1 hour incubation, the Calcium Green solution was thoroughly washed out using zebrafish ringers solution. Calcium imaging was performed using a QImaging Retiga Exi camera (Surry, BC, Canada) on a fixed-stage Olympus BX51 WI upright microscope. Confocal microscopy was not necessary for this experiment due to the efficient and specific loading of motor neurons. Data were acquired in 20 second trials during which a number of spontaneous and electrically evoked swimming episodes were recorded. Multiple trials (typically 10) were acquired for each field of view, with at least one minute between trials. Movement artifacts during data acquisition were corrected by registering frames from all trials to a common reference image (Preibisch et al., 2010). Optical and electrophysiological data were synchronized using the “Frame ON” TTL output of the QImaging camera.

Calcium imaging experiments were analyzed using Regions of Interest (ROIs) to separate the fluorescence signals from each cell in the field of view. The change in fluorescence as a percent of the mean baseline fluorescence ($\Delta F/F$) and the frame-by-frame signal to noise ratio (SNR, frame fluorescence divided by the standard deviation of the baseline frames) of the fluorescence were calculated for each trial of each cell. For motor neuron calcium imaging experiments, the most dorsal and most ventrally filled neurons in the field of view were used to

define the dorsoventral height of the motor column. Based on these boundaries, the motor column was divided into three bands of equal height: dorsal, intermediate, and ventral. A z-score was calculated for the ΔSNR of each cell in each frame and a cell was categorized as active during a fictive swimming episode if the z-score exceeded 2.5 during the episode (equivalent to a $p < 0.005$). The firing probability of the neuron was calculated for three frequency ranges: low (<35 Hz), mid-range (35 – 45 Hz) and high (>45 Hz). The frame rate of V3 calcium imaging data was not high enough to perform the z-score analysis. Instead, a T-test was used to compare the ΔF/F before and after electrically stimulating the larvae, a *p*-value of 0.05 was used to determine if each cell was active during the trial.

Laser Ablation of V3 Neurons

Acute ablation of the V3 neurons was performed using a Micropoint pulsed nitrogen pumped dye laser generating a 440 nm wavelength beam (Andor Technology, Belfast, Northern Ireland). Light was delivered via an Olympus BX51 WI microscope using a 60x / NA 1.0 water dipping objective lens. The laser was focused to apply maximal light intensity to the imaging plane of the microscope, the intensity of the laser was calibrated to produce a 4.5 – 5.0 μm hole in a mirror slide (this optimal intensity was determined empirically), and the x-y coordinates of the laser point in the field of view were indicated on a digital display. Three to six dpf zebrafish larvae were anesthetized in 0.02% Tricane in zebrafish ringers solution and embedded laterally in a gel composed of 3% methylcellulose and

0.02% Tricane in zebrafish ringers saline. A coverslip was placed over the gel and secured at the edges with agarose to stabilize the position of the larvae.

Laser ablation of V3 neurons was performed by positioning the microscope objective such that a neuron was in the x-y position at which the Micropoint laser was focused. Laser pulses were applied at 33 Hz for 10 seconds, a protocol that had been determined to destroy >95% of VGlut2:DsRed^{+} neurons (data not shown). Following the train of laser pulses, the microscope was repositioned to focus on another identified V3 neuron, and the protocol was repeated. Larvae were embedded for approximately 50 minutes in order to perform bilateral ablation of V3 neurons between S5 and S20 (Fig. 4.5), or 25 minutes to perform bilateral ablation of neurons between S12 and S18 (Fig. 4.6, 4.7). Sham control larvae were treated identically to V3 ablation larvae, but the x-y position of the laser was offset by 5 – 20 μm from each V3 cell, producing non-specific damage to neurons other than the V3 population.

Whole Cell Patch Recordings of Synaptic Currents

Whole cell patch clamp of motor neurons followed our published protocols (Masino and Fetcho, 2005). Briefly, larvae were prepared according to our PN recording protocol. Following skinning, trunk muscle was removed from a small region of the spinal cord. Motor neurons were targeted for patch clamp using differential contrast imaging (DIC) to identify the characteristic morphology of primary motor neurons. Since the goal of our whole cell patch experiments was

to measure synaptic currents, a patch saline of the following concentrations was used that inhibited intrinsic membrane currents: $CeMeSO_3$ (122 mM), HEPES (10 mM), Mg-ATP (4 mM), $MgCl_2$ (3 mM), EGTA (1 mM), QX314-Cl (1 mM), TEA-Cl (1 mM). Patch clamp electrodes had a tip resistance of approximately 12 MΩ, access resistance in whole cell configuration was 30-100 MΩ. The liquid junction potential of the patch saline and zebrafish ringers solution was calculated to be approximately +10 mV; the voltage clamp (VC) target potential was adjusted to compensate. Synaptic currents were measured using custom Matlab code.

Statistical Analysis

Statistical analysis of data was performed using two-sample t-tests, ANOVA tests, and least-squares linear regression. Statistical tests were carried out using SigmaPlot 12 software (SyStat Software, San Jose, CA) or Microsoft Excel (Microsoft, Seattle, WA). An α level of 0.05 was used to determine statistical significance. Data are reported as means and standard deviation.

RESULTS

V3 Neurons can be Identified in Larval Zebrafish Using the Tg(VGlut2:DsRed) Transgenic Line

In order to characterize the function of V3 neurons *in vivo*, it was necessary to reliably target the neurons for recording and perturbation. While there are no published transgenic zebrafish lines that specifically label neurons expressing *sim1a* (the zebrafish V3 marker), it is possible to infer V3 identity from their other

characteristics. V3 neurons proliferate ventral to the central canal and are glutamatergic (Zhang et al., 2008; Yang et al., 2010). In zebrafish, there is >90% overlap of vesicular glutamate transporter 2 (VGlut2) and *sim1a* expression in the ventral spinal cord at the embryonic stage (1.5 dpf) (Yang et al., 2010). However, it is possible that the embryonic ventral glutamatergic neurons migrate or are replaced by a non-V3 population between 1.5 dpf and the free-swimming larval stage (>3 dpf).

In order to test the hypothesis that the ventral VGlut2^{+} neurons observed at 4 – 6 dpf are V3 neurons, we measured the colocalization of Tg(VGlut2:DsRed) and Tg(Nkx2.2a:GFP-CAAX), a marker of p3 progenitor neurons (Briscoe et al., 2000; Schäfer et al., 2007; Fig. 4.1). At 4 – 6 dpf, Nkx2.2a expression was exclusively present ventral to the central canal (Fig.4.1A). The p3 domain of the

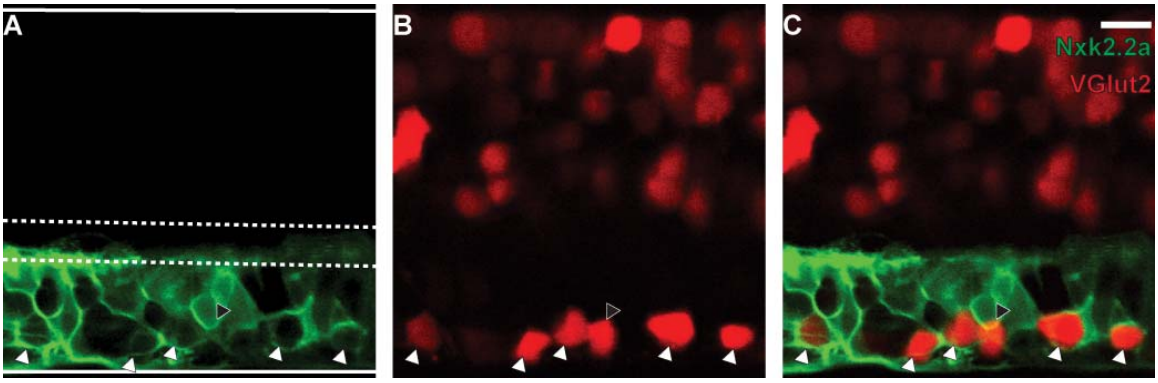

Figure 4.1 – Colocalization of Ventral VGlut2 and Nkx2.2a expression. A representative single confocal optical section of (A) Nkx2.2a:GFP-CAAX, (B) VGlut2:DsRed, and (C) a composite in the larval zebrafish spinal cord. The larva was mounted laterally, with dorsal up and rostral to the left. The boundaries of the spinal cord and central canal are illustrated by solid and dashed white lines, respectively, in panel A. White triangles indicate VGlut2^{+}/Nkx2.2a^{+} neurons and the black triangle indicates the only VGlut2^{+}/Nkx2.2a^{-} neuron in the field of view. Scale bar: 10 μm.

zebrafish spinal cord also produces Kolmer-Agduhr (KA) neurons (Yang et al., 2010), and likely other neuronal types, so it was not unexpected that there were more Nkx2.2a^{+} neurons than VGlut2^{+} neurons (Fig. 4.1 C). There was high overlap of ventral VGlut2^{+} neurons and Nkx2.2a^{+} neurons: 90% of VGlut2^{+} neurons ventral to the central canal were also positive for Nkx2.2a (*n* = 6 larvae, 162 neurons), and therefore confirmed to be V3 neurons. There was not a significant difference between the dorsoventral position of the VGlut2^{+} neurons that also expressed Nkx2.2a and those that did not (Two-sample T-test; $t = 1.6$; $p = 0.10$), so there was not a way to reliably segregate the VGlut2^{+} /Nkx2.2a^{+} neurons from the VGlut2^{+} /Nkx2.2a^{-} neurons in the Tg(VGlut2:DsRed) line without an additional transgene. However, the overwhelming majority of the VGlut2 neurons ventral to the central canal were confirmed to be V3 neurons, and the lack of confirmed transgene overlap in the remaining cells may be due to variegated transgene expression rather than the presence of a Non-V3 ventral glutamatergic neuronal population. Based on this experiment, we will treat the ventral VGlut2^{+} neurons as the V3 population, with the caveat that a small fraction may be misidentified.

V3 Neurons are Located in the Ventral-Medial Spinal Cord and are Distributed Along the Rostrocaudal Axis of the Spinal Cord

In mice, the V3 neurons migrate following differentiation to form spatially segregated dorsal and ventral populations that have different cellular properties and may be necessary for different behaviors (Borowska et al., 2013). In order to

determine if there are multiple populations of spatially segregated V3 neurons in zebrafish larvae, we used confocal microscopy to create 3-D reconstructions of the spinal cords of 4 – 6 dpf Tg(VGlut2:DsRed) zebrafish larvae (Fig. 4.2 A,B). The center of mass of each V3 neuron in the most rostral 2 mm of the spinal cord was tagged, and the distribution of the neurons within the spinal cord was calculated based on the imputed borders of the spinal cord (see *Methods*).

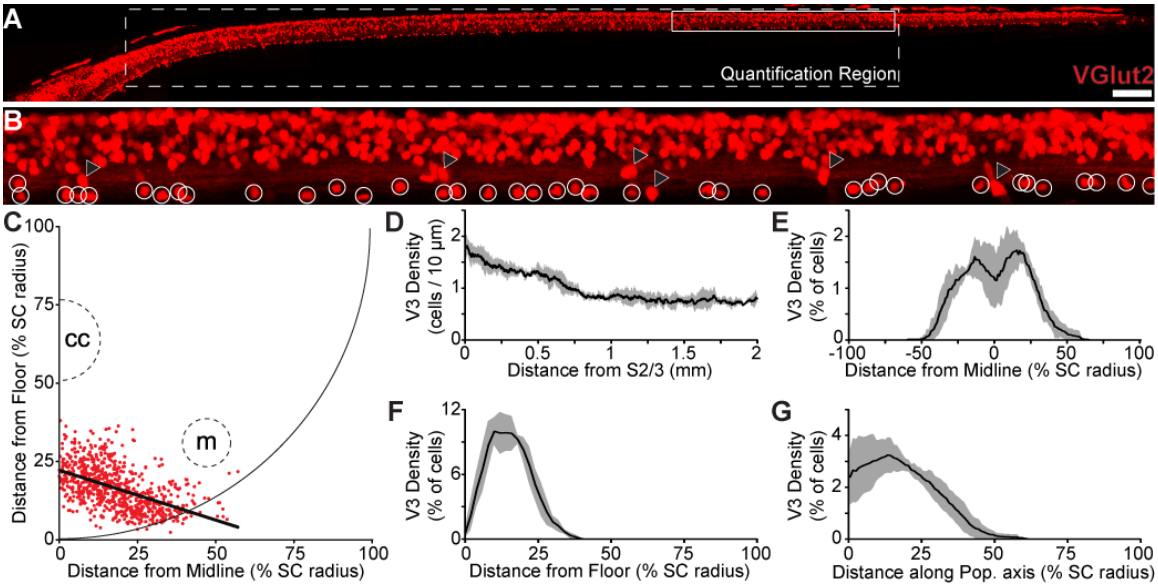

Figure 4.2 – Distribution of V3 Neuron Cell Bodies in the Spinal Cord. (A) Maximum intensity projection of a confocal stack of the spinal cord of a 5 dpf Tg(VGlut2:DsRed) zebrafish larva. The dashed white outline indicates the region of the cord in which cells were counted. The solid white outline is the region of the image shown at higher magnification in (B). (B) A higher magnification field of view. White circles indicate V3 neurons, black triangles indicate DRG neurons located lateral of the spinal cord. (C) Distribution of location of all quantified V3 neurons (red dots) projected in the coronal plane of the spinal cord. The outline of the spinal cord (solid grey line), as well as the location of the central canal (cc) and Mauthner axon (m) are indicated. The heavy black line indicates the line of best fit that best describes the axis of the V3 neuronal population. (D-G) The windowed moving average of V3 density along the rostrocaudal axis (D; window width: 250 µm), mediolateral axis (E; window width: 15% SC radius), dorsoventral axis (F; window width: 15% SC radius), and along the population axis illustrated on left (G; window width: 15% SC radius). Black lines are the mean, grey area indicates the standard deviation. SC: spinal cord. Scale bar: 100 µm (Panel A), 19 µm (Panel B).

Neurons in the far caudal spinal cord were not counted because the dimensions of the spinal cord taper to the extent that it was difficult to determine the location of the central canal and Mauthner axons. All of the neurons (*n* = 4 larvae; 797 neurons) were ventral to the central canal and almost all were medial of the Mauthner axon (Fig. 4.2 C). V3 neuron density is highest in the rostral spinal cord, but remains close to 1 cell per 10 μm high throughout the cord (Fig. 4.2 D). The V3 neurons are approximately 5 μm long in the rostrocaudal axis, so a density of ~1 cell per 10 μm is sufficient to thoroughly tile the ventral spinal cord. The V3 neuron population is a ventral-medial population, the majority of the cells are located in the most medial and most ventral 25% of the spinal cord (Fig. 4.2 E,F). There is no parasagittal plane through the spinal cord that is unoccupied by V3 neurons (Fig. 4.2E), so the V3 population may be considered a midline population. However, the density of neurons is not highest at the sagittal midline of the spinal cord, and when cell density is plotted along the population axis of the V3 neurons (Fig. 4.2C), the point of highest density is relatively far from the spinal cord midline (Fig. 4.2G). Because of this, I hypothesize that there are left and right populations of V3 neurons, but due to the tight packing of neurons in the ventral spinal cord, the populations contact and mingle on the spinal cord midline.

V3 Neurons Project Bilaterally and Have Descending Processes

Previous literature has described the ventral glutamatergic neurons as being members of the VeMe morphological class (Higashijima et al., 2004b). In order to

determine if this morphology is typical of V3 neurons, and to characterize the putative synaptic connectivity of the V3 neurons, I measured the 3-D morphology of individual V3 neurons using confocal microscopy (Fig. 4.3). The density of

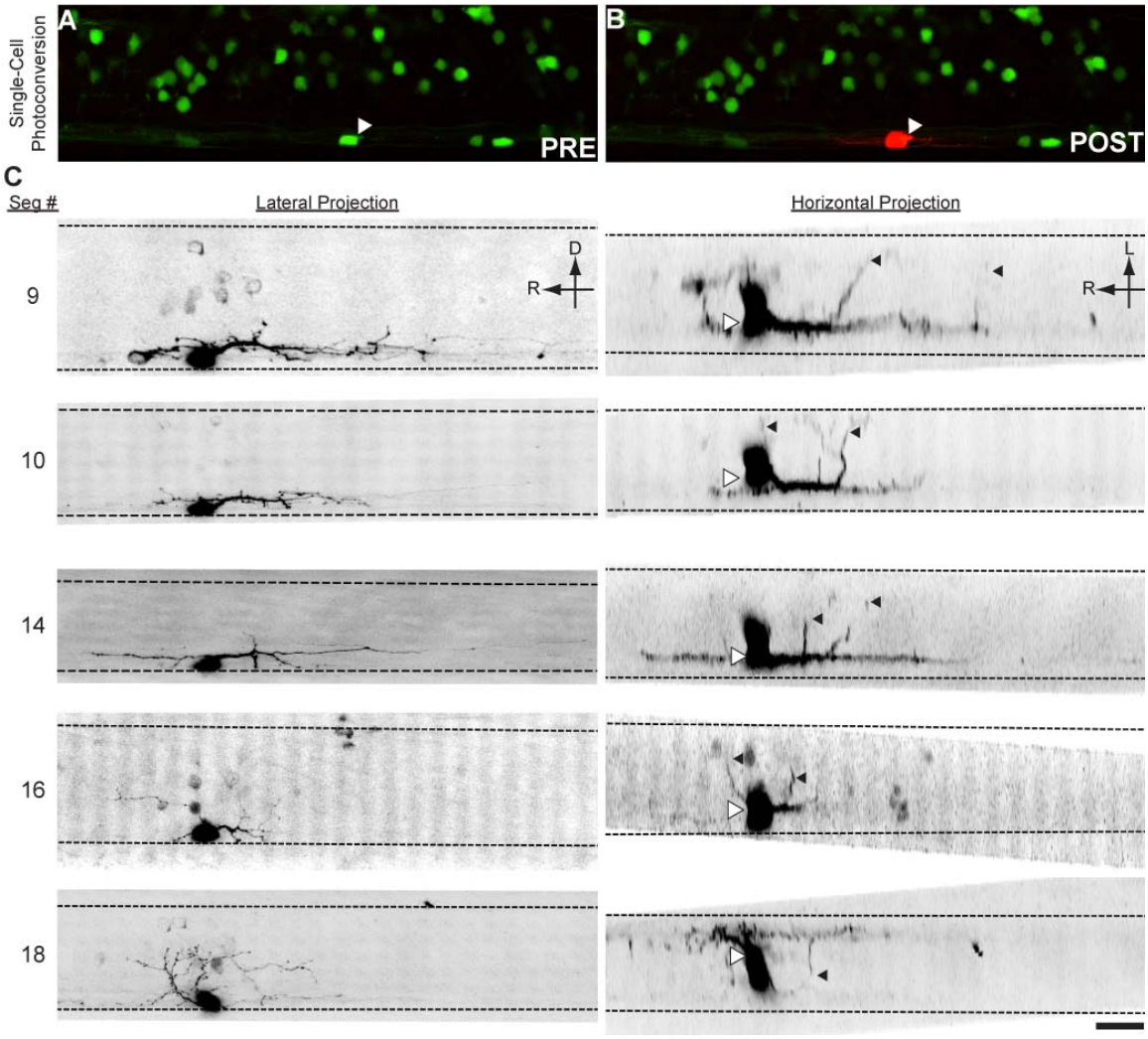

Figure 4.3 – V3 neurons are descending, bilaterally projecting cells. Kaede expression is driven in VGlut2+ neurons in VGlut2:Gal4/UAS:Kaede double transgenic larvae (A). A single neuron is exposed to UV laser light, converting the Kaede protein from green fluorescence to red (B). (C) Inverted contrast projections of Kaede-red fluorescence in 5 neurons. Each row of images is a neuron shown in a lateral/parasagittal projection (left) and horizontal projection (right). On the horizontal projections, the center of the cell body (white triangles) and contralateral projections (black triangles) are indicated. Lateral projections: Rostral left, dorsal up. Horizontal projections: Rostral left, lateral up. Scale bar: 20 μm.

DsRed fluorescence is too high in the Tg(VGlut2:DsRed) transgenic line to accurately trace the processes of a single neuron, so I used Tg(VGlut2:Gal4, UAS:Kaede) transgenic larvae to identify and photoconvert single V3 neurons (Fig. 4.3A,B). Following photoconversion, it was possible to obtain clear images of the full morphology of V3 neurons (*n* = 5 neurons, 4 larvae; Fig. 4.3C). Based on this preliminary sample of V3 morphology, it is clear that there is some variation in the projection pattern of the V3 neurons. For example, the V3 imaged in S10 had minimal projection density dorsal or rostral to the cell body, while the V3 neuron in S18 predominantly projected rostrally and dorsally (Fig. 4.3 C). Despite these differences, there are some common features of this initial sample of V3 morphologies. First, 5/5 cells have bilateral projections, but a higher density of processes ipsilateral to the cell body (Fig. 4.3 C, *right*). Second, 5/5 cells have the greatest density of processes close to the cell body and longer caudal projections than rostral projections (Fig. 4.3 C, *left*). Third, while the full extent of the processes of the S9 and S14 neurons is not presented in Fig. 4.3C, 5/5 V3 neurons had a maximum projection distance shorter than 300 μm. The projection pattern of the V3 neurons appears to innervate the ventral spinal cord, populated by V3 neurons, KA neurons and serotonin neurons (McLean and Fetcho, 2004; Yang et al., 2010), and the region of the spinal cord containing motor neurons and V2a interneurons (Eklöf-Ljunggren et al., 2012; Menelaou and McLean, 2012). This projection pattern is inconsistent with the morphology of VeMe neurons (Hale et al., 2001), evidence that the VeMes are a relatively uncommon subset of the ventral glutamatergic neurons.

The Majority of V3 Neurons are Active During Fictive Swimming

There is indirect evidence that a subset of V3 neurons are active during mouse locomotion (Borowska et al., 2013), but the activity of V3 neurons during fictive

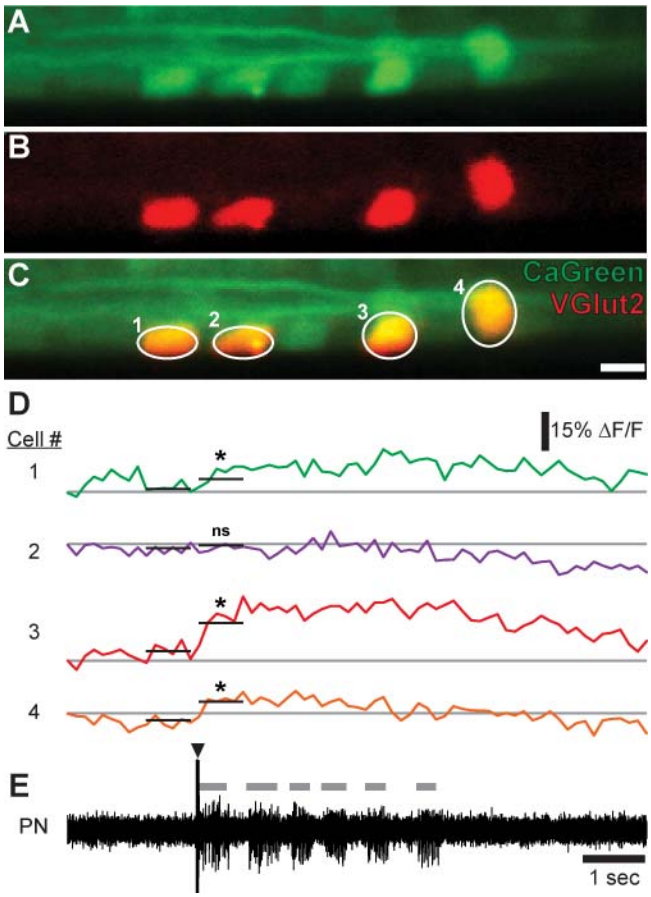

Figure 4.4 – V3 neurons are active during fictive locomotion. (A-C) Neurons in the spinal cord of VGlut2:DsRed were non-selectively filled with Calcium Green (A). V3 neurons were identified by VGlut2:DsRed expression and location (B), and dye-loaded V3 neurons were identified by overlay of the red and green channels (C). Each V3 neuron in the field of view was assigned a ROI (C). Synchronized recordings of Calcium Green fluorescence (D) and fictive swimming (E) were performed. Swimming-related neuronal activity was identified by testing for a significant difference in fluorescence between the 5 frames pre-stimulus v. 5 frames post-stimulus (black horizontal lines). (E) Swimming was induced with an electrical stimulation (stimulation artifact indicated by black triangle), which induced several episodes of swimming (gray bars). * Significant difference. Scale bar: 5 μm.

locomotion has not been measured. In order to test the hypothesis that the V3 neurons provide excitatory drive to the locomotor CPG, I measured the activity of the V3 neurons during fictive swimming using calcium imaging. Spinal neurons in 4 – 6 dpf Tg(VGlut2:DsRed) larvae were non-selectively loaded with Calcium Green 1 dye (*n* = 4 larvae; Fig.4.4 A-C). The activity of V3 neurons and fictive motor output following electrical stimulation of the larvae was measured via simultaneous confocal imaging and peripheral nerve recording (Fig. 4.4 D,E). Across all animals and trials, 78% (21/27) of V3 neurons were active during at least one episode of fictive swimming. The design of the experiment cannot distinguish neurons without swim related activity from those that were active but not sufficiently filled with dye to show changes in fluorescence, so 78% should be treated as a lower bound of the true proportion of V3 neurons that have swimming-related activity. Among the V3 neurons that showed activity, the neurons were active during 61% (45/74) of swimming episodes. The signal-to-noise ratio of bulk-loaded Calcium Green 1 AM was relatively low in the V3 neurons, and as above, this activity estimate should be considered a lower bound on the true recruitment probability.

Laser Ablation of V3 Neurons has no Effect on the Properties of Fictive Swimming

The previous experiments demonstrated that the V3 neurons have morphology, neurotransmitter expression, and activity consistent with providing excitatory drive to the locomotor CPG, but did not demonstrate the function of the V3

neurons or their necessity for behavior. In order to determine which features of fictive swimming require V3 activity, I performed laser ablation of a large percentage of the V3 neuron population and measured fictive swimming. Three experimental groups were used: 1) The V3 ablation group, in which all V3 neurons on both sides of the spinal cord between S5 and S20 were laser ablated (*n* = 6 larvae; 145(SD 9.6) neurons per larva). A representative example of laser ablation effectiveness in a restricted region is shown in Fig. 4.5 A,B. 2) The sham ablation, in which laser pulses were delivered 5 – 20 μm rostral to each V3 cell body (*n* = 6 larvae; 130(SD 10.8) sham targets per larva). 3) The unmanipulated control group was not embedded or exposed to laser pulses (*n* = 6 larvae).

The day following laser ablation or sham, the fictive swimming of each larva was measured using PN recordings (Fig. 4.5 C-E). The features of fictive swimming measured did not significantly differ between unmanipulated, sham and ablation experimental groups in spontaneous (slow) swimming (One-way ANOVAs; all $F < 1.3$; all $p > 0.29$; Fig. 4.5 C), or spinalized, NMDA-induced swimming (One-way ANOVAs; all $F < 2.9$; all $p > 0.08$; Fig. 4.5 E). One parameter of electrically-evoked (fast) swimming, mean burst frequency, reached nominal statistical significance (One-way ANOVA; $F = 3.8$; $p = 0.047$; Fig. 4.5 D), but correction for multiple hypothesis testing eliminates the significance of this trend.

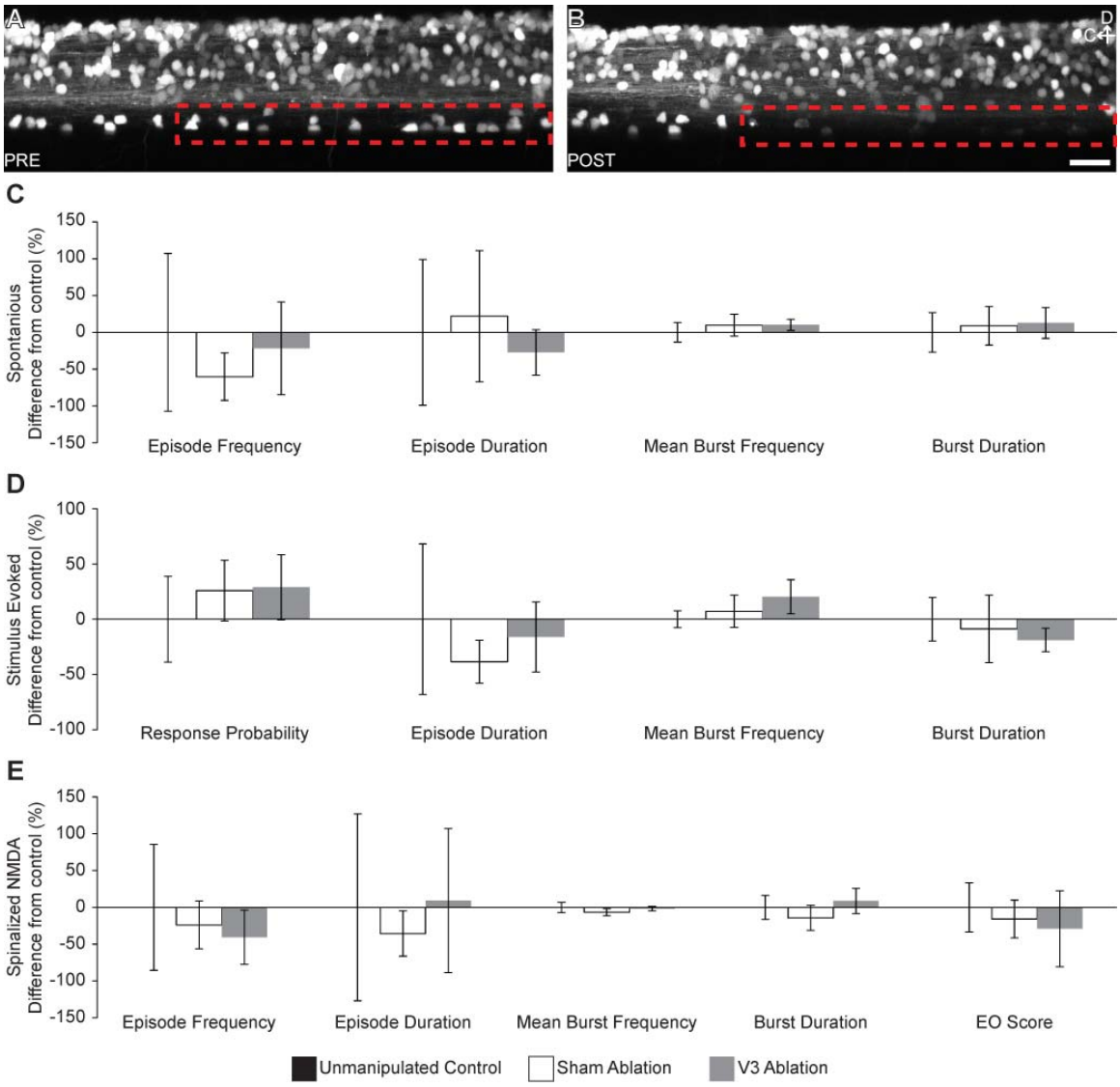

Figure 4.5 - Ablation of V3 Neurons does not Affect the Properties of Fictive Swimming. (A,B) Confocal stacks of the same VGlut2:DsRed zebrafish larva before (A) and 12 hours after (B) laser ablation of the V3 neurons in the region indicated (red dashed lines). (C-E) Plots of the p
roperties of fictive swimming in unmanipulated control larvae, sham ablation larvae, and V3 ablation larvae. Data are presented as percent change from unmanipulated control, so only the error bars are visible for this group. Spontaneous (C), stimulus evoked (D), and Spinalized, NMDA (E) induced fictive swimming were measured.

Laser Ablation of V3 Neurons Reduces the Firing Probability and Frequency-Dependent Recruitment of Motor Neurons

One limitation of PN recordings is that they only capture the activity of the subset of the neurons that innervates the intermyotomal cleft, a population of ventrally located, low-threshold motor neurons (Menelaou and McLean, 2012). Perturbation of other motor neuron populations, such as the high-threshold, dorsal motor neurons, would not affect fictive motor output as measured by PN

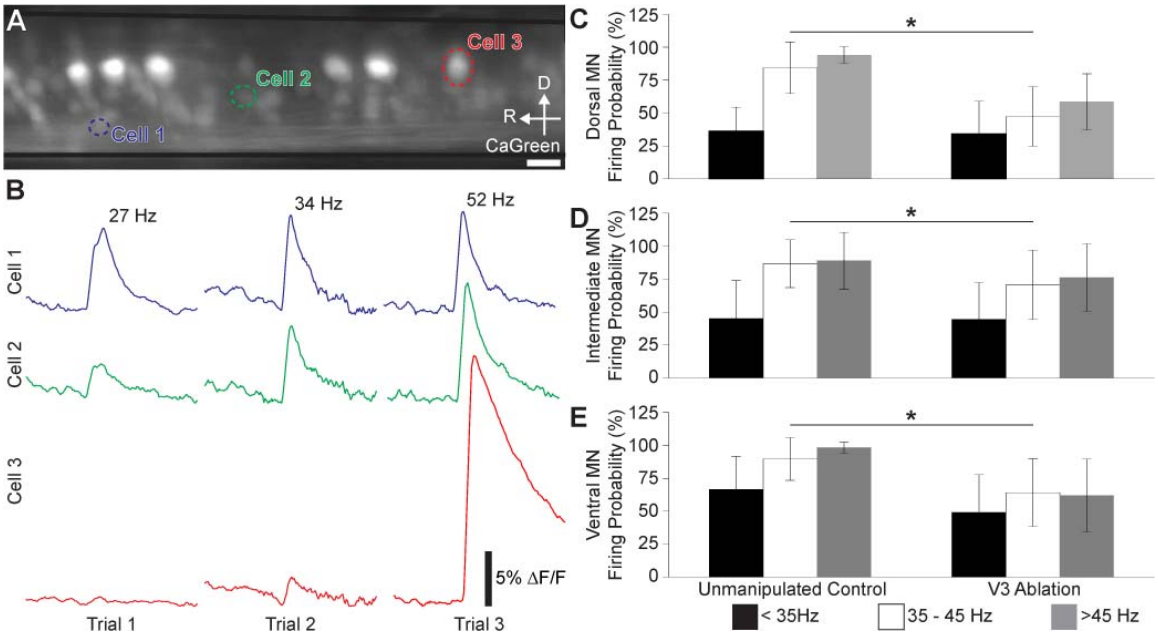

Figure 4.6 - Laser Ablation of V3 Neurons Reduces the Firing Probability and Frequency-Dependent Recruitment of Motor Neurons. (A) Epiflurescent image of motor neurons loaded with Calcium Green 1 AM. ROIs surround three neurons: a ventral motor neuron (Cell 1; blue), an intermediate motor neuron (Cell 2; green), and a dorsal motor neuron (Cell 3; red). Black lines indicate the dorsal and ventral borders of the spinal cord. (B) Calcium signal ΔF/F for each cell indicated in (A). The activity of the cell is shown during a low speed fictive swimming episode (27 Hz peak burst frequency; left column), a mid-range episode (34 Hz peak; center column), and a high speed episode (52 Hz peak; right column). (C-E) Plots of the firing probability for motor neurons in the dorsal (C), intermediate (D), and ventral (E) regions of the motor pool. Scale bar: 10 μm. * Statistically significant difference.

recordings. Therefore, a different recording technique, calcium imaging, was used to monitor the activity of the motor neuron population during fictive locomotion (Fig. 4.6). Motor neurons in unmanipulated control and V3 laser ablation zebrafish larvae were loaded with Calcium Green 1 AM dye via the peripheral motor nerves (*n* = 1 control larva, 39 imaged neurons; 2 ablation larvae, 60 imaged neurons; Fig. 4.6 A). Motor neuron calcium signal and fictive motor output (PN) were recorded during both stimulus evoked and spontaneous fictive swimming. Larval zebrafish motor neurons are recruited with increasing probability with increasing fictive burst frequency (McLean et al., 2007), but the kinetics of Calcium Green 1 are slow relative to the speed of larval zebrafish locomotion, so it was not possible to measure motor neuron activity during each cycle of fictive locomotion. Instead, the peak burst frequency of each episode was used as a measure of the recruitment potential for the episode as a whole. The activity of each motor neuron was measured in each episode (Fig. 4.6 B), and the data were subdivided based on the properties of the episode and motor neuron locations. Episodes were divided into three categories based on peak burst frequency: low frequency (<35 Hz), mid-range (35 – 45 Hz) and high frequency (>45 Hz). The motor neuron region was split into 3 equal-height regions: dorsal, intermediate, and ventral, and neurons were assigned to a category based on the location of the center of the cell. The recruitment probability for neurons in each spatial region and in each frequency domain was calculated (Fig. 4.6 C-E). Laser ablation of V3 neurons had the main effect of significantly decreasing the firing probability of motor neurons in all three spatial

regions (Two-way ANOVA; all F > 3.9; all $p < 0.05$). There was also a significant main effect of frequency-dependent recruitment; firing probability increased with peak burst frequency in all three spatial domains (Two-way ANOVA; all F > 8.7; all $p < 0.001$), consistent with previous reports (McLean et al., 2007). Finally, there was a significant interaction of experimental group and recruitment in the dorsal region (Two-way ANOVA; F = 6.1; $p < 0.004$), due to weaker frequency-dependence changes in firing probability in the V3 ablation group. In summary, V3 ablation has the effect of reducing the reliability of motor neuron firing during locomotion, and decreasing the recruitment of dorsal motor neurons during medium and high frequency fictive swimming.

Laser Ablation of V3 Neurons Reduces the Correlation Between Fictive Swimming Burst Frequency and Excitatory Synaptic Drive

In order to explore the mechanism for disruption of frequency-dependent recruitment of motor neurons following V3 ablation, I performed whole cell patch recordings of motor neurons in control and V3 ablated zebrafish larvae ($n = 4$ per group). The patch saline contained fluorescent dye to confirm neuronal targeting (Fig. 4.7 A), and channel inhibitors to suppress the intrinsic membrane currents of the patched neuron (see *Methods*). Neurons were voltage clamped to the reversal potential of glycenergic receptors (-90 mV), isolating only the glutamateric and electrical synaptic inputs. Simultaneous voltage clamp and PN recordings were performed to measure the burst-frequency dependent excitatory synaptic inputs to the motor neurons (Fig. 4.7 B,C). In control larvae, there is a

strong correlation between burst frequency and peak phasic excitatory synaptic drive (Fig. 4.7 D), consistent with previous reports (Kishore et al., 2014). In contrast, there was no apparent correlation between burst frequency and synaptic drive in the motor neurons of V3 ablation larvae (Fig. 4.7 E). The

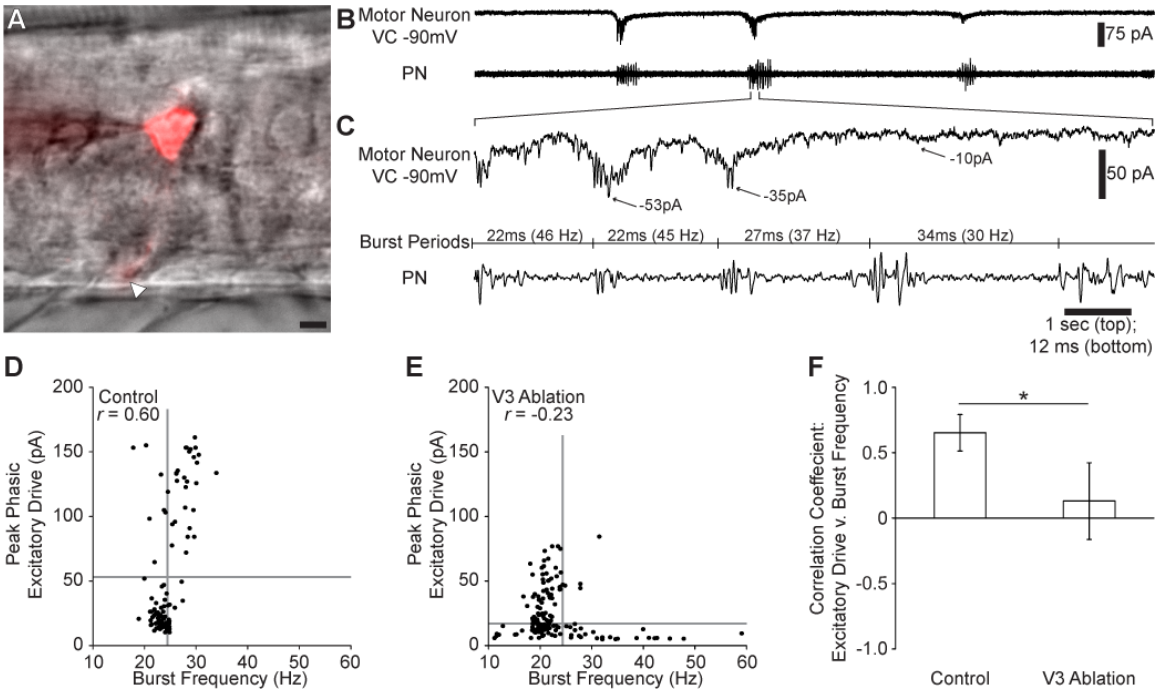

Figure 4.7 – Ablation of V3 neurons disrupts correlation between swimming burst frequency and excitatory pre-motor drive. (A) Motor neurons were patched and filled with fluorescent dye for identification based on soma position and the presence of an axon leaving the spinal cord (white triangle). Scale bar: 5 μm (B,C) Simultaneous recordings of motor neuron synaptic currents (top trace of each pair) and a peripheral nerve recording (bottom trace of each pair). (B) Each fictive swimming episode is accompanied by inward synaptic currents. (C) The indicated region of (B) on a fine time scale. The peak phasic synaptic drive for each burst (arrows) and the respective burst period are indicated. (D,E) Plots of the correlation between peak excitatory synaptic drive and the burst frequency for each burst in a representative control (D) and V3 ablation (E) larva. Each point is a single burst, the horizontal and vertical gray lines indicate the mean peak phasic excitatory drive and burst frequency, respectively. (F) Plot of the mean correlation between burst frequency and phasic excitatory drive for control and V3 ablation larvae. * Statistically significant difference.

correlation coefficient between instantaneous burst frequency and peak excitatory synaptic drive is significantly lower in V3 ablation larvae than in unmanipulated control larvae (two-sample T-test; $t = 3.2$; $p = 0.02$; Figure 4.7 F).

DISCUSSION

In this study I performed a preliminary characterization of the potential roles of V3 neurons in the larval zebrafish locomotor CPG. The V3 population can be identified, with some caveats, using the Tg(VGlut2:DsRed) and Tg(VGlut2:Gal4) transgenic lines (Fig 4.1). The V3 neurons are a numerous ventromedial population distributed across the rostrocaudal axis of the spinal cord (Fig 4.2). The V3 neurons project to both sides of the spinal cord, with a richer innervation of the ipsilateral side of the spinal cord (Fig. 4.3). Unlike other characterized zebrafish CPG neurons (Higashijima et al., 2004a; Menelaou et al., 2014), the V3 neurons do not extend lengthy processes rostrally or caudally. Instead, they appear to send local, dorsal projections into the region of the spinal cord containing motor neurons and V2a interneurons (Eklöf-Ljunggren et al., 2012; Menelaou and McLean, 2012), and some neurons have ipsilateral descending processes extending less than 300 μm. In this preliminary dataset, there are several different V3 projection patterns (Fig. 4.3 C). The observed diversity of cell morphology is confounded by ongoing development in the nervous system, and the rostrocaudal developmental gradient (Cole and Ross, 2001). Further experiments are necessary to clarify if these morphologies represent distinct V3 sub-types, developmental stages of a single morphological family, or regional

specializations of the V3 neurons. One potentially informative experiment would be to photoconvert individual V3 neurons at a pre-free swimming developmental stage (i.e., 2 dpf) and observe the growth of the V3 neurites over several days. It is also important to characterize the sites of vesicular release on the V3 processes to determine the putative input and output regions of the neurons (Menelaou et al., 2014).

The majority of V3 neurons were found to be active during fictive swimming using our experimental design (Fig. 4.4), but there are several caveats to this finding. First, the quality of the calcium signal was low, increasing the probability of Type II errors during data analysis, and potentially masking swim related V3 activity. Second, only stimulus evoked (fast) fictive swimming was observed, and burst frequency is extremely important to the recruitment properties of other excitatory pre-motor interneurons (McLean et al., 2008). Third, if the V3 neurons are a heterogeneous population, bulk loading the spinal cord does not facilitate identification of the active V3 sub-types. A future experiment that would clarify these issues would use the Tg(VGlut2:Gal4) transgenic line to drive expression of a genetically encoded calcium indicator, such as GCaMP6 (Chen et al., 2013), in a small subset of neurons (Downes et al., 2002). With sufficiently sparse labeling of VGlut2-expressing neurons, it would be possible to characterize the activity and structure of neurons without using photoconvertible proteins. It may also be possible to use a higher density of GCaMP6 expressing neurons if co-

expressed with a red to far-red photoconvertable protein (Subach et al., 2011), but these proteins have not been tested in zebrafish.

Given the importance of V3 neurons for mouse locomotion (Zhang et al., 2008), it was surprising that laser ablation of V3 neurons in larval zebrafish had no effect on the features of fictive motor output measured in this experiment (Fig. 4.5). One interpretation of this finding is that PN recordings in larval zebrafish are not truly comparable to ventral root recordings in mice because of the heavy subsampling of motor neuron subtypes in PN recordings, and V3 neurons may have a conserved function in both species. Another interpretation is that despite similarities in gene expression and neurotransmitter profile, pre-motor interneuron function is divergent between axial and tetrapod locomotion. The latter argument has been advanced regarding the V2a interneurons (Dougherty and Kiehn, 2010; Dougherty et al., 2013); the different effects (or lack thereof) of V3 ablation in zebrafish and mice may be a second example of the trend. An important difference between the current study and mouse knock out experiments is the mechanism of ablation. In the current study, V3 neurons were ablated acutely, and little time was given for circuit compensation. In the mouse experiments, on the other hand, V3 neurons were ablated or silenced chronically (Zhang et al., 2008; Rabe Bernhardt et al., 2012), leaving opportunity for developmental changes. Acute silencing experiments using optogenetics could be performed in both species (Arrenberg et al., 2009; Hägglund et al., 2013), and

may demonstrate that this difference between species is due to the experimental manipulation rather than the underlying neural circuit.

The effects of V3 ablation observed in this study were an overall reduction in motor neuron recruitment and the loss of burst-frequency dependent recruitment (Fig. 4.6), presumably through the reduction in burst-frequency correlated excitatory synaptic input (Fig. 4.7). This finding is somewhat surprising because both the V2a pre-motor circuitry and intrinsic membrane properties of motor neurons promote a ventral to dorsal motor neuron recruitment order (Menelaou and McLean, 2012; Ampatzis et al., 2014). Furthermore, it does not seem likely that the V3 neurons are necessary for V2a activity, because perturbation of V2a neurons alters fictive burst frequency (Eklöf-Ljunggren et al., 2012), and we do not observe this effect following V3 ablation. Counterintuitively, dorsal motor neurons have both the highest spike threshold and receive synaptic drive from the smallest number of V2a neurons (Menelaou and McLean, 2012; Menelaou et al., 2014). In this study, V3 ablation has the strongest effect on the recruitment of dorsal motor neurons (Fig. 4.6), and the majority of the neurons patched for recording of synaptic drive were dorsal motor neurons (data not shown). I hypothesize that the net V2a synaptic drive to dorsal motor neurons is not strong enough to consistently drive them to firing threshold during the temporal window for burst activity, and the V3 neurons act to boost the phasic synaptic drive. This function would be consistent with activity of V3 neurons during fast swimming (Fig. 4.4), but predicts that V3 neurons would be recruited in a burst frequency

dependent fashion. This hypothesis does not explain the presence of bilateral projections from the V3 neurons (Fig. 4.3), but it may be that the contralateral projections are dendritic, and the V3 neurons only excite ipsilateral motor neurons. An alternative hypothesis is that the V3 neurons provide excitatory drive specifically to high burst frequency V2a neurons, and these neurons are hypoactive in V3 ablation larvae. This hypothesis could be distinguished from the direct pre-motor hypothesis by measuring depolarization of V2a and motor neurons following optogenetic activation of V3 neurons. A third hypothesis is that the V3 neurons provide excitatory drive to spinal neuromodulatory neurons (McLean and Fetcho, 2004), and the effects of V3 ablation on motor neuron activity and synaptic drive are due to lack of neuromodulatory tone. This hypothesis could be tested by performing an ablation of the spinal neuromodulatory cells directly, and observing the effect on motor neuron recruitment.

The current study provides a promising glimpse into the function of the V3 neurons, but requires additional experiments in order to make conclusions regarding their role. The suggested role, providing excitatory drive to high threshold motor pathways, is important for determining the outcome of predator-prey interactions (Domenici and Blake, 1997). These interactions cannot be simulated and evaluated convincingly with immobilized larvae and fictive swimming using current techniques, and the negative results of our fictive swimming experiments (Fig. 4.5) suggest that developing richer behavioral

paradigms will be important for characterizing the function of spinal motor circuits.

CHAPTER 5: CONCLUSION AND FUTURE DIRECTIONS

This research has addressed two fundamental unknowns in the characterization of the larval zebrafish locomotor circuit. First, the lack of an empirically supported high-level model of the locomotor CPG undermined the formulation of clear hypotheses about the function of spinal interneurons. Second, the properties of larval zebrafish swimming are not fully accounted for by the functions of characterized spinal interneurons. In this Dissertation, I have described a framework for approaching research on the vertebrate locomotor CPG (Chapter 1), tested models of the higher-level organization of the zebrafish locomotor CPG (Chapters 2 & 3) and characterized the function of a poorly understood interneuron population (V3 neurons; Chapter 4). In this final chapter, I will more fully describe a high-level model of the function of the larval zebrafish locomotor CPG, describe the role of the V3 neurons in terms of the behavioral features they support, and propose future directions for research on larval zebrafish locomotion.

High-Level Functional Organization of the Larval Zebrafish Locomotor Network

In spite of recent advances in characterizing pre-motor interneurons in larval zebrafish (Ampatzis et al., 2014; Bagnall and McLean, 2014; Kishore et al., 2014; Ljunggren et al., 2014; Menelaou et al., 2014), there is still a lack of synapse-level information on interneuron interactions, making any proposed circuit diagram of the locomotor CPG reliant upon assumptions of homology or

unsupported hypotheses. In the absence of detailed, synaptic-level information, it is helpful to have a higher level understanding of how the locomotor circuit works. Higher level descriptions provide a starting place for formulating and rejecting hypotheses, and a template into which more detailed synaptic data can be placed. At the most abstract level of description, the larval zebrafish spinal cord transforms simple inputs into a spatially patterned output via a robust, spatially distributed circuit.

The inputs to the spinal circuit are simple because at the larval stage there are a limited number of projection neurons from the brain to the spinal cord. According to one estimate, there are only 200 descending fibers carrying information from the brain to the spinal cord (Budick and O'Malley, 2000). Of these fibers, approximately 60 are serotonergic (McLean and Fetcho, 2004) and >30 are dopaminergic (Lambert et al., 2012). So, according to the estimate of Budick and O'Malley (2000), there are only 100 descending fibers carrying all of the fast synaptic communication between the brain and spinal cord. Even if this number is an underestimate by a factor of 2, the information carrying capacity of this number of fibers is still relatively limited when compared with the complexity of the motor outputs produced by larval zebrafish.

This limited number of fibers initiate and maintain locomotor activity in the spinal cord (Arrenberg et al., 2009; Kimura et al., 2013), act as command-like neurons for specialized behaviors (e.g., escape (Liu and Fetcho, 1999)) and set the speed

and turning angle of swimming episodes (Huang et al., 2013; Severi et al., 2014; Thiele et al., 2014; Wang and McLean, 2014). Controlled turning in larval zebrafish (in contrast to high amplitude, escape-like turning) is due to the summation of a single turn movement superimposed on a routine swim episode (Trivedi and Bollmann, 2013), and the turn command-like neurons are not necessary for descending drive to the swimming CPG (Huang et al., 2013). The only known fast synaptic signal from the brain to the spinal swimming CPG, distinct from other behavioral circuits, is an “ON” signal with an intensity dial (Arrenberg et al., 2009; Kimura et al., 2013; Wang and McLean, 2014).

This simple input is transformed into a tightly regulated pattern of bilateral alternation and rostrocaudal progression of activity by the spinal locomotor CPG. The goal of the work presented in Chapters 2 & 3 of this dissertation was to determine if the spinal locomotor network was segmentally organized or not. The results of both the experiments presented here, as well as recent reports (Eklöf-Ljunggren et al., 2012; Bagnall and McLean, 2014; Ljunggren et al., 2014), instead suggest that the larval zebrafish CPG is an unsegmented network of microcircuits. This network has three main functions: terminate episodes after a period of time set by the neuromodulatory tone and level of excitation (Lambert et al., 2012; Wiggin et al., 2012), maintain side-to-side alternation of activity at 50% phase, and maintain rostrocaudal progression of activity at 3% phase/body segment, all at a wide range of burst frequencies (Masino and Fetcho, 2005; Wiggin et al., 2014). The episode termination mechanism is not segmental and is

functionally independent of the burst-phase setting (or coordination) mechanisms (Chapter 2). The coordination circuit is also not segmental, and phase-setting of rostrocaudal delay and side-to-side alternation appear to depend on shared neuronal mechanisms (Chapter 3).

Limitations of Our Experimental Paradigm in Evaluating the Effect of Perturbing V3 Neurons

The properties of fictive swimming that we typically measure in PN recordings are intended to capture relevant features of behavior. Fictive episode duration matches well with behavioral measures of swim duration (Lambert et al., 2012), fictive burst frequency captures the cycle frequency of lateral undulation (Masino and Fetcho, 2005), and burst duration is a proxy for swimming intensity. However, these descriptions of motor activity were not sufficient to capture the effect of perturbing V3 neurons (Fig. 4.5), despite our finding that V3 ablation reduces the activity of motor neurons (Fig. 4.6 & 4.7).

Reduced motor neuron recruitment probability should be expected to reduce neuronal output to muscles, so it is somewhat puzzling that laser ablation of V3 neurons did not produce any apparent difference in a direct measure of motor neuron output to muscles: a PN recording. However, PN recordings only sample the most ventral, most excitable motor neurons (Menelaou and McLean, 2012), a population that has a 50% firing probability even following V3 ablation (Fig. 4.6). Because the number of motor neuron spikes per PN burst cannot be reliably

measured, subtle changes in recruitment probability cannot be quantified using this technique. Whole cell patch recordings from muscle cells recruited during high speed swimming would complement PN recording by measuring the probability and intensity of synaptic drive in the dorsal-fast swim pathway (Buss and Drapeau, 2000; Drapeau et al., 2001; Cui et al., 2004).

An alternative method for assessing the behavioral effect of interneuron ablation is high-speed video recording of larval zebrafish behavior (Ingebretson and Masino, 2013). If V3 neurons reduce the firing probability of motor neurons, they should be expected to reduce the number of muscle fibers recruited by each motor burst, which would, in turn, result in reducing swimming speed at a given tail beat frequency. However, preliminary data characterizing the free-swimming behavioral effects of V3 neuronal ablation did not reveal a speed deficit (data not shown). This lack of behavioral impact likely occurred because the design of the V3 ablation experiment did not take into consideration the kinematics of larval zebrafish swimming. During routine, low-speed swimming, the peak body curvature of the zebrafish is in the most caudal 30% of the animal (Budick and O'Malley, 2000). In a typical zebrafish larva, this is caudal to body segment 20. The laser ablations of V3 neurons performed did not target segments caudal to S20, and if V3 neurons are primarily locally projecting as we predict (Fig. 4.3), the ablations did not affect the motor neurons in the region most responsible for generating forward thrust during slow swimming. V3 neurons in the ablation region would be expected to participate in fast swimming, which has peak body

curvature located at approximately S16, but our behavioral paradigm does not regularly evoke fast swims (Ingebretson and Masino, 2013). In order to observe the behavioral effect of reduced motor neuron recruitment, it would be necessary to either evoke high speed swims, perform caudal V3 laser ablations, or both.

Our results indicate that the V3 neurons are likely a component of the zebrafish swimming circuit, but our experimental design and behavioral assessments were not comprehensive enough to detect a change. While specific additions or modifications to our data collection procedures will allow us to assess the behavioral impact of V3 neuron ablation, it may be helpful to develop richer behavioral paradigms and behavioral data capture techniques to avoid missing the effect of interneuron activation or perturbation in future studies.

Future Directions

The results presented here have overcome one of the barriers to understanding the larval zebrafish locomotor CPG identified in Chapter 1, but they have also highlighted additional barriers to completing the characterization of the spinal motor circuits.

While the work presented is a promising first step in characterizing the function of V3 neurons, significant work remains. Some of these experiments have been outlined in Chapter 4, such as describing the morphological development and categories of V3 neurons and determining if there is burst-frequency dependent

recruitment of V3 neurons, or V3 sub-populations. More broadly, the V3 neurons need to be placed in both a network and behavioral context. The network context of the V3 neurons is captured by their synaptic connections, which are unknown. Morphology and use of fluorescent markers of related to pre- and post- synaptic specializations (Menelaou et al., 2014) are a first step toward developing a circuit map that includes the V3 neurons, but apposition of processes does not always imply active synapses. The use of transgenically-expressed wheat germ agglutinin (WGA) to identify synaptic connections in larval zebrafish cerebellum was recently reported (Takeuchi et al., 2014), this transgenic line would also be extremely helpful in identifying the synaptic inputs and outputs of V3 neurons, and providing targets for paired whole cell electrophysiology to measure synaptic connections from V3 neurons to their targets. Determining the behavioral context in which the V3 neurons are active will require identifying behaviors for which the V3 neurons are necessary. Our results indicate that the V3 neurons are important for fast, but not necessarily escape-related, behaviors. Acquiring and analyzing these data will require sensory stimulation of the larvae and automated kinematic analysis of high speed video (Bhandiwad et al., 2013; Mirat et al., 2013).

The addition of sensory stimulation of larvae to our free-swimming behavioral swimming paradigm may facilitate the characterization of V3 neurons, but *ad hoc* additions of stimuli have the effect of making it more difficult to compare behavior across experiments and across labs. A behavioral paradigm that encouraged the

expression of a broader range of motor behaviors applied consistently across experiments would both increase the probability of detecting the functional role of specialized interneurons, and increase the portability of experimental data. Two behaviors that could be added to our standard paradigm are prey capture and predator avoidance. Prey capture behaviors, in which larval zebrafish hunt paramecia, are essential for zebrafish survival and are generally slow, precise, goal-directed, visually-guided swimming behaviors (Budick and O'Malley, 2000; Borla et al., 2002; Patterson et al., 2013; Trivedi and Bollmann, 2013; Personal communication, Aaron Lambert). Addition of a low concentration of paramecia to the experimental chamber would promote these behaviors without compromising our ability to monitor larval behavior. Predator avoidance behaviors are also essential for survival, but are not typically recorded in zebrafish behavioral paradigms. Introduction of predators to the experimental chamber (von Reyn et al., 2014) could assist in promoting the expression of escape behaviors, fast swimming and struggle. Unfortunately, larval zebrafish can only fail predator evasion one time, so a high-throughput method for interneuron perturbation would be necessary to acquire a sufficient number of predator-prey interactions for analysis. An alternative to genuine predator interaction that would not consume experimental animals would be interaction with a projected virtual object or robotic predator object that induces avoidance responses (Bianco et al., 2011; Zabala et al., 2012).

Finally, it will be important to develop a strategy for comprehensively labeling spinal cord interneurons. The strategy of labeling cells based on developmental domain is beginning to show its limits. In both fish and mice, progenitor domains are subdivided into multiple functional populations (Tables 1.2, 1.3), and important populations of CPG interneurons are not captured by any progenitor domain markers (Dougherty et al., 2013). Comprehensive coverage of spinal neurons is both difficult to achieve and verify because of numeric complexity, but the larval zebrafish is an ideal model organism for developing the technology (Satou et al., 2013).

Summary

There has been substantial progress in the field of larva zebrafish motor circuits over the last 5 years, and I believe that the work presented here is an important contribution to that work. Because of this research, we have evidence that the larval zebrafish spinal cord is not composed of segmental oscillators, but is instead a continuous circuit (Chapters 2 & 3). The neural circuit that ends swimming episodes is functionally independent of the neural circuit that coordinates the timing of motor output at different points along the body of the zebrafish (Chapter 2). The termination of swimming episodes does not depend upon fast synaptic inhibition, but coordination of burst timing across the body does (Chapter 3). While the work presented on the V3 neurons is incomplete, the preliminary evidence presented suggests that the V3 neurons act synergistically with the V2a interneuron at the motor neuron level, or may provide pre-synaptic

excitatory drive to the V2a interneurons (Chapter 4). The framework for the locomotor system proposed in Chapters 2 and 3 will be important for synthesizing the work of many labs in characterizing the interneurons that comprise the CPG (Higashijima et al., 2004a; Liao and Fetcho, 2008; Eklöf-Ljunggren et al., 2012; Ljunggren et al., 2014; Menelaou et al., 2014), and the addition of the V3 neurons as an excitatory pre-motor interneuron population will be helpful in constructing models of how the spinal circuit drives and terminates locomotion.

REFERENCES

Ampatzis K, Song J, Ausborn J, El Manira A. Separate microcircuit modules of distinct v2a interneurons and motoneurons control the speed of locomotion. *Neuron* 83: 934–43, 2014.

Andersson LS, Larhammar M, Memic F, Wootz H, Schwochow D, Rubin C-J, Patra K, Arnason T, Wellbring L, Hjälm G, Imsland F, Petersen JL, McCue ME, Mickelson JR, Cothran G, Ahituv N, Roepstorff L, Mikko S, Vallstedt A, Lindgren G, Andersson L, Kullander K. Mutations in DMRT3 affect locomotion in horses and spinal circuit function in mice. *Nature* 488: 642–6, 2012.

Arrenberg AB, Del Bene F, Baier H. Optical control of zebrafish behavior with halorhodopsin. *Proc. Natl. Acad. Sci. U. S. A.* 106: 17968–73, 2009.

Bagnall MW, McLean DL. Modular Organization of Axial Microcircuits in Zebrafish. *Science* 343: 197–200, 2014.

Batista MF, Jacobstein J, Lewis KE. Zebrafish V2 cells develop into excitatory CiD and Notch signalling dependent inhibitory VeLD interneurons. *Dev. Biol.* 322: 263–75, 2008.

Batty RS. Development of swimming movements and musculature of larval herring (Clupea harengus). *J. Exp. Biol.* 110: 217–29, 1984.

Berens P. CircStat: A MATLAB Toolbox for Circular Statistics. *J. Stat. Softw.* 31: 1–21, 2009.

Bhandiwad AA, Zeddies DG, Raible DW, Rubel EW, Sisneros JA. Auditory sensitivity of larval zebrafish (Danio rerio) measured using a behavioral prepulse inhibition assay. *J. Exp. Biol.* 216: 3504–13, 2013.

Bianco IH, Kampff AR, Engert F. Prey capture behavior evoked by simple visual stimuli in larval zebrafish. *Front. Syst. Neurosci.* 5: 101, 2011.

Borla MA, Palecek B, Budick S, O'Malley DM. Prey capture by larval zebrafish: evidence for fine axial motor control. *Brain. Behav. Evol.* 60: 207–29, 2002.

Borowska J, Jones CT, Zhang H, Blacklaws J, Goulding M, Zhang Y. Functional subpopulations of V3 interneurons in the mature mouse spinal cord. *J. Neurosci.* 33: 18553–65, 2013.

Briscoe J, Pierani A, Jessell TM, Ericson J. A Homeodomain Protein Code Specifies Progenitor Cell Identity and Neuronal Fate in the Ventral Neural Tube. *Cell* 101: 435–445, 2000.

Broughton RE, Betancur-R R, Li C, Arratia G, Ortí G. Multi-locus phylogenetic analysis reveals the pattern and tempo of bony fish evolution. *PLoS Curr.* 5, 2013.

Brown TG. On the nature of the fundamental activity of the nervous centres; together with an analysis of the conditioning of rhythmic activity in progression, and a theory of the evolution of function in the nervous system. *J. Physiol.* 48: 18–46, 1914.

Buchanan J, Grillner S. Newly identified “glutamate interneurons” and their role in locomotion in the lamprey spinal cord. *Science.* 236: 312–314, 1987.

Buchanan JT, Grillner S, Cullheim S, Risling M. Identification of excitatory interneurons contributing to generation of locomotion in lamprey: structure, pharmacology, and function. *J Neurophysiol* 62: 59–69, 1989.

Buchanan JT. Identification of interneurons with contralateral, caudal axons in the lamprey spinal cord: synaptic interactions and morphology. *J Neurophysiol* 47: 961–975, 1982.

Buchanan JT. Contributions of identifiable neurons and neuron classes to lamprey vertebrate neurobiology. *Prog. Neurobiol.* 63: 441–466, 2001.

Budick SA, O’Malley DM. Locomotor repertoire of the larval zebrafish: swimming, turning and prey capture. *J. Exp. Biol.* 203: 2565–79, 2000.

Bullock TH. Revisiting the concept of identifiable neurons. *Brain. Behav. Evol.* 55: 236–40, 2000.

Buss RR, Bourque CW, Drapeau P. Membrane properties related to the firing behavior of zebrafish motoneurons. *J. Neurophysiol.* 89: 657–64, 2003.

Buss RR, Drapeau P. Physiological properties of zebrafish embryonic red and white muscle fibers during early development. *J. Neurophysiol.* 84: 1545–57, 2000.

Buss RR, Drapeau P. Synaptic Drive to Motoneurons During Fictive Swimming in the Developing Zebrafish. *J Neurophysiol* 86: 197–210, 2001.

Butler AB, Hodos W. Comparative Vertebrate Neuroanatomy: Evolution and Adaptation John Wiley & Sons. 2005

Cangiano L, Grillner S. Fast and slow locomotor burst generation in the hemispinal cord of the lamprey. *J. Neurophysiol.* 89: 2931–42, 2003.

Cangiano L, Grillner S. Mechanisms of rhythm generation in a spinal locomotor network deprived of crossed connections: the lamprey hemicord. *J. Neurosci.* 25: 923–35, 2005.

Cazalets JR, Sqalli-Houssaini Y, Clarac F. Activation of the central pattern generators for locomotion by serotonin and excitatory amino acids in neonatal rat. *J. Physiol.* 455: 187–204, 1992.

Cazalets JR. Metachronal propagation of motoneurone burst activation in isolated spinal cord of newborn rat. *J. Physiol.* 568: 583–97, 2005.

Charrier V, Cabelguen J-M. Fictive rhythmic motor patterns produced by the tail spinal cord in salamanders. *Neuroscience* 255: 191–202, 2013.

Chen T-W, Wardill TJ, Sun Y, Pulver SR, Renninger SL, Baohan A, Schreiter ER, Kerr RA, Orger MB, Jayaraman V, Looger LL, Svoboda K, Kim DS. Ultrasensitive fluorescent proteins for imaging neuronal activity. *Nature* 499: 295–300, 2013.

Cohen AH, Wallen P. The neuronal correlate of locomotion in fish. *Exp. brain Res.* 41: 11–18, 1980.

Cole LK, Ross LS. Apoptosis in the developing zebrafish embryo. *Dev. Biol.* 240: 123–42, 2001.

Cowley KC, Schmidt BJ. Effects of inhibitory amino acid antagonists on reciprocal inhibitory interactions during rhythmic motor activity in the in vitro neonatal rat spinal cord. *J Neurophysiol* 74: 1109–1117, 1995.

Crone SA, Quinlan KA, Zagoraiou L, Droho S, Restrepo CE, Lundfald L, Endo T, Setlak J, Jessell TM, Kiehn O, Sharma K. Genetic Ablation of V2a Ipsilateral Interneurons Disrupts Left-Right Locomotor Coordination in Mammalian Spinal Cord. *Neuron* 60: 70–83, 2008.

Crone SA, Zhong G, Harris-Warrick R, Sharma K. In mice lacking V2a interneurons, gait depends on speed of locomotion. *J. Neurosci.* 29: 7098–109, 2009.

Cui WW, Saint-Amant L, Kuwada JY. shocked Gene is required for the function of a premotor network in the zebrafish CNS. *J. Neurophysiol.* 92: 2898–908, 2004.

Dale N. Reciprocal inhibitory interneurones in the Xenopus embryo spinal cord. *J. Physiol.* 363: 61–70, 1985.

Deliagina TG, Orlovsky GN, Pavlova G. The capacity for generation of rhythmic oscillations is distributed in the lumbosacral spinal cord of the cat. *Exp. brain Res.* 53: 81–90, 1983.

Dimitrijevic MR, Gerasimenko Y, Pinter MM. Evidence for a spinal central pattern generator in humans. *Ann. N. Y. Acad. Sci.* 860: 360–76, 1998.

Domenici P, Blake R. The kinematics and performance of fish fast-start swimming *J. Exp. Biol.* 200: 1165–1178, 1997.

Dougherty KJ, Kiehn O. Functional organization of V2a-related locomotor circuits in the rodent spinal cord. *Ann. N. Y. Acad. Sci.* 1198: 85–93, 2010.

Dougherty KJ, Zagoraiou L, Satoh D, Rozani I, Doobar S, Arber S, Jessell TM, Kiehn O. Locomotor Rhythm Generation Linked to the Output of Spinal Shox2 Excitatory Interneurons. *Neuron* 80: 920–933, 2013.

Downes GB, Granato M. Supraspinal input is dispensable to generate glycine-mediated locomotive behaviors in the zebrafish embryo. *J. Neurobiol.* 66: 437–51, 2006.

Downes GB, Waterbury JA, Granato M. Rapid in vivo labeling of identified zebrafish neurons. *Genesis* 34: 196–202, 2002.

Drapeau P, Ali DW, Buss RR, Saint-Amant L. In vivo recording from identifiable neurons of the locomotor network in the developing zebrafish. *J. Neurosci. Methods* 88: 1–13, 1999.

Drapeau P, Buss RR, Ali DW, Legendre P, Rotundo RL. Limits to the development of fast neuromuscular transmission in zebrafish. *J. Neurophysiol.* 86: 2951–6, 2001.

Drapeau P, Saint-Amant L, Buss RR, Chong M, McDearmid JR, Brustein E. Development of the locomotor network in zebrafish. *Prog. Neurobiol.* 68: 85–111, 2002.

Eklöf-Ljunggren E, Haupt S, Ausborn J, Dehnisch I, Uhlén P, Higashijima S, El Manira A. Origin of excitation underlying locomotion in the spinal circuit of zebrafish. *Proc. Natl. Acad. Sci. U. S. A.* 109: 5511–6, 2012.

Fetcho JR, Liu KS. Zebrafish as a model system for studying neuronal circuits and behavior. *Ann. N. Y. Acad. Sci.* 860: 333–45, 1998.

Fetcho JR, McLean DL. Some principles of organization of spinal neurons underlying locomotion in zebrafish and their implications. *Ann. N. Y. Acad. Sci.* 1198: 94–104, 2010.

Fetcho JR, Svoboda KR. Fictive swimming elicited by electrical stimulation of the midbrain in goldfish. *J. Neurophysiol.* 70: 765–80, 1993.

Fetcho JR. The utility of zebrafish for studies of the comparative biology of motor systems. *J. Exp. Zool. B. Mol. Dev. Evol.* 308: 550–62, 2007.

Fuiman LA, Webb PW. Ontogeny of routine swimming activity and performance in zebra danios (Teleostei: Cyprinidae). *Anim. Behav.* 36: 250–261, 1988.

Gosgnach S, Lanuza GM, Butt SJB, Saueressig H, Zhang Y, Velasquez T, Riethmacher D, Callaway EM, Kiehn O, Goulding M. V1 spinal neurons regulate the speed of vertebrate locomotor outputs. *Nature* 440: 215–9, 2006.

Goulding M. Circuits controlling vertebrate locomotion: moving in a new direction. *Nat Rev Neurosci* 10: 507–518, 2009.

Grillner S, Jessell TM. Measured motion: searching for simplicity in spinal locomotor networks. *Curr. Opin. Neurobiol.* 19: 572–86, 2009.

Grillner S, Perret C, Zangger P. Central generation of locomotion in the spinal dogfish. *Brain Res.* 109: 255–269, 1976.

Grillner S, Wallen P. Cellular bases of a vertebrate locomotor system - steering, intersegmental and segmental co-ordination and sensory control. *Brain Res. Rev.* 40: 92–106, 2002.

Grillner S. On the generation of locomotion in the spinal dogfish.*Exp. brain Res.* 20: 459–70, 1974.

Grillner S. Biological pattern generation: the cellular and computational logic of networks in motion. *Neuron* 52: 751–66, 2006.

Grossmann KS, Giraudin A, Britz O, Zhang J, Goulding M. Genetic dissection of rhythmic motor networks in mice. *Prog. Brain Res.* 187: 19–37, 2010.

Guertin PA. The mammalian central pattern generator for locomotion. *Brain Res. Rev.* 62: 45–56, 2009.

Hägglund M, Borgius L, Dougherty KJ, Kiehn O. Activation of groups of excitatory neurons in the mammalian spinal cord or hindbrain evokes locomotion. *Nat. Neurosci.* 13: 246–52, 2010.

Hägglund M, Dougherty KJ, Borgius L, Itohara S, Iwasato T, Kiehn O. Optogenetic dissection reveals multiple rhythmogenic modules underlying locomotion. *Proc. Natl. Acad. Sci. U. S. A.* 110: 11589–94, 2013.

Hale ME, Ritter DA, Fetcho JR. A confocal study of spinal interneurons in living larval zebrafish. *J. Comp. Neurol.* 437: 1–16, 2001.

Hampel FR. The Influence Curve and its Role in Robust Estimation. *J. Am. Stat. Assoc.* 69: 383–393, 1974.

Han X, Chow BY, Zhou H, Klapoetke NC, Chuong A, Rajimehr R, Yang A, Baratta M V, Winkle J, Desimone R, Boyden ES. A high-light sensitivity optical neural silencer: development and application to optogenetic control of non-human primate cortex. *Front. Syst. Neurosci.* 5: 18, 2011.

Hedges SB, Dudley J, Kumar S. TimeTree: a public knowledge-base of divergence times among organisms. *Bioinformatics* 22: 2971–2, 2006.

Heil M, Karban R. Explaining evolution of plant communication by airborne signals. *Trends Ecol. Evol.* 25: 137–44, 2010.

Herrero-Carrón F, Rodríguez FB, Varona P. Bio-inspired design strategies for central pattern generator control in modular robotics. *Bioinspir. Biomim.* 6: 016006, 2011.

Higashijima S, Masino MA, Mandel G, Fetcho JR. Imaging neuronal activity during zebrafish behavior with a genetically encoded calcium indicator. *J. Neurophysiol.* 90: 3986–97, 2003.

Higashijima S, Masino MA, Mandel G, Fetcho JR. Engrailed-1 Expression Marks a Primitive Class of Inhibitory Spinal Interneuron. *J. Neurosci.* 24: 5827 – 5839, 2004a.

Higashijima S-I, Schaefer M, Fetcho JR. Neurotransmitter properties of spinal interneurons in embryonic and larval zebrafish. *J. Comp. Neurol.* 480: 19–37, 2004b.

Hill AA V, Masino MA, Calabrese RL. Intersegmental coordination of rhythmic motor patterns. *J. Neurophysiol.* 90: 531–8, 2003.

Hirata H, Saint-Amant L, Downes GB, Cui WW, Zhou W, Granato M, Kuwada JY. Zebrafish bandoneon mutants display behavioral defects due to a mutation in the glycine receptor beta-subunit. *Proc. Natl. Acad. Sci. U. S. A.* 102: 8345–50, 2005.

Ho S, O'Donovan M. Regionalization and intersegmental coordination of rhythm-generating networks in the spinal cord of the chick embryo. *J. Neurosci.* 13: 1354–1371, 1993.

Huang K-H, Ahrens MB, Dunn TW, Engert F. Spinal projection neurons control turning behaviors in zebrafish. *Curr. Biol.* 23: 1566–73, 2013.

Ikenaga T, Urban JM, Gebhart N, Hatta K, Kawakami K, Ono F. Formation of the spinal network in zebrafish determined by domain-specific pax genes. *J. Comp. Neurol.* 519: 1562–79, 2011.

Ingebretson JJ, Masino MA. Quantification of locomotor activity in larval zebrafish: considerations for the design of high-throughput behavioral studies. *Front. Neural Circuits* 7: 109, 2013.

Jacobson RD, Hollyday M. Electrically evoked walking and fictive locomotion in the chick. *J. Neurophysiol.* 48: 257–70, 1982.

Jankowska E. Spinal interneuronal networks in the cat: elementary components. *Brain Res. Rev.* 57: 46–55, 2008.

Jiang Z, Carlin KP, Brownstone RM. An in vitro functionally mature mouse spinal cord preparation for the study of spinal motor networks. *Brain Res.* 816: 493–499, 1999.

Kahn JA, Roberts A. Experiments on the central pattern generator for swimming in amphibian embryos. *Philos. Trans. R. Soc. Lond. B. Biol. Sci.* 296: 229–43, 1982.

Kiehn O. Development and functional organization of spinal locomotor circuits. *Curr. Opin. Neurobiol.* 21: 100–9, 2011.

Kimura Y, Okamura Y, Higashijima S. alx, a zebrafish homolog of Chx10, marks ipsilateral descending excitatory interneurons that participate in the regulation of spinal locomotor circuits. *J. Neurosci.* 26: 5684–97, 2006.

Kimura Y, Satou C, Fujioka S, Shoji W, Umeda K, Ishizuka T, Yawo H, Higashijima S. Hindbrain V2a Neurons in the Excitation of Spinal Locomotor Circuits during Zebrafish Swimming. *Curr. Biol.* 23: 843–849, 2013.

Kishore S, Bagnall MW, McLean DL. Systematic shifts in the balance of excitation and inhibition coordinate the activity of axial motor pools at different speeds of locomotion. *J. Neurosci.* 34: 14046–54, 2014.

Kjaerulff O, Kiehn O. Distribution of networks generating and coordinating locomotor activity in the neonatal rat spinal cord in vitro: a lesion study. *J. Neurosci.* 16: 5777–5794, 1996.

Koyama M, Kinkhabwala A, Satou C, Higashijima S, Fetcho J. Mapping a sensory-motor network onto a structural and functional ground plan in the hindbrain. *Proc. Natl. Acad. Sci. U. S. A.* 108: 1170–5, 2011.

Kristan WB, Calabrese RL, Friesen WO. Neuronal control of leech behavior. *Prog. Neurobiol.* 76: 279–327, 2005.

Kucenas S, Snell H, Appel B. nkx2.2a promotes specification and differentiation of a myelinating subset of oligodendrocyte lineage cells in zebrafish. *Neuron Glia Biol.* 4: 71–81, 2008.

Kwan AC, Dietz SB, Webb WW, Harris-Warrick RM. Activity of Hb9 interneurons during fictive locomotion in mouse spinal cord. *J. Neurosci.* 29: 11601–11613, 2009.

Kwan KM, Fujimoto E, Grabher C, Mangum BD, Hardy ME, Campbell DS, Parant JM, Yost HJ, Kanki JP, Chien C-B. The Tol2kit: a multisite gateway-based construction kit for Tol2 transposon transgenesis constructs. *Dev. Dyn.* 236: 3088–3099, 2007.

Kyriakatos A, Mahmood R, Ausborn J, Porres CP, Büschges A, El Manira A. Initiation of locomotion in adult zebrafish. *J. Neurosci.* 31: 8422–31, 2011.

Lambert AM, Bonkowsky JL, Masino MA. The conserved dopaminergic diencephalospinal tract mediates vertebrate locomotor development in zebrafish larvae. *J. Neurosci.* 32: 13488–500, 2012.

Lanuza GM, Gosgnach S, Pierani A, Jessell TM, Goulding M. Genetic Identification of Spinal Interneurons that Coordinate Left-Right Locomotor Activity Necessary for Walking Movements. *Neuron* 42: 375–386, 2004.

Lee S-K, Jurata LW, Funahashi J, Ruiz EC, Pfaff SL. Analysis of embryonic motoneuron gene regulation: derepression of general activators function in concert with enhancer factors. *Development* 131: 3295 –3306, 2004.

Legendre P, Korn H. Glycinergic inhibitory synaptic currents and related receptor channels in the zebrafish brain. *Eur. J. Neurosci.* 6: 1544–57, 1994.

Li W-C, Higashijima S, Parry DM, Roberts A, Soffe SR. Primitive roles for inhibitory interneurons in developing frog spinal cord. *J. Neurosci.* 24: 5840–8, 2004.

Li W-C, Moult PR. The control of locomotor frequency by excitation and inhibition. *J. Neurosci.* 32: 6220–30, 2012.

Li W-C, Roberts A, Soffe SR. Specific brainstem neurons switch each other into pacemaker mode to drive movement by activating NMDA receptors. *J. Neurosci.* 30: 16609–20, 2010.

Li W-C, Soffe SR, Wolf E, Roberts A. Persistent responses to brief stimuli: feedback excitation among brainstem neurons. *J. Neurosci.* 26: 4026–35, 2006.

Liao JC, Fetcho JR. Shared versus Specialized Glycinergic Spinal Interneurons in Axial Motor Circuits of Larval Zebrafish. *J. Neurosci.* 28: 12982 –12992, 2008.

Liew WC, Bartfai R, Lim Z, Sreenivasan R, Siegfried KR, Orban L. Polygenic sex determination system in zebrafish. *PLoS One* 7: e34397, 2012.

Liu KS, Fetcho JR. Laser ablations reveal functional relationships of segmental hindbrain neurons in zebrafish. *Neuron* 23: 325–35, 1999.

Ljunggren EE, Haupt S, Ausborn J, Ampatzis K, El Manira A. Optogenetic activation of excitatory premotor interneurons is sufficient to generate coordinated locomotor activity in larval zebrafish. *J. Neurosci.* 34: 134–9, 2014.

Marder E, Calabrese RL. Principles of rhythmic motor pattern generation. *Physiol. Rev.* 76: 687 –717, 1996.

Marder E, Goaillard J-M. Variability, compensation and homeostasis in neuron and network function. *Nat. Rev. Neurosci.* 7: 563–74, 2006.

Masino MA, Fetcho JR. Fictive swimming motor patterns in wild type and mutant larval zebrafish. *J. Neurophysiol.* 93: 3177–88, 2005.

Matsushima T, Grillner S. Intersegmental co-ordination of undulatory movements--a “trailing oscillator” hypothesis. *Neuroreport* 1: 97–100, 1990.

McCrea DA, Rybak IA. Organization of mammalian locomotor rhythm and pattern generation. *Brain Res. Rev.* 57: 134–46, 2008.

McDearmid JR, Drapeau P. Rhythmic motor activity evoked by NMDA in the spinal zebrafish larva. *J. Neurophysiol.* 95: 401–17, 2006.

McLean DL, Fan J, Higashijima S, Hale ME, Fetcho JR. A topographic map of recruitment in spinal cord. *Nature* 446: 71–5, 2007.

McLean DL, Fetcho JR. Ontogeny and innervation patterns of dopaminergic, noradrenergic, and serotonergic neurons in larval zebrafish. *J. Comp. Neurol.* 480: 38–56, 2004.

McLean DL, Fetcho JR. Movement, technology and discovery in the zebrafish. *Curr. Opin. Neurobiol.* 21: 110–5, 2011.

McLean DL, Masino MA, Koh IYY, Lindquist WB, Fetcho JR. Continuous shifts in the active set of spinal interneurons during changes in locomotor speed. *Nat Neurosci* 11: 1419–1429, 2008.

Meinertzhagen IA, Okamura Y. The larval ascidian nervous system: the chordate brain from its small beginnings. *Trends Neurosci.* 24: 401–410, 2001.

Menelaou E, McLean DL. A Gradient in Endogenous Rhythmicity and Oscillatory Drive Matches Recruitment Order in an Axial Motor Pool. *J. Neurosci.* 32: 10925–10939, 2012.

Menelaou E, VanDunk C, McLean DL. Differences in the morphology of spinal V2a neurons reflect their recruitment order during swimming in larval zebrafish. *J. Comp. Neurol.* 522: 1232–48, 2014.

Miller S, van der Meché FG. Coordinated stepping of all four limbs in the high spinal cat. *Brain Res.* 109: 395–8, 1976.

Mink JW, Blumenschine RJ, Adams DB. Ratio of central nervous system to body metabolism in vertebrates: its constancy and functional basis. *Am. J. Physiol.* 241: R203–12, 1981.

Mirat O, Sternberg JR, Severi KE, Wyart C. ZebraZoom: an automated program for high-throughput behavioral analysis and categorization. *Front. Neural Circuits* 7: 107, 2013.

Miyasaka N, Morimoto K, Tsubokawa T, Higashijima S, Okamoto H, Yoshihara Y. From the Olfactory Bulb to Higher Brain Centers: Genetic Visualization of Secondary Olfactory Pathways in Zebrafish. *J. Neurosci.* 29: 4756 –4767, 2009.

Mori S, Nishimura H, Kurakami C, Yamamura T, Aoki M. Controlled locomotion in the mesencephalic cat: distribution of facilitatory and inhibitory regions within pontine tegmentum. *J. Neurophysiol.* 41: 1580–91, 1978.

Moult PR, Cottrell GA, Li W-C. Fast silencing reveals a lost role for reciprocal inhibition in locomotion. *Neuron* 77: 129–40, 2013.

Muller UK, Von Leeuwen J. Swimming of larval zebrafish: ontogeny of body waves and implications for locomotory development. *J. Exp. Biol.* 207: 853–868, 2004.

Mullins OJ, Hackett JT, Buchanan JT, Friesen WO. Neuronal control of swimming behavior: comparison of vertebrate and invertebrate model systems. *Prog. Neurobiol.* 93: 244–69, 2011.

Mulloney B, Smarandache-Wellmann C. Neurobiology of the crustacean swimmeret system. *Prog. Neurobiol.* 96: 242–67, 2012.

Noga BR, Kettler J, Jordan LM. Locomotion produced in mesencephalic cats by injections of putative transmitter substances and antagonists into the medial reticular formation and the pontomedullary locomotor strip. *J. Neurosci.* 8: 2074–86, 1988.

O'Malley DM, Kao YH, Fetcho JR. Imaging the functional organization of zebrafish hindbrain segments during escape behaviors. *Neuron* 17: 1145–55, 1996.

Patterson BW, Abraham AO, MacIver MA, McLean DL. Visually guided gradation of prey capture movements in larval zebrafish. *J. Exp. Biol.* 216: 3071–83, 2013.

Pietri T, Manalo E, Ryan J, Saint-Amant L, Washbourne P. Glutamate drives the touch response through a rostral loop in the spinal cord of zebrafish embryos. *Dev. Neurobiol.* 69: 780–95, 2009.

Preibisch S, Saalfeld S, Schindelin J, Tomancak P. Software for bead-based registration of selective plane illumination microscopy data. *Nat. Methods* 7: 418–9, 2010.

Preibisch S, Saalfeld S, Tomancak P. Globally optimal stitching of tiled 3D microscopic image acquisitions. *Bioinformatics* 25: 1463–5, 2009.

Rabe Bernhardt N, Memic F, Gezelius H, Thiebes A-L, Vallstedt A, Kullander K. DCC mediated axon guidance of spinal interneurons is essential for normal locomotor central pattern generator function. *Dev. Biol.* 366: 279–89, 2012.

Rabe N, Gezelius H, Vallstedt A, Memic F, Kullander K. Netrin-1-dependent spinal interneuron subtypes are required for the formation of left-right alternating locomotor circuitry. *J. Neurosci.* 29: 15642–9, 2009.

Ramer LM, Ramer MS, Bradbury EJ. Restoring function after spinal cord injury: towards clinical translation of experimental strategies. *Lancet Neurol.* 13: 1241–1256, 2014.

Von Reyn CR, Breads P, Peek MY, Zheng GZ, Williamson WR, Yee AL, Leonardo A, Card GM. A spike-timing mechanism for action selection. *Nat. Neurosci.* 17: 962–70, 2014.

Rihel J, Schier AF. Behavioral screening for neuroactive drugs in zebrafish. *Dev. Neurobiol.* 72: 373–85, 2012.

Roberts A, Conte D, Hull M, Merrison-Hort R, al Azad AK, Buhl E, Borisyuk R, Soffe SR. Can Simple Rules Control Development of a Pioneer Vertebrate Neuronal Network Generating Behavior? *J. Neurosci.* 34: 608–621, 2014.

Roberts A, Kahn JA, Soffe SR, Clarke JD. Neural control of swimming in a vertebrate. *Science* 213: 1032–4, 1981.

Roberts A, Li W-C, Soffe SR. How neurons generate behavior in a hatchling amphibian tadpole: an outline. *Front. Behav. Neurosci.* 4: 16, 2010.

Roberts A, Soffe SR, Wolf ES, Yoshida M, Zhao FY. Central circuits controlling locomotion in young frog tadpoles. *Ann. N. Y. Acad. Sci.* 860: 19–34, 1998.

Sapir T, Geiman EJ, Wang Z, Velasquez T, Mitsui S, Yoshihara Y, Frank E, Alvarez FJ, Goulding M. Pax6 and engrailed 1 regulate two distinct aspects of renshaw cell development. *J. Neurosci.* 24: 1255–64, 2004.

Satou C, Kimura Y, Higashijima S. Generation of multiple classes of V0 neurons in zebrafish spinal cord: progenitor heterogeneity and temporal control of neuronal diversity. *J. Neurosci.* 32: 1771–83, 2012.

Satou C, Kimura Y, Hirata H, Suster ML, Kawakami K, Higashijima S. Transgenic tools to characterize neuronal properties of discrete populations of zebrafish neurons. *Development* 140: 3927–31, 2013.

Satou C, Kimura Y, Kohashi T, Horikawa K, Takeda H, Oda Y, Higashijima S. Functional role of a specialized class of spinal commissural inhibitory neurons during fast escapes in zebrafish. *J. Neurosci.* 29: 6780–93, 2009.

Sautois B, Soffe SR, Li W-C, Roberts A. Role of type-specific neuron properties in a spinal cord motor network. *J. Comput. Neurosci.* 23: 59–77, 2007.

Schäfer M, Kinzel D, Winkler C. Discontinuous organization and specification of the lateral floor plate in zebrafish. *Dev. Biol.* 301: 117–129, 2007.

Schindelin J, Arganda-Carreras I, Frise E, Kaynig V, Longair M, Pietzsch T, Preibisch S, Rueden C, Saalfeld S, Schmid B, Tinevez J-Y, White DJ, Hartenstein V, Eliceiri K, Tomancak P, Cardona A. Fiji: an open-source platform for biological-image analysis. *Nat. Methods* 9: 676–82, 2012.

Schoenwolf GC, Smith JL. Mechanisms of neurulation: traditional viewpoint and recent advances. *Development* 109: 243–70, 1990.

Scott EK, Mason L, Arrenberg AB, Ziv L, Gosse NJ, Xiao T, Chi NC, Asakawa K, Kawakami K, Baier H. Targeting neural circuitry in zebrafish using GAL4 enhancer trapping. *Nat. Methods* 4: 323–6, 2007.

Severi KE, Portugues R, Marques JC, O'Malley DM, Orger MB, Engert F. Neural Control and Modulation of Swimming Speed in the Larval Zebrafish. *Neuron* 83: 692–707, 2014.

Smarandache-Wellmann C, Weller C, Mulloney B. Mechanisms of Coordination in Distributed Neural Circuits: Decoding and Integration of Coordinating Information. *J. Neurosci.* 34: 793–803, 2014.

Soffe SR, Roberts A, Li W-C. Defining the excitatory neurons that drive the locomotor rhythm in a simple vertebrate: insights into the origin of reticulospinal control. *J. Physiol.* 587: 4829–44, 2009.

Stein PSG. Swimming movements elicited by electrical stimulation of the turtle spinal cord: The high spinal preparation. *J. Comp. Physiol. ? A* 124: 203–210, 1978.

Stein PSG. Motor pattern deletions and modular organization of turtle spinal cord. *Brain Res. Rev.* 57: 118–24, 2008.

Stepien AE, Arber S. Probing the locomotor conundrum: descending the "V" interneuron ladder. *Neuron* 60: 1–4, 2008.

Subach OM, Patterson GH, Ting L-M, Wang Y, Condeelis JS, Verkhusha V V. A photoswitchable orange-to-far-red fluorescent protein, PSmOrange. *Nat. Methods* 8: 771–777, 2011.

Suster ML, Kania A, Liao M, Asakawa K, Charron F, Kawakami K, Drapeau P. A novel conserved evx1 enhancer links spinal interneuron morphology and cis-regulation from fish to mammals. *Dev. Biol.* 325: 422–433, 2009.

Svane I, Young C. The ecology and behaviour of ascidian larvae. *Ocean. Mar Biol*. 27:45-90, 1989

Takeuchi M, Matsuda K, Yamaguchi S, Asakawa K, Miyasaka N, Lal P, Yoshihara Y, Koga A, Kawakami K, Shimizu T, Hibi M. Establishment of Gal4 transgenic zebrafish lines for analysis of development of cerebellar neural circuitry. *Dev. Biol.* 397: 1–17, 2014.

Talpalar AE, Bouvier J, Borgius L, Fortin G, Pierani A, Kiehn O. Dual-mode operation of neuronal networks involved in left-right alternation. *Nature* 500: 85–8, 2013.

Talpalar AE, Endo T, Löw P, Borgius L, Hägglund M, Dougherty KJ, Ryge J, Hnasko TS, Kiehn O. Identification of minimal neuronal networks involved in flexor-extensor alternation in the mammalian spinal cord. *Neuron* 71: 1071–84, 2011.

Thiele TR, Donovan JC, Baier H. Descending control of swim posture by a midbrain nucleus in zebrafish. *Neuron* 83: 679–91, 2014.

Trivedi CA, Bollmann JH. Visually driven chaining of elementary swim patterns into a goal-directed motor sequence: a virtual reality study of zebrafish prey capture. *Front. Neural Circuits* 7: 86, 2013.

Wadden T, Hellgren J, Lansner A, Grillner S. Intersegmental coordination in the lamprey: simulations using a network model without segmental boundaries. *Biol. Cybern.* 76: 1–9, 1997.

Wallén P, Grillner S, Feldman JL, Bergelt S. Dorsal and ventral myotome motoneurons and their input during fictive locomotion in lamprey. *J. Neurosci.* 5: 654–61, 1985.

Wang W-C, McLean DL. Selective responses to tonic descending commands by temporal summation in a spinal motor pool. *Neuron* 83: 708–21, 2014.

Waters CM, Bassler BL. Quorum sensing: cell-to-cell communication in bacteria. *Annu. Rev. Cell Dev. Biol.* 21: 319–46, 2005.

Westerfield M. The Zebrafish Book. A Guide for the Laboratory Use of Zebrafish (Danio rerio), 5th Edition. University of Oregon Press. 2007

Wheatley M, Edamura M, Stein RB. A comparison of intact and in-vitro locomotion in an adult amphibian. *Exp. brain Res.* 88: 609–14, 1992.

Wheatley M, Jovanovic K, Stein RB, Lawson V. The activity of interneurons during locomotion in the in vitro necturus spinal cord. *J. Neurophysiol.* 71: 2025–2032, 1994.

Wiggin TD, Anderson TM, Eian J, Peck JH, Masino MA. Episodic Swimming in the Larval Zebrafish is Generated by a Spatially Distributed Spinal Network with Modular Functional Organization. *J. Neurophysiol.* 108: 925–34, 2012.

Wiggin TD, Peck JH, Masino MA. Coordination of fictive motor activity in the larval zebrafish is generated by non-segmental mechanisms. *PLoS One* 9: e109117, 2014.

Williams TL, Grillner S, V. SV, Wallen P, Kashin S, Rossignol S. LOCOMOTION IN LAMPREY AND TROUT: THE RELATIVE TIMING OF ACTIVATION AND MOVEMENT. *J. Exp. Biol.* 143: 559–566, 1989.

Wilson SW, Houart C. Early Steps in the Development of the Forebrain. *Dev. Cell* 6: 167–181, 2004.

Wolf E, Soffe SR, Roberts A. Longitudinal neuronal organization and coordination in a simple vertebrate: a continuous, semi-quantitative computer model of the central pattern generator for swimming in young frog tadpoles. *J. Comput. Neurosci.* 27: 291–308, 2009.

Wyart C, Del Bene F, Warp E, Scott EK, Trauner D, Baier H, Isacoff EY. Optogenetic dissection of a behavioural module in the vertebrate spinal cord. *Nature* 461: 407–10, 2009.

Yang H, Inokuchi H, Adler J. Phototaxis away from blue light by an Escherichia coli mutant accumulating protoporphyrin IX. *Proc. Natl. Acad. Sci. U. S. A.* 92: 7332–6, 1995.

Yang L, Rastegar S, Strähle U. Regulatory interactions specifying Kolmer-Agduhr interneurons. *Development* 137: 2713 –2722, 2010.

Zabala F, Polidoro P, Robie A, Branson K, Perona P, Dickinson MH. A simple strategy for detecting moving objects during locomotion revealed by animal-robot interactions. *Curr. Biol.* 22: 1344–50, 2012.

Zagoraiou L, Akay T, Martin JF, Brownstone RM, Jessell TM, Miles GB. A cluster of cholinergic premotor interneurons modulates mouse locomotor activity. *Neuron* 64: 645–662, 2009.

Zhang J, Lanuza GM, Britz O, Wang Z, Siembab VC, Zhang Y, Velasquez T, Alvarez FJ, Frank E, Goulding M. V1 and v2b interneurons secure the

alternating flexor-extensor motor activity mice require for limbed locomotion. *Neuron* 82: 138–50, 2014.

Zhang Y, Narayan S, Geiman E, Lanuza GM, Velasquez T, Shanks B, Akay T, Dyck J, Pearson K, Gosgnach S, Fan C-M, Goulding M. V3 Spinal Neurons Establish a Robust and Balanced Locomotor Rhythm during Walking. *Neuron* 60: 84–96, 2008.

Zhong G, Shevtsova NA, Rybak IA, Harris-Warrick RM. Neuronal activity in the isolated mouse spinal cord during spontaneous deletions in fictive locomotion: insights into locomotor central pattern generator organization. *J. Physiol.* 590: 4735–59, 2012.